Design of Efficient, Cost Effective Three Phase Induction Motors for Ceiling Fans in India

by

Mohammad Mowafaq Qasim

B.S. American University of Sharjah (2011)
S.M. Masdar Institute of Science and Technology (2013)

Submitted to the Department of Electrical Engineering and Computer Science
in partial fulfillment of the requirements for the degree of

Master of Science in Computer Science and Engineering

at the

MASSACHUSETTS INSTITUTE OF TECHNOLOGY

June 2019

Signature redacted

Author .....
Department of Electrical Engineering and Computer Science
May 23, 2019

Signature redacted

Certified by .....
James L. Kirtley Jr.
Professor of Electrical Engineering and Computer Science
Thesis Supervisor

Signature redacted

Accepted by .....
Leslie A. Kolodziejski
Professor of Electrical Engineering and Computer Science
Chair, Department Committee on Graduate Students

Design of Efficient, Cost Effective Three Phase Induction Motors for Ceiling Fans in India

by

Mohammad Mowafaq Qasim

Submitted to the Department of Electrical Engineering and Computer Science
on May 23, 2019, in partial fulfillment of the
requirements for the degree of
Master of Science in Computer Science and Engineering

Abstract

In developing economies such as India, improving the efficiency of home appliances is of high priority in locations which are characterized by a weak electric distribution system. Ceiling fans are one of the most used home appliances in India. They typically operate for many hours, and since most of them are driven by inefficient, low cost single phase induction motors, the total power loss is nontrivial. To overcome the inefficiency of single phase induction motors, brushless dc motors have been increasingly used in ceiling fans to achieve high efficiency and power factor at multiple speed settings. However, they are more expensive than conventional ceiling fan motors due to the additional cost of permanent magnets and power electronic drive circuit.

Three phase in contrast to single phase induction motors have proven to have a superior performance especially for high power applications. From a manufacturing point of view, they are no more expensive to build than single phase induction motors. Also, three phase induction motors require no permanent magnets, which makes them economically attractive. To be able to use three phase induction motors in home appliances at variable speed, a power electronic drive is required to convert the single phase supply to three phase. The drive circuit can also be controlled to improve the input power factor. With the advancement of power electronic technology and integrated control devices, such motor drives can be made efficient and cost effective.

This thesis explores the design and optimization of three phase squirrel cage induction motors for the application of ceiling fans in India, with the objective of achieving a balance between efficiency and cost. A detailed analytical model for a low speed, low power three phase squirrel cage induction motor is developed. The analytical model is validated using finite-element analysis. This thesis also optimizes the motor design using genetic algorithms. The optimized design weighs $4.5kg$ and achieves 70% efficiency, which proves more efficient than existing ceiling fan motors in India. The optimized design is also validated in finite-element analysis. Finally, this thesis presents a simulation study of the motor drive implementation for the proposed three phase induction motor.

Thesis Supervisor: James L. Kirtley Jr.
Title: Professor of Electrical Engineering and Computer Science

And say, "My Lord, increase me in knowledge."

Quran [20:114]

Acknowledgments

First, I would like to express my sincere thanks and appreciations to my advisor Professor James Kirtley for his generous teaching, relentless guidance, encouragement and support throughout this thesis. His great knowledge, experience, and enthusiasm for electric machines have inspired me to pursue the field of electric machines. This thesis would not have been possible without his guidance.

I also would like to thank Professor David Perreault for his generous time to answer my questions related to power electronics. His outstanding teaching, generosity with his knowledge and experience, his great efforts to organize seminars and field trips for graduate students, and his invaluable advice in research, is very inspiring.

During the course of this work, I had the great opportunity to work with Professor Vivek Agarwal and Arpan Hota, our collaborators at the power electronics and power systems group at the Indian Institute of Technology, Bombay. Prof. Agarwal's input on the design of the power electronic drive part of the project has been very valuable. To him, I say "Thank you!". I also would like to thank Arpan whom I have been working with closely for this project. The many technical discussions we had, his accommodation of the time difference in our conference calls, his generous help to acquire and ship the test ceiling fans to Boston, were instrumental in the success of this work.

I would like to express my sincere gratitude to all LEES faculty and staff who have been very helpful, including Dr. Stephen Umans (whose generosity with time to discuss challenging problems with the machine design and analytical modeling is extraordinary), Professor Steven Leeb (who have played a major role in LEES renovation to provide students with necessary equipment and lab facility), Professor Jeffery Lang, David Otten and Donna Gale.

Great thanks to my friends and colleagues who have made LEES a great place to work, including Alexander Jurkov, Anas Al Bastami, Colm O'Rourke, Lukasz Huchel, Po Hsu Huang, Krishan Kant, Sajjad Mohammadi, Alex Hanson, Edwin Fonkwe, Matthew Overlin, William Taft, Yiou He, Rakesh Kumar, Jessica Boles, Tony Zhang, Mike Ranjram, Intae Moon, Adedayo Aderibole, Nathan Monroe, Daisy Green, Jie Mei, and many others.

Words can never do justice to express my gratitude to my family. It is to my parents Mowaffaq Qasim and Wedad Mousa that this thesis is dedicated. I have become what I am now due to them. Their unconditional love, endless care and continuous encouragement are my main source of inspiration. My sister, Mona Qasim, may God bless her soul, was always supportive of my academic pursue, and her belief in me is a treasure I cherish and a motivation to reach to greater heights. Much credit goes to my siblings. It is their love, support and advice that I will not trade for the whole world.

I also would like to express my gratitude to my friends in Boston, including Mohamed Radwan, Edmond Awad, Nasir Almasri, Mohamed Ibrahim, Sally El Henawy, Shahd Labib, Cynthia Hajal, Christian Adib, Shaheen Tomah, Abdullah Al-Dujaili, Sana Al-Dujaili, Rabeeya Arif, and many others.

Finally, I would like to thank MIT Tata Center for supporting this research. Special thanks go to Professor Robert Stoner, Professor Chintan Vaishnav and Reja Amatya for connecting me with local ceiling fan companies in India and their great mentor-ship to help me develop the techno-economic analysis for my research. I also would like to thank Usha Limited for providing us with ceiling fans data and efficiency reports.

Contents

List of Figures

List of Tables

Chapter 1

Background and Motivation

Electric motors are the single largest electrical load, accounting for 43% of all global electricity consumption in 2006, 9% of which are appliance motors used in the residential sector [64]. Among the highest energy-consuming electric motor driven appliances are refrigerators, heating, ventilation and air-conditioning (HVAC) systems, pumps, and fans. The performance of these motors are characterized by three indices: efficiency, power factor, and current distortion. Each of the indices are of a particular interest to emerging economies such as India, which is characterized by a relatively weak power system, and relatively large number of isolated distribution systems that can be considered microgrids. For example, on July the 30th, 2012, the largest power outage in history, which affected most of northern and eastern India, left more than 600 million people in the dark. These power outages, planned and unplanned, are not only due to the large energy demand, but also due to inefficiencies at both the distribution and consumer ends. A lot of home appliances driven by motors are being produced and increasingly used in India by a large population which is constantly increasing as individuals get wealthier. Therefore, hundreds, if not thousands of Terra-Watt of energy, can be saved annually by adopting efficient appliances at the consumer end. One of the inefficient appliances that are widely used in India are ceiling fans.

Fans are the main source of residential cooling in India as opposed to air-conditioning systems in the developed countries. It is reported that they accounted for 6% of the total residential energy use in India in 2000 and is expected to account for at least 9% in 2020

[19]. Furthermore, fans are also well-known to be a cost-effective solution for reducing air conditioner electricity consumption. Therefore, improving the performance of electric motors that drive ceiling fans can play an important role in reducing the overall energy consumption in many countries, not only in India. Furthermore, a study on the potential global benefits of improving ceiling fan energy efficiency [50] shows that using the existing motor technology, 50% improvement on the motor efficiency can be achieved which results in more than 50 Terra-Watt-Hour energy saving by 2020 in India.

The most commonly used motor for driving fractional horse power appliances is the single phase induction motor. Two common types of single phase induction motor are widely used for driving ceiling fans: shaded pole induction motor [56] which is popular in Europe and the United States, and permanent split capacitor induction motor [14], prevalent in India. Ceiling fans driven by these motors have a power consumption of 70 W [16]. Another type of ceiling fans motors that are becoming more popular is brushless DC motors (BLDC). BLDC motor is a permanent magnet synchronous motor driven by solid state devices. It had first appeared in 1962 by William and Trickey [66]. In that time, these motors were not economically attractive due to the high cost of permanent magnets and power electronics. With the advancement in semi-conductor technology, BLDC motors have succeeded to replace conventional brush DC motors in the higher horse-power range [35]. However, it was not until 2009 when BLDC motors came into the ceiling fan industry in the US, and a few years later in India.

Ceiling fans driven by BLDC motors are efficient and can operate over a range of speeds since they rotate in synchronism with the airgap magnetic field (no slip loss), provide excitation at no loss by the PMs, and operate over a range of speeds by a power electronic drive circuit. They are considered the most efficient in the household fan market, as they draw less power in the range of 28 - 35 W as at rated speed compared to the 70 W conventional ceiling fan. However, they are more expensive than the conventional single phase induction motors due to the added cost of the permanent magnets and power electronic circuit.

Three phase induction motors, are simple, rugged, easy to build, and reliable. Generally, they can be designed to have a satisfactory efficiency and can be operated stably at variable speeds by a suitable power electronic drive circuit. However, it is still considered

until now unconventional to use three phase induction motors in low power applications such as home appliances. The main reason is the absence of three phase supply in households. However with semiconductor power devices becoming increasingly cheaper, it is worth considering three phase induction motors for powering home appliances due to their aforementioned advantages. For example, Arpan et al. [27] have shown that a power electronic drive system for three phase induction motors of domestic fan applications can be made cost effective, efficient, and more reliable by using a simple dc-link capacitor reduction strategy accompanied with a modified PWM scheme [27]. In this thesis, we attempt to show that three phase squirrel cage induction motors, equipped with a power electronic drive, can be designed with relatively high efficiency and satisfactory power factor for ceiling fans.

1.1 Problem Statement

The distribution electric grids are relatively weak in India. Part of their inefficiency is due to the use of inefficient loads and appliances at the consumer end. Ceiling fans is a primary appliance that is used in almost every house in India. The majority of these ceiling fans use single phase induction motors which are quite inefficient. The existing ceiling motor technology, such as brushless dc motors or improved design of split phase induction motor through means of thinner laminations (affect eddy current losses), rotor bars of copper instead of aluminum (affect conduction losses) and smaller airgap (affect torque), can potentially reduce power consumption of conventional ceiling fans by 50% or more, resulting in great savings. However, this comes at the expense of cost. For example, the price of a BLDC ceiling fan is four times more expensive than the conventional capacitor-run motor ceiling fan, which makes it economically unattractive and sometime unattainable to many end-users in India. Similarly, improved lamination, and higher rotor bar conductivity adds to the cost of SPIMs. Thus, designing a motor is a challenging task of achieving a balance between many trade-offs, such as efficiency, power factor, cost, weight, volume, etc.

The two types of ceiling fan motors (SPIMs and BLDC) showcase a situation of conflicting requirements, namely efficiency and cost. The first type of motor is inexpensive

to manufacture but its efficiency is limited, and can be designed to operate at maximum efficiency and power factor only at a single speed. However, the second motor is inherently efficient, and being driven by a power electronic package enables variable speed operation without using lossy resistors as in SPIMs. The main drawback of this motor is its higher cost, which is primarily due to its PMs and secondarily due to the cost of power electronics. Reaching to a middle ground between these two technologies is a challenging task, nonetheless attainable by induction motors with a smart control. Three phase squirrel cage induction motors can provide the balance between efficiency and cost since they are fairly efficient, do not require PMs, and can be driven at variable speeds using a power electronic package while maintaining high efficiency at lower speeds. In this thesis, a three phase induction motor driven by a power electronic circuit at variable speeds is proposed for ceiling fans in India.

The proposed motor system for ceiling fans is shown in Fig. 1-1. It consists of a three phase induction motor, a power rectifier, and DC link capacitor followed by an inverter. The rectifier is used to convert the AC power to DC, stored in the form of electric energy in the dc link capacitor. The inverter is controlled by a microcontroller and pulse-width-modulation scheme to convert the DC power into three phase AC power suitable for driving the three phase induction motor. The motor can operate at several speeds via Volt-Hz open loop control implemented by the microcontroller upon receiving an input command from the fan's remote control or a speed control knob.

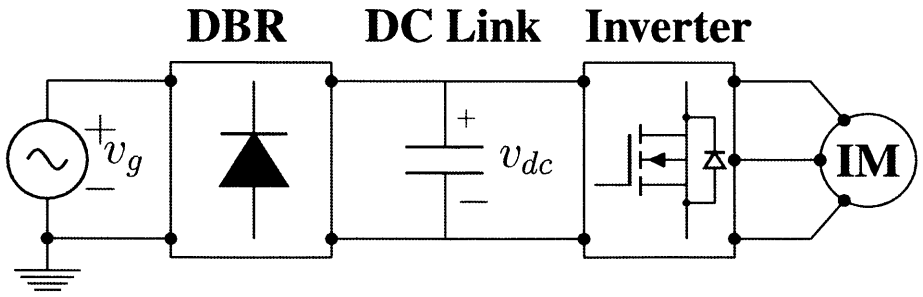

Figure 1-1: Block diagram of three phase induction motor with power electronic drive circuit: the motor drives home ceiling fan

1.2 Thesis Contributions

This thesis explores the design of squirrel cage induction motor for household ceiling fans in India with the objective of achieving overall improvements and balance between efficiency, and cost to overcome the inefficiency of single phase induction motors used in conventional ceiling fans and the higher cost of brushless dc motors of the new generation of ceiling fans. The thesis contributions are summarized as follows:

(1) The analytical model of the three phase squirrel cage induction motor is developed, considering higher order space harmonics and core losses. The authors adopts the methods shown by P. Alger [3], J. Kirtley [31] and T. Lipo [38] in developing the analytical model. The calculation of the equivalent circuit parameters are described in detail and the performance of the motor is evaluated based on solving the equivalent circuit. A detailed procedure on evaluating the performance of the motor based on the analytical model is summarized.

(2) The analytical model is validated in 2D and 3D finite-element (FE) transient analysis in ANSYS Maxwell.

(3) Based on the verified analytical model, an optimized motor design is obtained by employing genetic algorithm optimization. Several optimization objective functions were explored, and an optimal design is chosen to satisfy the best compromise between efficiency and weight (and thus cost). The selected optimized motor design has 70% efficiency ($21.4W$ input power, $15W$ mechanical power), has 0.5 power factor, weighs $4.5kg$, which proves superior to existing ceiling fan motors in terms of energy consumption. The optimized motor maintains an overall high efficiency (60% to 70%) as the load is varied. The input power factor can be corrected if required by provision of a power factor correction circuit added to the drive circuit.

(4) The optimized motor is validated in Maxwell 2D FE transient analysis.

(5) The optimized motor with the power electric drive circuit is evaluated in MATLAB/Simulink using the rotor reference frame d-q dynamic simulation model. The

instantaneous torque, input power, mechanical power, and stator currents approximates that calculated from the analytical and FE models.

1.3 Thesis Outline

This thesis is divided into six chapters including this introductory chapter. Chapter 2 surveys the different type of motors used in ceiling fans, specifically single phase induction motors and brushless dc motors. The final part of the chapter discusses three phase induction motors in general as they are the proposed type of motors in this thesis for ceiling fans application.

Chapter 3 discusses the analytical model for squirrel cage induction motors in detail. This analytical model has the merit of describing the terminal behavior of the motor using a simple equivalent circuit model. The per phase equivalent circuit model is also discussed and the analytical expressions for the circuit parameters are provided. Furthermore, this chapter presents a detailed procedure on evaluating the performance of the motor through means of solving the equivalent circuit.

Chapter 4 presents the validation of the analytical model in 2D and 3D FE transient analysis in ANSYS Maxwell, and optimization of the motor design using a genetic algorithm optimization technique. The chapter starts by verifying the performance of initial design of the motor using finite-element models and then uses the analytical model to optimize the motor design. The second part of the chapter explores and compares between different optimization objective functions to reach to a trade-off between efficiency and active weight of the motor. The third part of the chapter selects an optimum design and presents the validation results of the optimized motor design in finite-element transient analysis.

Chapter 5 investigates the performance of the optimized induction motor with the power electronic drive circuit using d-q simulation dynamic model in MATLAB/Simulink. It is shown the optimized design of the proposed ceiling fan three phase phase induction motor can be driven by low cost variable speed drive with simple volt-Hz open loop control. The d-q model uses the equivalent circuit parameters corresponding to the fundamental airgap

flux density of the optimized motor. The second part of the chapter compares the steady state torque, input power, mechanical power, and stator currents obtained from motor with drive Matlab/Simulink simulations with those obtained from the analytical model and FE transient simulations.

Finally, Chapter 6 provides a summary of the ground covered in the thesis and presents recommendations for future work.

Chapter 2

Literature Review

There are two main type of motors used to drive ceiling fans: single phase induction motors and brushless dc motors. Single phase induction motors were prominent in driving home ceiling fans until 2009 when Emerson Electric introduced their first brushless dc motor *ecofan* model. Now, most efficient (and more expensive) ceiling fan motors use brushless dc motors. In this thesis, three phase induction motors equipped with power electronic drive circuit is proposed for household ceiling fans as the can be designed with higher efficiency than single phase induction motors, and lower overall cost (including cost of the drive) than brushless dc motors. In this chapter, we will give a brief background the major motor technologies used in the ceiling fan industry, including single phase induction motors and brushless dc motors. We will also attempt to provide a general background about three phase induction motors and shed light on the major contributions in the modeling, design, optimization and drives of appliance motors.

2.1 Single Phase Induction Motors

From a structural point of view, single phase induction motors (SPIM) resemble three phase induction motors in structure with a difference only in the stator winding. The stator winding in single phase induction motors consists of two coils 90 electrical degrees displaced in space, such as in split phase motors and one winding in shaded pole motors. The rotor, on the other hand, is the same as in three phase squirrel cage induction motors. In fact, if one

of the phases of a three-phase induction machine was opened while the motor is running at rated speed, the machine may continue to operate as a single phase motor with line-to-line voltage across the other two connected lines. The same motor, however, will not restart with single phase supply according to the double revolving theory [57, 62].

The double revolving theory states that a stationary pulsating magnetic field of single phase motor can be decomposed into two revolving magnetic fields of equal magnitude but rotating in opposite directions. The induction motor will respond to each magnetic field separately producing its own torque-speed characteristic curve, and the net torque is the superposition of the two torques produced by the forward and backward magnetic fields. By symmetry and superposition, such a motor inherently produces no starting torque at standstill, as the two oppositely rotating magnetic fields produce torques of equal magnitude and opposite signs. However, if the motor was started by auxiliary means, the net torque will be in the direction in which it is started, and the motor will naturally continue to run. This torque is the average torque, however the instantaneous torque will be alternating at twice the line-frequency of the stator with zero average per cycle. This pulsation will cause the motor to vibrate making it noisier than a three phase induction motor of the same size. This inherit vibration must be allowed for in the mechanical design of the motor [62].

As mentioned earlier, SPIMs can be started by auxiliary means, and are commonly classified according to their starting technique into three main categories: split-phase with resistive auxiliary winding, split phase with capacitive auxiliary winding known as capacitor motors, and shaded-pole motors. Selection of the appropriate motor is based on the efficiency, power factor requirements, starting and running torque requirements of the load, and the limitations on starting and running current drawn from the supply line [57].

2.1.1 Split Phase Motors with Resistive Auxiliary Winding

Split phase induction motors have two windings: the main winding and the auxiliary winding as shown in Fig. 2-1. The axes of these windings are set 90 electrical degrees apart in space along the stator. The main windings have a lower resistance-to-reactance (R/X) ratio than the auxiliary winding, and hence the current in the auxiliary winding leads the

rent in the main winding [31,57]. This means that the flux density of the auxiliary winding peaks before that of the main winding, making one of the oppositely rotating magnetic field stronger than the other providing a net starting torque for the motor. The direction of rotation of the rotor is determined by whether the space angle between the main and auxiliary winding is +90 or -90 electrical degrees. Thus the direction of rotation can be reversed by switching the connections of the auxiliary winding. To obtain a higher R/X ratio for the auxiliary winding, a smaller wire than the main winding is usually used for that purpose. Although the auxiliary winding have higher losses due to the higher resistance, it is used only at the stating of the motor as it is disconnected later via a centrifugal switch once the rotor reaches up to 75% of synchronous speed. Split-phase motors have moderate stating torque with a fairly low stating current. Their efficiency is typically from $40-55\%$. Typical appliance that use SPIM include blowers, centrifugal pumps, and fans.

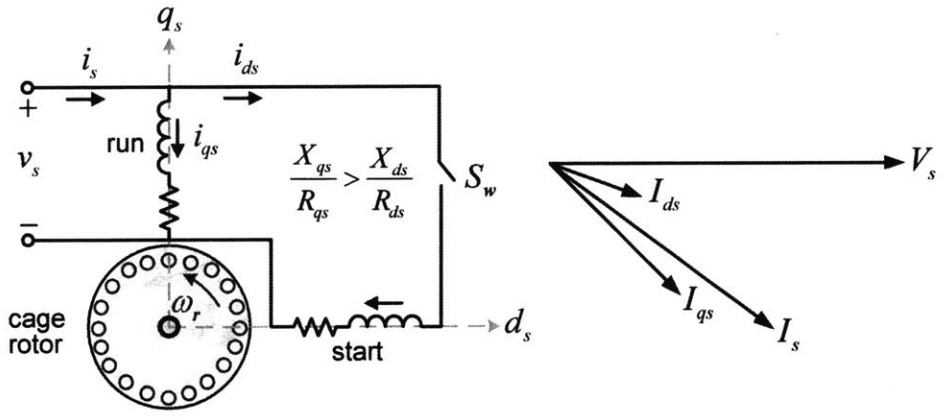

Figure 2-1: Split phase induction motor

2.1.2 Capacitor Motor

The capacitor start motor is a split phase motor, but the time-phase displacement between the two currents is provided by means of capacitor connected in series with the auxiliary winding (2-2). By the choosing the right value of capacitance, the auxiliary current can be designed to lead the main current at 90 electrical degrees, resulting in uniform rotating field. Similar to the split-phase motor, the auxiliary winding is disconnected after the motor the motor has started. In permanent-split-capacitor motor, the capacitor is not disconnected

from the auxiliary winding after starting. Capacitor-type motors have better starting and running torques as compared to split-phase motors, and thus can be used to start loads that require higher starting torque. Furthermore, in case of permanent-split-capacitor motor, the power factor, efficiency, and torque pulsations can be improved by designed for perfect two-phase operation at any one desired load condition. The capacitor can smooth out the pulsations in input power and torque improving the overall efficiency and power factor, but at the expense of a lower starting torque [3, 57, 62].

This type of motor is widely used for the ceiling fans in India due to its low cost. They are usually rated for $70W$ power and deliver not more than $20W$ mechanical power at rated speed making them inefficient. This suggests that even with improved designs of capacitor motors, better efficiency can be achieved at the expense of slight increase in cost. For example, some ceiling fan manufacturers in India, such as Usha [58], have in the market $50W$ capacitor motor ceiling fans.

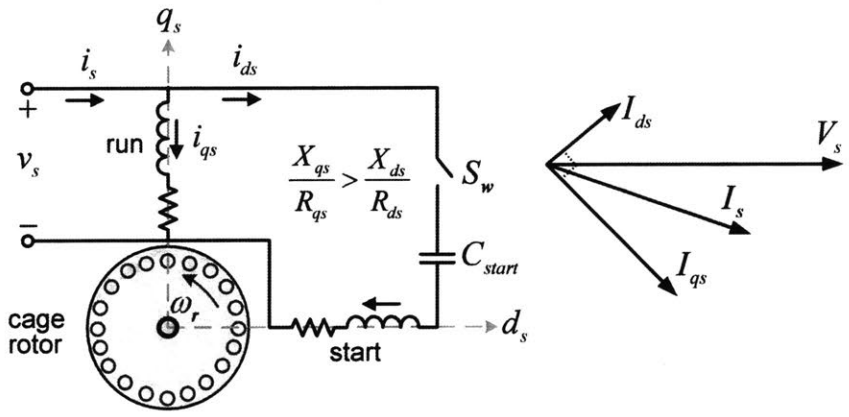

Figure 2-2: Capacitor start motor

2.1.3 Shaded Pole Motor

Shaded pole motors have only one main winding, and instead of auxiliary winding, they have salient poles with one portion of each pole surrounded by a short-circuited coil called a shading coil. Time-varying flux in the main winding induces voltage and current in the shading coil. This causes the flux in the shaded pole to lag the flux in the other portion resulting in a rotating magnetic field in the direction from the unshaded to the shaded

portion of the pole [13, 17, 18, 44, 45, 56, 57, 59, 62]. A low starting torque is produced from this process. This type of SPIM has the lowest efficiency ($\sim 40\%$), however, they are can be attractive in some appliances due their low cost. Conventional ceiling fans in the United States use this type of motor due to their relatively low cost and extreme simplicity.

2.2 Brushless DC Motors

Brushless dc motors are electronically commutated permanent magnet (PM) synchronous motors. They are driven with rectangular waveform supply as compared to PM synchronous motors which are usually driven by a sinusoidal supply. They are commonly of surface mounted magnets morphology with magnets mounted on the surface of the rotor and a conventional stator winding similar to that of poly-phase induction motor. Brushless dc motors work based on the interaction of the magnetized stator coils and the permanent magnet. The stator coils are energized in such a way that there are forces of attraction and repulsion between the stator and rotor poles to produce the highest torque possible. The main outstanding feature of brushless dc motors is their dc torque output, unlike SPIMs which have an inherently pulsating torque. As the name suggests, brushless dc motors have no brushes, thus are commutatorless unlike conventional PM dc commutator motors. Therefore, they clearly have no brush maintenance cost, and are considered relatively 'safer'to operate in inflammable environments due to the absence of the sparking associated normally associated with brushes [42]. Moreover, brushless dc motors have larger surface area available for the armature winding as opposed to commutator motors, and thus can withstand higher current densities enabling them to produce larger torque. With the aforementioned advantages, brushless dc motors tend to have higher efficiencies compared to commutator motors of the same size.

Compared to three phase induction motors, brushless dc motors have higher efficiency and power factor assuming the same size and cooling scheme. Both brushless dc motors and adjustable speed drives for three phase induction motors consist of the same power electronic components: a rectifier (if required) followed by a three leg inverter. However, the control scheme for brushless dc motor is simpler than pulse-width-modulation switch-

ing scheme typically employed in induction motor drives. Nevertheless, brushless dc motors comes with certain disadvantages. The weight and hence the cost of the PM increases with the size of the motor. Thus, brushless dc motors are usually used in applications with relatively low power due to the increased cost of the PM. For high power rating, induction motors become more attractive in terms of cost effectiveness, and their efficiencies improve. Furthermore, induction motors are capable of operating in the flux weakening region, enabling them to deliver constant power at higher speeds (above synchronous speed). This is more challenging to achieve in brushless dc motors, especially with larger machines at high speeds, where the PM are mounted on the rotor (mechanical constraint) [42].

The increased reduction in cost and power electronics have made brushless dc motors increasingly used in commercial, industrial, and medical technologies. Among their applications are computers (printers, hard disk drives), hand-held power tools, actuators for computer numerical control (CNC) machines, industrial robots, medical equipment and electric vehicles. Since 2012, there is a new trend in India to move towards brushless dc motors for super efficient ceiling fans. Recently brushless dc motor ceiling fans in India have reduced their power consumption to $< 30W$ at rated speed [54] at the sacrifice of four times the price of a conventional $70W$ ceiling fan.

Nowadays, brushless dc motors have been increasingly used in household and commercial fan applications. This has led to more research effort in the area of single-phase brushless dc motor design and drives (single phase refers to the power outlet supply). In particular, researchers are exploring methods and modeling tools to assist in designing brushless dc motors and their drives for appliances. For example, in [23], M. Fazil et al. propose a nonlinear dynamic model for brushless dc motors for ceiling fan application to reduce the simulation time compared to transient finite-element-model. Furthermore, in [46] a stator shape optimizing design is proposed to reduce the cogging torque of single phase brushless dc motor. As brushless dc motors is not the main focus of this thesis, we refer the authors to [4, 15, 21, 29, 36, 39, 40, 49, 51, 67, 69] for more literature on drive control strategies and design of single phase brushless dc motors for small power applications.

2.3 Three Phase Induction Motors

Three phase induction motors come mostly in large sizes, and in the aggregate, consume the largest amount of energy in the electric power grid. They are built for a wide range of applications ranging from fractional horse power up to few mega Watt power applications [1, 2] due to their simplicity, ruggedness, and economical importance. The induction motor can be thought of an electric transformer whose magnetic circuit is divided by the airgap into two parts: the stator and the rotor, moving relative to each other and one carrying the primary and the other the secondary windings [3]. Their stator is of conventional structure which consists of three windings inserted in slots spatially displaced 120 electrical degree apart from each other. The stator winding can be either distributed, such as in large machines or concentrated such as in fractional horse applications. When the stator is excited by a three phase supply, a flux traveling wave is produced and as it cuts the rotor conducting elements, a voltage and thus current is induced in the rotor circuit. The interaction of the induced currents with the traveling wave creates electromagnetic torque that causes the rotor to rotate [3, 31, 57].

Three phase induction motors are classified into two types based on their rotor circuit: wound rotor, and squirrel cage induction motors. Wound rotors have rotor windings similar to that of the stator, and their terminals are connected to slip rings mounted on the shaft. Mounted on the slip rings are carbon brushes bearing which provides access to the terminals of the rotor circuit. The advantage of wound rotors is that the rotor resistance can be adjusted, and thus the starting torque can be controlled. Wound rotors are less common than squirrel cage rotors, and they are generally used for specialized applications. Cage rotors, on the other hand, have rotor bars inserted in the slots instead of a conventional winding. The rotor bars are short circuited from both ends with end-rings. Rotor bars and end-rings are usually made of aluminum for low cost motors, and copper for high performance motors. The simple structure of cage induction motors and their economic value made them more prevalent over wound rotors.

Since the invention of induction motors by Nikola Tesla in 1886, extensive research has been done on the modeling of poly phase induction motors. From the vast research

published on the behaviour of poly phase induction machines and efforts that developed analytical models which aimed to describe their behaviour, we attempt here to give credit to the early research by citing some classical papers published in that area [7, 8, 10, 11, 22, 24, 33, 41, 48, 52, 53, 60, 61, 63].

With the advancement of semiconductor technology, power electronic devices, sensors, control circuitry, and microcontrollers, speed adjustable drives have become almost ubiquitous in induction motor applications. The power electronic drive usually consist of a rectifier (three phase or single phase depending on the size of the motor) followed by a six switching device inverter. With proper sensing of stator currents, voltages and in some cases rotor position, an open loop or closed loop feedback control scheme is employed by analog circuitry (using operation amplifiers) or digitally in micrcontrollers to generate the gate pulses for inverter switches to achieve torque or speed control. Selected references on control and drives of poly phase induction motors can be found in [9, 20, 26, 28, 34, 55, 68].

As power electronic devices continue to advance in size and cost, using three phase induction motor equipped with adjustable speed drives for home appliances is becoming more viable economically. In this thesis, we attempt to design a three phase induction motor for $< 30W$ household ceiling, which is driven by a power electronic circuit. In the next chapter, the analytical model of three squirrel cage induction motor is developed and discussed in detail.

Chapter 3

Analytical Model

The analytical model of three phase induction motors has been extensively studied since the invention of induction motors by Nikola Tesla. Although their basic operating principle is relatively simple, deriving a mathematical model that exactly predicts the behaviour of induction motors is quite difficult. Nonetheless, analytical models which attempt to describe the behaviour of induction machines through means of equivalent circuit have proved to be simple, tractable, and provide reasonable approximation to the real machine. In this chapter we provide the analytical model of three phase induction motors represented by a general equivalent circuit model.

This chapter is organized as follows. The general equivalent circuit model of three phase induction motors is described briefly in Section 3.1. Then, in Sections 3.2 – 3.4 the equivalent circuit parameters are derived and expressions to calculate each circuit parameter is provided. Finally in Section 3.5, steps to evaluate the performance of three phase induction motors based on the solving its equivalent circuit is outlined. Torque, input power, output power, efficiency and power factor are among the performance metrics used to evaluate a certain design.

3.1 Extended Equivalent Circuit Model

The notion of the equivalent circuit model of induction motors goes long back since its invention in the late 19^{th} century. It is inspired by the fact that the physics of induction

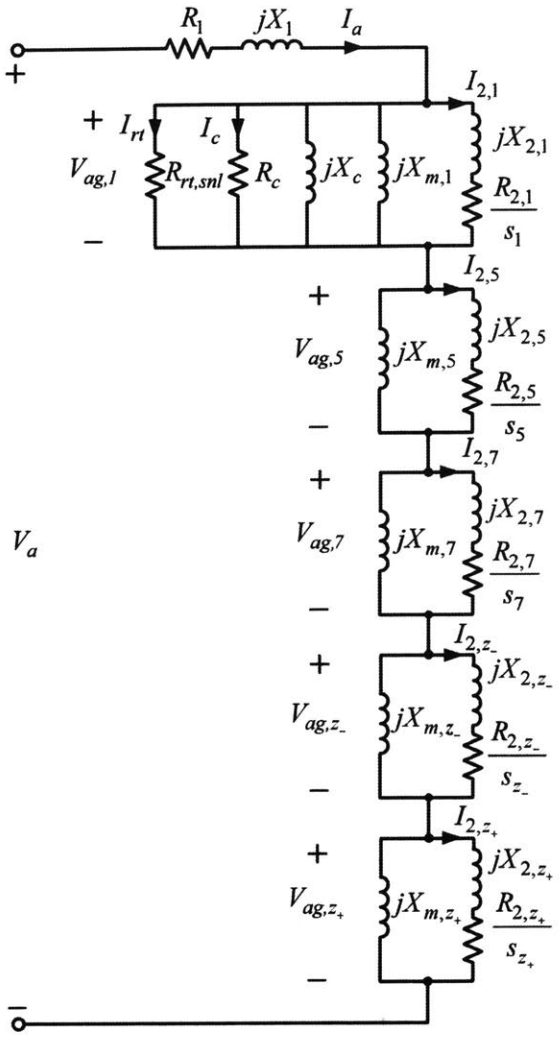

Figure 3-1: Extended equivalent circuit model of three phase induction motor

motors are similar to transformers as both works based electromagnetic induction. The purpose OF the equivalent circuit model is to provide a relatively simple analytical model of the electromechanical system that represents its terminal behavior, and provides a simple way to predict its performance including torque, converted power, efficiency, and power factor. There is a vast literature that deal with induction motors from first principle, however, the authors have relied heavily on J. Kirtley's course notes [31], P. Alger's [3], T. Lippo's [38], and S. Uman's [57] books to develop the analytical model. The extended single phase equivalent circuit model of three phase induction motors is shown in Fig. 3-1.

As described by Alger [3], one phase of the induction motor winding can be thought of

a series connected impedances.

In the depicted circuit model, R_1 denotes to the stator resistance, X_1 is the stator leakage reactance, X_m^n is the magnetizing reactance of the n^{th} space harmonic component of the airgap flux of the stator winding, R_c and X_c are the core loss impedance elements in the stator core behind the slots (back-iron) and stator teeth, $R_{rt,snl}$ models the no-load stray loss in the rotor teeth due to the modulation of the fundamental airgap flux by the stator teeth [31], R_{2n} and X_{2n} are the rotor resistance and leakage reactance referred to the stator due to the n^{th} space harmonic component of the stator airgap flux. The harmonic orders, $n = 2k \mp 1 = 5, 7$ refer to the negative (backward rotating) and positive (forward traveling) phase-belt harmonics for three phase machines {k is number of phase-belts or phases thus $k = 3$}, whereas, $n = z_{\mp} = \frac{N_s}{p} \mp 1$ subscripts refer to the zigzag negative and positive space harmonic orders, respectively, wherein N_s is the number of stator slots, and p is the number of pole pairs. The calculation of the circuit parameters are provided in the following subsections.

3.2 Stator Equivalent Circuit Parameters

3.2.1 Stator Resistance R_1

Assume the mean length of a turn can be approximated by simply following the path that a conductor takes to form a loop around one pole pitch,

$$l_c = \left[l + \frac{2\pi\left(\frac{D_{sg}}{2} - d_s - \frac{h_s}{2}\right)}{2p} \right] \times 2 \tag{3.1}$$

where, l is the axial length of the stator stack (usually known as the active length), D_{sg} the stator airgap diameter (stator outer diameter), d_s the stator depression depth (see Fig. 3-2), h_s the stator slot height, and p is the number of pole pairs. Note that the expression in (3.1) does not account for any extension lengths.

The length of stator winding per phase is equal to the mean length of a turn of the stator

coil (l_c) times the number turns in series per phase or simply what we refer as the number of turns per phase (N_a). Thus, the stator winding length per phase is,

$$\begin{aligned} l_1 &= N_a \cdot l_c \\ &= N_a \cdot \left[l + \frac{1}{2} \frac{2\pi\left(D_{sg} - d_s - \frac{h_s}{2}\right)}{p} \right] \times 2 \end{aligned} \tag{3.2}$$

The area of one wire/conductor is the slot area divided by the number of series connected turns per coil. Furthermore, the packing factor should be taken into account as well. The area of one conductor (A_w) can thus be expressed in terms of the stator slot area (A_{sslot}), packing factor (κ_{cu}), and number of turns per coil (N_c) as:

$$A_w = \kappa_{cu} \frac{A_{sslot}}{n_s} = \kappa_{cu} \frac{A_{sslot}}{2N_c} \tag{3.3}$$

where n_s is the number of turns of in series in a slot, and is equal number of coil sides multiplied by number of turns per coil side, and thus $n_s = 2N_c$. Also, note that a packing factor (κ_{cu}) of $\sim 0.3 - 0.5$ is typical for random-wound electric machines. In this design $\kappa_{cu} = 0.45$ is assumed.

From Ohm's law, and using (3.3) the stator resistance can be expressed as:

$$\begin{aligned} R_1 &= \frac{l_1}{\sigma_{cu} A_w} \\ &= \frac{N_a l_c}{\sigma_{cu} \kappa_{cu} \frac{A_{sslot}}{2N_c}} \\ &= 2N_c N_a \frac{l_c}{\sigma_{cu} \kappa_{cu} A_{sslot}} \end{aligned} \tag{3.4}$$

where σ_{cu} is the electrical conductivity of copper. Throughout this design, the conductivity of copper is considered at $25°C$: $\sigma_{cu} = 5.84 \times 10^7 S/m$.

The expression in (3.4) can be expressed in terms of number of stator slots and number of

turns per phase as:

$$\begin{aligned} R_1 &= 4N_c N_a \frac{l_c/2}{\sigma_{cu}\kappa_{cu}A_{sslot}} \\ &= 4\frac{N_a}{N_s/3}N_a \frac{l_c/2}{\sigma_{cu}\kappa_{cu}A_{sslot}} \\ &= 12\frac{N_a^2}{N_s}\frac{l_c/2}{\sigma_{cu}\kappa_{cu}A_{sslot}} \end{aligned} \tag{3.5}$$

where, l_c is as given by (3.2).

3.2.2 Magnetizing and Space Harmonics Reactances $X_{m,n}$

The fundamental space component of the stator inductance forms the magnetizing inductance of the equivalent circuit, whereas higher order space harmonic components of the stator airgap flux density contribute to stator leakage flux, as it does not contribute to real power or useful torque, rather to reactive power that is associated with losses. By superposition, these higher space harmonic inductances are stacked in series with the magnetizing branch forming higher order airgap inductances, as shown in Fig. 3-1.

For a three phase squirrel cage induction motor, excited by three voltage source, the peak of the radial air gap flux density can be expressed as:

$$B_{r,n} = \frac{3}{2}\frac{2}{n\pi}\frac{\mu_0(N_a k_{w,n})I_a}{pg_e} \qquad n = 1, 5, 7, 11, ... \tag{3.6}$$

where $\mu_0 = 4\pi \times 10^{-7} H/m$ is the permeability of air, N_a number of turns per phase, I_a terminal current in rms, p number of pole pairs, g_e effective airgap depth, and $k_{w,n}$ is the winding factor at the n^{th} space harmonic order.

The effective airgap depth g_e in (3.6) is the corrected airgap depth by carter's coefficient. Carter's suggests [38] that the slotted surface of the stator and rotor can be replaced with unslotted surface with the same cross section but with modified equivalent airgap depth:

$$g_e = \underbrace{\frac{\tau_\gamma}{\tau_\gamma - u + \frac{4g}{\pi}\ln(1+\frac{\tau_\gamma u}{4g})}}_{\kappa_c} g \tag{3.7}$$

where g is the physical airgap depth and κ_c is Carter's correction factor.

The airgap is corrected for both the stator and rotor slots:

$$g_e = \kappa_{c,s} \cdot \kappa_{c,r}\, g \tag{3.8}$$

$$g_e = \frac{\tau_{\gamma,s}}{\tau_{\gamma,s} - u_s + \frac{4g}{\pi}\ln(1+\frac{\tau_{\gamma,s} u_s}{4g})} \cdot \frac{\tau_{\gamma,r}}{\tau_{\gamma,r} - u_r + \frac{4g}{\pi}\ln(1+\frac{\tau_{\gamma,r} u_r}{4g})}\, g \tag{3.9}$$

The winding factor ($k_{w,n}$) seen in (3.6) is the product of the pitch ($k_{p,n}$) and breadth ($k_{b,n}$) {distribution} factors and can be expressed as:

$$k_{w,n} = k_{p,n} \times k_{b,n} \tag{3.10}$$

$$= \underbrace{sin(\frac{n\alpha}{2})\, sin(\frac{n\pi}{2})}_{k_{p,n}} \times \underbrace{\frac{sin(n\frac{m\gamma}{2})}{m \cdot sin(n\frac{\gamma}{2})}}_{k_{b,n}} \tag{3.11}$$

In (3.10), m is the number of stator slots per pole per phase, α is the winding pitch angle in electrical radians and γ is the stator slot angle in electrical radians, and can be expressed as:

$$m = \frac{N_s}{2p\,k} = \frac{N_s}{6p} \tag{3.12}$$

$$\alpha = \pi\, p_f = \pi \frac{N_{ct}}{\tau_p}$$

$$= \pi \frac{3m - N_{sp}}{3m} \tag{3.13}$$

$$\gamma = \frac{\pi}{3m} \tag{3.14}$$

where N_s is the number of stator slots, k number of phases ($k = 3$ for three phase electric

machines), p_f is the pitch factor or coil-throw N_{ct} to pole pitch τ_p ratio, N_{sp} the number of slots by which the coil is being short-pitched.

The airgap voltage (per phase) induced by the rotating field on the rotor bars (sometimes referred as the back emf) can be driven from electromotive force equation resulting from the rotating airgap flux lines cutting the rotor bars:

$$\begin{aligned} V_{ag.n} &= 2v\ B_{r,n}\ l\ (N_a k_{w,n}) \\ &= 2R_g \frac{\omega_{r,n}}{p} B_{r,n}\ l(N_a k_{w,n}) \\ &= 2R_g \frac{s\omega}{np} B_{r,n}\ l(N_a k_{w,n}) \end{aligned} \tag{3.15}$$

Note that the quantity $n \cdot p$ in the denominator of $\omega/(n \cdot p)$ is referred as the number of harmonic poles and reflects slower synchronous speed of machines with higher number of poles pairs, as well as $1/n$ of synchronous speed for the corresponding n^{th} higher order space harmonic flux wave component. R_g is the airgap radius, l is the active length, ω is the electrical synchronous frequency of the fundamental airgap flux wave in rad/s and is determined by the drive frequency (frequency of the drive voltage produced by the power electronic drive circuit), $\omega_{r,n} = \omega_r/n = s\omega/n$ is the rotor electric frequency (also commonly known as the slip frequency) corresponding to the n^{th} space harmonic airgap flux density, s is the slip ratio between the synchronous (stator) and rotor physical speeds with respect to the synchronous speed:

$$s = \frac{\omega - p \cdot \omega_m}{\omega} \tag{3.16}$$

where ω_m is the physical (mechanical) speed of the motor in mechanical rad/s and $p \cdot \omega_m$ is its electrical equivalent.

Substituting (3.6) in (3.15):

$$
\begin{aligned}
V_{ag,n} &= 2R_g \frac{s\omega}{np} \frac{3}{2} \frac{2}{n\pi} \frac{\mu_0 (N_a k_{w,n}) I_a}{p g_e} \, l(N_a k_{w,n}) \\
&= s\omega \frac{3}{2} \frac{4}{\pi} \frac{\mu_0 (N_a k_{w,n})^2 R_g l}{(np)^2 g_e} I_a \\
&= s \, X_{m,n} I_a = s \hat{V}_{ag,n}
\end{aligned} \tag{3.17}
$$

where $\hat{V}_{ag,n}$ is the maximum (in rms) induced voltage at standstill (unity-slip/locked-rotor condition).

By inspection of equation (3.17), the magnetizing inductance $L_{m,n}$ and reactance $X_{m,n}$ corresponding to the n^{th} space harmonic of the airgap flux are:

$$
L_{m,n} = \frac{3}{2} \frac{4}{\pi} \frac{\mu_0 (N_a k_{w,n})^2 R_g l}{(np)^2 g_e} \tag{3.18}
$$

$$
\begin{aligned}
X_{m,n} &= \omega L_{m,n} \\
&= (2\pi f) \frac{3}{2} \frac{4}{\pi} \frac{\mu_0 (N_a k_{w,n})^2 R_g l}{(np)^2 g_e} \qquad\qquad n = 1, 5, 7, z_-, z_+
\end{aligned} \tag{3.19}
$$

As mentioned before, $z_{\mp}$ are the forward and backward zigzag harmonic orders respectively from the top $(+)$ to the bottom $(-)$ subscript, and they can be expressed as in terms of the number of slots per pole per phase (m) as:

$$
\begin{aligned}
z_{\mp} &= \frac{N_s}{p} \mp 1 = 6 \, \frac{N_s}{6p} \mp 1 \\
&= 6 \, m \mp 1
\end{aligned} \tag{3.20}
$$

It is also clear from (3.20) that for concentrated windings ($k_{b,n} = 1$) for which $m = 1$, the zigzag harmonics are the same as the phase-belt harmonics, i.e. $z_{\mp} = 5, 7$, unlike distributed winding ($k_{b,n} < 1$) where $m > 1$ resulting slot (zigzag) harmonics of distinct order numbers (e.g $z_{\mp} = 29, 31$ for 60 stator slots, 4 pole three-phase machine $\{m = 5\}$).

For convenience in developing the analytical model later in MATLAB, It is practical to

express the airgap radius in terms of rotor or stator physical diameters (design parameters):

$$R_g = \frac{1}{2}(D_{rg} \mp g_e) \tag{3.21}$$

$$= \frac{1}{2}(D_{sg} \pm g_e) \tag{3.22}$$

where D_{rg} is the rotor airgap diameter and D_{sg} is the stator airgap diameter. The '$-$' sign in (3.21) refers to outer-rotor inner-stator (hub) structure, whereas, the '$+$' sign refers to the commonly used outer-stator inner rotor structure.

3.2.3 Stator Leakage Reactance X_1

Any flux that is produced by the stator winding and does not cross the airgap (produce no useful torque) is considered part of the stator leakage flux. The stator leakage flux, thus, consists of: (1) slot leakage flux that links that coils in the stator slot but not the rotor, (2) coil-end leakage, (3) space harmonics leakage, and (4) skew leakage.

Leakage due to higher order harmonics of the airgap flux is taken into account in the equivalent circuit as the magnetizing components of the smaller transformers stacked in series with the main transformer representing the fundamental airgap flux sine wave. And the leakage flux due to skewing of the rotor bars can be incorporated as part of the stator leakage or rotor leakage. In this work, it is incorporated in the rotor circuit referred to the stator. The per-phase stator leakage reactance (X_1), therefore, has two main components: stator slot leakage reactance ($X_{1s,l}$) and coil-end leakage (X_{1e}), and can be expressed as:

$$\begin{aligned} X_1 &= X_{1s,l} + X_{1e} \\ &= \omega L_{1s,l} + \omega L_{1e} \end{aligned} \tag{3.23}$$

Analytical expressions for $L_{1s,l}$ and L_{1e} will be derived in the following subsections (Subsection 1 and 2, respectively).

1 Stator Slot Leakage Inductance $L_{1s,l}$

The currents in the stator slots will produce flux that links the stator conductors but not the rotor bars. This is represented by the slot leakage flux, which corresponds to slot leakage inductance. This inductance depends on the geometry of the slot. A simple rectangular slot shape is considered as shown in 3-2. As shown in the figure, w is the width of the slot, h the height of the slot, and u and d are the depression (slot opening) width and depth, respectively. This might not be the most practical slot shape, but can provide a reasonable approximation to a more realistic slot shape such as the tapered trapezoidal slot which is widely used in induction machine stators. It will be shown later, that this slot shape can provide a reasonable approximation to trapezoidal slots, especially for small induction motors. Furthermore, a tapered, trapezoidal stator slot shape will be considered later for a more accurate analytical expression for the stator slot leakage inductance.

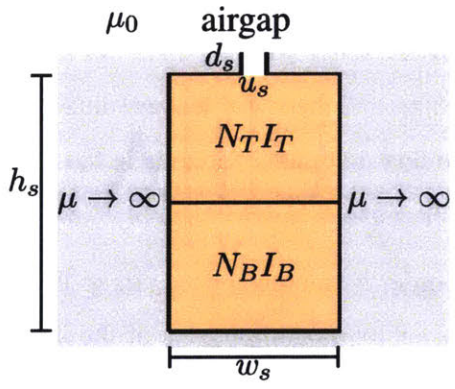

Figure 3-2: Rectangular semi-closed stator slot of a double layer winding

A double layer winding in the stator slots will be assumed throughout the derivation of the stator slot leakage inductance. First, the slot permeance will be derived, then an expression for the inductance per phase is provided for a full pitch winding, and finally a general expression will be derived for the case of short-pitched winding.

In Fig. 3-2, the coil in the bottom side has N_B turns per coil side; whereas, the top coil has N_T turns. At start of the derivation, when we derive the slot permeance expression, we will assume currents in the bottom and top sides, I_B and I_T, respectively, are from the same phase ($I_B = I_T$). Then we will see the effect of short pitching on the slot permeance

and the corresponding slot inductance per phase taking into account any mutual inductance in slots where I_T and I_B are from different phases.

The magnetic field in the conductor winding portion of the slot and in the slot depression area can be found by applying Ampere's law around a loop as shown by contours c_1, c_2 and c_3 in Fig. 3-3.

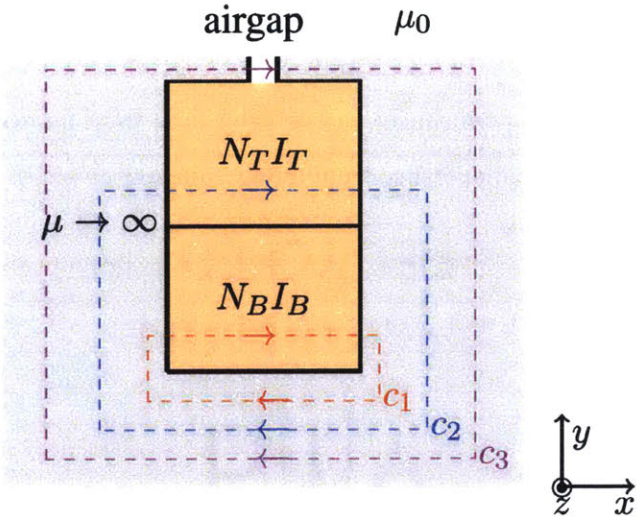

Figure 3-3: Ampere's loops to derive magnetic field in different regions of the slot

Apply Ampere's current law in the integral form around loop c_1:

$$\begin{aligned} \oint_{c_1} \vec{H}.\vec{dl} &= I_{enc} \\ H_x w &= N_B I_B \frac{y}{h/2} \\ H_x &= \frac{2N_B I_B}{wh} y \qquad\qquad 0 \le y \le h/2 \end{aligned} \tag{3.24}$$

Similarly for the top coil (contour c_2):

$$\begin{aligned} H_x &= \frac{N_B I_B + N_T I_T \frac{y-h/2}{h/2}}{w} \\ &= \frac{N_B I_B}{w} + \frac{N_T I_T}{w} \frac{2y-h}{h} \\ &= \frac{N_B I_B - N_T I_T}{w} + \frac{2N_T I_T}{wh} y \qquad\qquad h/2 \le y \le h \end{aligned} \tag{3.25}$$

Finally, from Ampere's loop c_3, the magnetic field in the depression region can be expressed as:

$$H_x = \frac{N_B I_B + N_T I_T}{u} \qquad 0 \le y' \le d \tag{3.26}$$

The slot inductance (and permeance) can be calculated from the so called energy approach (one can calculate the inductance from the flux linkage as well). The energy stored in the slot can be expressed as:

$$\begin{aligned}
W_{sslot} &= \iiint \frac{1}{2}\mu_0 H_x^2 \, dx \, dy \, dz \\
&= \frac{1}{2}\mu_0 l \Bigg[\Big(\frac{2N_B I_B}{wh}\Big)^2 w \int_0^{h/2} y^2 dy \\
&+ w \int_{h/2}^{h} \Big(\frac{N_B I_B - N_T I_T}{w} + \frac{2N_T I_T}{wh} y\Big)^2 dy \\
&+ ud\Big(\frac{N_B I_B + N_T I_T}{u}\Big)^2 \Bigg] \\
W_{sslot} &= \frac{1}{2}\mu_0 l \Bigg[\Big(\frac{2N_B I_B}{wh})^2\Big) w\frac{h^3}{24} + w\frac{h}{2}\frac{(N_B I_B)^2 - 2N_B I_B N_T I_T + (N_T I_T)^2}{w^2} \\
&+ 2w\frac{N_B I_B - N_T I_T}{w}\frac{3h^2}{8} + w\Big(\frac{2N_T I_T}{wh})^2\Big) w\frac{7h^3}{24} \\
&+ ud\frac{(N_B I_B)^2 + 2N_B I_B N_T I_T + (N_T I_T)^2}{u^2} \Bigg] \\
W_{sslot} &= \frac{1}{2}\mu_0 l \Bigg[(N_B I_B)^2\Big(\frac{1}{6}\frac{h}{w} + \frac{1}{2}\frac{h}{w} + \frac{d}{u}\Big) + (N_T I_T)^2\Big(\frac{1}{2}\frac{h}{w} + \frac{3}{2}\frac{h}{w} + \frac{7}{6}\frac{h}{w} + \frac{d}{u}\Big) \\
&+ (N_T I_T N_B I_B)\Big(- \frac{h}{w} + \frac{3}{2}\frac{h}{w} + 2\frac{d}{u}\Big)
\end{aligned} \tag{3.27}$$

Thus, the energy stored in the stator slot can be written as:

$$W_{sslot} = \frac{1}{2}\mu_0 l\Bigg[(N_B I_B)^2\Big(\frac{2}{3}\frac{h}{w} + \frac{d}{u}\Big) + (N_T I_T)^2\Big(\frac{1}{6}\frac{h}{w} + \frac{d}{u}\Big) + (N_T I_T N_B I_B)\Big(\frac{1}{2}\frac{h}{w} + 2\frac{d}{u}\Big)\Bigg] \tag{3.28}$$

Taking into account the two currents i_B and i_T in the slot, the corresponding flux linkages can be expressed as:

$$\lambda_B = L_B i_B + L_{BT} i_T \tag{3.29}$$

$$\lambda_T = L_{BT} i_B + L_T i_T \tag{3.30}$$

Using the co-energy definition, the energy stored in the stator slot can be expressed in terms of the bottom and top coil currents can be expressed:

$$\begin{aligned} W_{sslot} &= \int_{path} \lambda di \\ &= \int_{i_B, i_T = 0} \lambda_B di_B + \int_{i_T, i_B = I_B} \lambda_T di_T \\ &= \frac{1}{2} L_B \, I_B^2 + \frac{1}{2} L_T I_T^2 + L_{BT} I_B I_T \end{aligned} \tag{3.31}$$

By comparing equations (3.27) and (3.31), the bottom (L_B), top (L_T), and the mutual inductance between the bottom and top coils (L_{BT}) can be expressed as:

$$L_B = N_B^2 \, \mathcal{P}_B = N_B^2 \, \mu_0 l\Big(\frac{2}{3}\frac{h}{w} + \frac{d}{u}\Big) \tag{3.32a}$$

$$L_T = N_T^2 \, \mathcal{P}_T = N_T^2 \, \mu_0 l\Big(\frac{1}{6}\frac{h}{w} + \frac{d}{u}\Big) \tag{3.32b}$$

$$L_{BT} = N_{BT}^2 \, \mathcal{P}_{BT} = N_B N_T \, \mu_0 l\Big(\frac{1}{4}\frac{h}{w} + \frac{d}{u}\Big) \tag{3.32c}$$

where $\mathcal{P}_B$, $\mathcal{P}_T$, and $\mathcal{P}_{BT}$ are the corresponding permeances to the top, bottom, mutual

permeance between the bottom and top coils, respectively.

Full-Pitch Winding

For a full pitched winding, the currents in top and bottom coils are from the phase: $I_B = I_T = I$. Thus, we can rewrite equation (3.31) as:

$$W_{sslot} = \frac{1}{2}\left(L_B + L_T + 2L_{BT}\right) I^2 \tag{3.33}$$

where $L_{sslot} = L_B + L_T + 2L_{BT}$ is the stator slot inductance.

Assume the number of turns in the bottom and top coil sides are equal: $N_B = N_T = N_c$. Substituting in equations (3.32) & (3.34), the co-energy in the slot can be rewritten as:

$$W_{sslot} = \frac{1}{2}N_c^2\left(\mathcal{P}_B + \mathcal{P}_T + 2\mathcal{P}_{BT}\right) I^2 \tag{3.34}$$

Thus, the slot permeance for a double layer, full pitched winding can be expresses as:

$$\mathcal{P}_{sslot} = \mathcal{P}_B + \mathcal{P}_T + 2\mathcal{P}_{BT} \tag{3.35}$$

We can express the stator slot inductance in terms of its permeance as:

$$L_{sslot} = N_c^2\mathcal{P}_{sslot} \tag{3.36}$$

Assuming a full-pitch distributed winding and thus same phases in each slot, the top coil side is connected in series with the bottom coil side. Thus, the number of turns of series connected coils in a slot of the same phase, denoted as n_s, is twice the number of turns per coil side:

$$n_s = 2N_c \tag{3.37}$$

The slot inductance in equation (3.36) can be rewritten as:

$$
\begin{aligned}
L_{sslot} &= \left(\frac{n_s}{2}\right)^2 \mathcal{P}_{sslot} \\
&= n_s^2 \frac{\mathcal{P}_{sslot}}{4} \\
&= 4N_c^2 \mathcal{P}'_{sslot}
\end{aligned} \tag{3.38}
$$

where $\mathcal{P}'_{sslot}$ is the equivalent permeance and can be expressed as,

$$
\begin{aligned}
\mathcal{P}'_{sslot} &= \frac{\mathcal{P}_{sslot}}{4} \\
&= \frac{\mathcal{P}_B}{4} + \frac{\mathcal{P}_T}{4} + \frac{2\mathcal{P}_{BT}}{4} \\
&= \mathcal{P}'_B + \mathcal{P}'_T + 2\mathcal{P}'_{BT}
\end{aligned} \tag{3.39}
$$

Substituting $\mathcal{P}_B$, $\mathcal{P}_T$ and $\mathcal{P}_{BT}$ in equation (3.39) yields,

$$
\begin{aligned}
\mathcal{P}'_{sslot} &= \frac{1}{4}\left(\left(\frac{2}{3} + \frac{1}{6} + 2\frac{1}{4}\right)\frac{h}{w} + (1+1+2)\frac{d}{u}\right)\mu_0 l \\
&= \mu_0 l\left(\frac{1}{3}\frac{h}{w} + \frac{d}{u}\right)
\end{aligned} \tag{3.40}
$$

Note that this permeance (slot permeance due to a double layer, full-pitch winding configuration as per equation (3.40)) is equivalent to that of a single layer configuration with one coil in the slot having $2N_c$ turns per coil. To verify this, the permeance in the single layer case is derived by inspecting the coenergy in the slot:

$$
\begin{aligned}
W_{sslot} &= \frac{1}{2}\mu_0 l\left(\left(\frac{2N_c I}{wh}\right)^2 w\int_0^h y^2 dy + d\,u\left(\frac{2N_c I}{u}\right)^2\right) \\
&= \underbrace{\frac{1}{2}4N_c^2\underbrace{\mu_0 l\left(\frac{1}{3}\frac{h}{w}+\frac{d}{u}\right)}_{\mathcal{P}'_{sslot}}}_{L_{sslot}} I^2
\end{aligned} \tag{3.41}
$$

As seen from equation (3.41), the slot permeance of a double layer, full-pitch winding with N_c turns per coil side is equivalent to that of a single layer winding with $2N_c$ turns per coil. This is expected since if we divide the single layer winding in half to create the double layer winding.

The per phase slot self inductance ($L_{1s,s}$) can be expressed as:

$$
L_{1s,s} = \underbrace{L_{sslot}\times m}_{L_{sslot,phase-belt}} \times \underbrace{2p}_{\text{number of series connected coils}} \tag{3.42}
$$

where m is the number of stator slots per pole per phase and p the number of pole pairs.

In $L_{1s,s}$ the subscript '1' denotes to the per phase stator quantities in the equivalent circuit, the first 's' refers to '*slot*', and the second 's' is a short term for '*self*'.

Or,

$$
\begin{aligned}
L_{1s,s} &= 4N_c^2 P'_{sslot}\times 2mp \\
&= 4\left(\frac{N_a}{2mp}\right)^2 P'_{sslot}\times 2mp \\
&= 4\frac{N_a^2}{2mp}P'_{sslot} \\
&= 12\frac{N_a^2}{N_s}P'_{sslot} \\
&= 12\frac{N_a^2}{N_s}\left(\frac{\mathcal{P}_B}{4}+\frac{\mathcal{P}_T}{4}+\frac{\mathcal{P}_{BT}}{2}\right)
\end{aligned} \tag{3.43}
$$

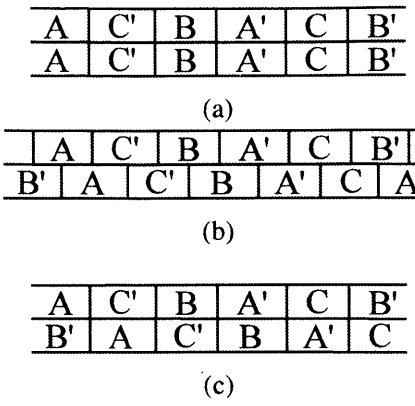

Figure 3-4: Snippets showing the phase sequence of a double-layer winding as it is being short-pitched from $p_f = 1$ to $p_f = 2/3$: (a) full-pitch $p_f = 1$, (b) short-pitched $2/3 < p_f < 1$, (c) short-pitched $p_f = 2/3$

And the stator slot reactance is:

$$\begin{aligned} X_{1s,s} &= 2\pi f L_{1s,s} \\ &= 2\pi f \times 12 \frac{N_a^2}{N_s} \left(\frac{\mathcal{P}_B}{4} + \frac{\mathcal{P}_T}{4} + \frac{\mathcal{P}_{BT}}{2} \right) \end{aligned} \tag{3.44}$$

Short-Pitch Winding

It is possible to short-pitch the two-layer coils, reducing their end lengths, and thus reducing the reactive flux space harmonic components with only a small reduction in the useful fundamental flux, and thus resulting in a more favorable *mmf* pattern [3].

The approach to derive the slot permeance for a fractional-pitch (short-pitch) winding is based on Lippo's [38] and Alger's [3]. Consider an ordinary, 2-layer distributed winding with 60° phase-belt ($p\theta_{PB} = p \times 360/(2p*3) = 60°elect.$), and m slots per phase-belt (per pole per phase). The phase sequence of the two-layer winding short-pitched from unity to two-third pitch factor is shown in Fig. 3-4 (a)-(c). In each phase-belt there is m slots per pole per phase. Therefore, one can also think of short pitching in terms of number of slots as well as pitch factor. Notice in Fig. 3-4b the bottom layer is being shifted to the right reducing the coil throw (pitch factor $2/3 < p_f < 1$) and in Fig. 3-4c the winding is short-pitched by one phase-belt which is equivalent to a pitch factor of $p_f = \frac{180^{oe}-60^{o}}{180} = 2/3$.

By examining Figs. 3-4a, it is clear that that the self permeance term due to mutual flux between the top and bottom coils of the same phase is as calculated before and equals to $\mathcal{P}'_{BT}$. However, it start decreasing as the slot is partially shared by a different phase-belt (Fig. 3-4b), and goes to zero when the winding is short-pitched by one phase-belt ($p_f = 2/3$) (Fig. 3-4c). On the other hand, the permeance due to mutual coupling between the top and bottom coils from different phases reaches to a negative maximum (negative due to opposite sense of current directions) when the winding at $p_f = 2/3$ and is zero at full pitch ($p_f = 1$). We can repeat this exercise by short-pitching the winding further until the pitch factor becomes zero (short pitched by three phase-belts or $180°elect.$).

We can rewrite the slot permeance in equation 3.39 to incorporate the effect of short-pitching as:

$$\mathcal{P}'_{sslot} = \frac{\mathcal{P}_{sslot}}{4} = \frac{\mathcal{P}_B}{4} + \frac{\mathcal{P}_T}{4} + \frac{\mathcal{P}_{BT}}{2} \times k_s \tag{3.45}$$

where, k_s refers to the self coil-pitch factor and can be expressed as a function of pitch-factor when the winding is short pitched by one, two, and three phase-belts, respectively:

$$k_s = \begin{cases} 3p_f - 2 & 2/3 \leq p_f \leq 1 \\ 0 & 1/3 \leq p_f \leq 2/3 \\ 3p_f - 1 & 0 \leq p_f \leq 1/3 \end{cases} \tag{3.46}$$

Thus, the slot self inductance per phase becomes:

$$\begin{aligned} L_{1s,s} &= \left(L'_B + L'_T + 2k_s L'_{BT}\right) \\ &= 12\frac{N_a^2}{N_s}\left(\mathcal{P}'_B + \mathcal{P}'_T + 2k_s\mathcal{P}'_{BT}\right) \\ &= 12\frac{N_a^2}{N_s}\left(\frac{\mathcal{P}_B}{4} + \frac{\mathcal{P}_T}{4} + k_s \times \frac{\mathcal{P}_{BT}}{2}\right) \end{aligned} \tag{3.47}$$

The inductance due to mutual coupling between the top and bottom coils from different phases, or simply the mutual inductance, can be expressed as:

$$
\begin{aligned}
L_{1s,m} &= k_m L_{BT}^{'} \\
&= k_m \times 12 \frac{N_a^2}{N_s} \left(\frac{\mathcal{P}_{BT}}{4} \right)
\end{aligned} \tag{3.48}
$$

where k_m is the mutual coil-pitch factor and can be expressed as a function of the pitch-factor as:

$$
k_m = \begin{cases} 3p_f - 3 & 2/3 \leq p_f \leq 1 \\ 3(1 - 2p_f) & 1/3 \leq p_f \leq 2/3 \\ 3p_f & 0 \leq p_f \leq 1/3 \end{cases} \tag{3.49}
$$

Assuming a symmetrical stator winding, the slot leakage flux linkages can be written as:

$$
\begin{bmatrix} \lambda_{1s,s}^a \\ \lambda_{1s,s}^b \\ \lambda_{1s,s}^c \end{bmatrix} = \begin{bmatrix} L_{1s,s} & L_{1s,m} & L_{1s,m} \\ L_{1s,m} & L_{1s,s} & L_{1s,m} \\ L_{1s,m} & L_{1s,m} & L_{1s,s} \end{bmatrix} \begin{bmatrix} i_a \\ i_b \\ i_c \end{bmatrix} \tag{3.50}
$$

Assume the winding is connected in Star and with the neutral being left disconnected (three-phase three-wire induction motor):

$$
i_a + i_b + i_c = 0 \tag{3.51}
$$

Therefore, the stator slot leakage flux linkages in equation (3.50) can be expressed as:

$$
\begin{aligned}
\lambda_{1s,s}^a &= \left(L_{1s,s} - L_{1s,m} \right) i_a = L_{1s,l} i_a \\
\lambda_{1s,s}^b &= \left(L_{1s,s} - L_{1s,m} \right) i_b = L_{1s,l} i_b \\
\lambda_{1s,s}^c &= \left(L_{1s,s} - L_{1s,m} \right) i_c = L_{1s,l} i_c
\end{aligned} \tag{3.52}
$$

where $L_{1s,l}$ is the per phase stator slot leakage inductance. By substituting $L_{1s,s}$ (3.47) and

$L_{1s,m}$ (3.48) in the slot leakage $L_{1s,l}$, it can be expressed in terms of self and mutual coil pitch factors as:

$$\begin{aligned} L_{1s,l} &= L_{1s,s} - L_{1s,m} \\ &= 12\frac{N_a^2}{N_s}\left(\mathcal{P}_B^{'} + \mathcal{P}_T^{'} + (2k_s - k_m)\mathcal{P}_{BT}^{'}\right) \\ &= \left(L_B^{'} + L_T^{'} + k_l L_{BT}^{'}\right) \end{aligned} \tag{3.53}$$

where, $k_l = 2k_s - k_m$ is the leakage coil-pitch factor and thus can be calculated as:

$$k_l = \begin{cases} 3p_f - 1 & 2/3 \leq p_f \leq 1 \\ 3(2p_f - 1) & 1/3 \leq p_f \leq 2/3 \\ 3p_f - 2 & 0 \leq p_f \leq 1/3 \end{cases} \tag{3.54}$$

It is useful also to write k_l in terms of the number of slots by which the coil is being short-pitched (N_{sp}) in case of a double layer distributed winding. From (3.13) that the pitch factor can be expressed in terms of N_{sp} as:

$$p_f = 1 - \frac{N_{sp}}{3m} \tag{3.55}$$

Substitute p_f, given in (3.55), in (3.54), k_s, k_m, and k_l can be expressed in terms of N_{sp} & m as:

$$k_l = \begin{cases} 2 - \frac{N_{sp}}{m} & 0 \leq N_{sp} \leq m \\ 3 - \frac{2N_{sp}}{m} & m \leq N_{sp} \leq 2m \\ 1 - \frac{N_{sp}}{m} & 2m \leq N_{sp} \leq 3m \end{cases} \tag{3.56}$$

The self, mutual and leakage coil-pitch factors (k_s, k_m, k_l, respectively) for a double layer winding short pitched by a maximum of 3 phase-belts (considering 60_{circ} phase-belt machine) is summarized in Table. 3.1.

Table 3.1: Self, mutual, and leakage coil-pitch factors

p_f or N_{sp}	k_s	k_m	$k_l = 2k_s - k_m$
$2/3 \leq p_f \leq 1/3$	$3p_f - 2$	$3p_f - 3$	$3p_f - 1$
$0 \leq N_{sp} \leq m$	$1 - \frac{N_{sp}}{m}$	$\frac{-N_{sp}}{m}$	$2 - \frac{N_{sp}}{m}$
$1/3 \leq p_f \leq 2/3$	0	$3(1 - 2p_f)$	$3(2p_f - 1)$
$m \leq N_{sp} \leq 2m$	0	$-3 + 2\frac{N_{sp}}{m}$	$3 - \frac{2N_{sp}}{m}$
$0 \leq p_f \leq 1/3$	$3p_f - 1$	$3p_f$	$3p_f - 2$
$2m \leq N_{sp} \leq 3m$	$2 - \frac{N_{sp}}{m}$	$3 - \frac{N_{sp}}{m}$	$1 - \frac{N_{sp}}{m}$

2 End Winding Leakage Inductance L_{1e}

End-winding leakage inductance is one of the most complex inductances to estimate. We found that Alger's [3] expression end-winding leakage reactance is a good start for small induction motors where the end-winding inductance is generally small. According to [3], the end-winding reactance can be roughly approximated as:

$$\begin{aligned} X_{1e} &= \omega L_{1e} \\ &\approx 2\pi f \left[\frac{21}{2\pi p^2} N_a^2 D_{sg} \left(\frac{N_{ct}}{\tau_p} - 0.3 \right) 10^{-6} \right] \end{aligned} \tag{3.57}$$

3.3 Rotor Equivalent Circuit Parameters

The rotor impedances referred to the stator side of the per-phase equivalent circuit is described in this section. The rotor impedance of the n^{th} transformer (Fig. 3-1) consist of a rotor resistance (R_{2n}) and leakage reactance (X_{2n}) components. Before we provide the analytical expressions for the rotor impedances, we will first define the skew factor as it affects the calculation of rotor parameters referred to the stator.

3.3.1 Skew Effect

Skewing the rotor or stator slots (commonly rotor bars in squirrel cage motors) reduces the coupling between rotor and stator, which in-turn corresponds to reduction in the amplitude of the air-gap flux density space harmonics with slight decrease in the fundamental sine wave component. This as a result help to reduce the stray-load loss due to belt and zigzag harmonics. In general, stray-load loss due to belt harmonics can reduced by short-pitching the stator winding by an appropriate pitch factor; however, this is not possible for the zigzag harmonics, and the only way to reduce stray-load loss due to zigzag harmonics is by skewing the rotor or stator [31]. Furthermore, skewing can help to suppress the parasitic torque components, including those due to the positive sequence harmonic components of the flux wave, which has the potential to introduce dips in starting regime of the torque-speed curve, and in extreme cases can lead to asynchronous crawling (failure to start) in addition to losses. Thus, skewing does not only result in a smooth torque-speed curve, but also a cleaner voltage waveform that is closer to a pure sinusoid, and potentially less noise [3], [38].

Since skewing reduces coupling between stator and rotor as mentioned previously, it is equivalent to increasing the total leakage inductance of the motor, nonetheless. This results in reducing the useful torque (due to reduction in the magnitude of the fundamental-frequency component of the flux density) and thus shifting the torque speed curve down a little. To maintain the same starting and breakdown torque, the stator voltage (hence stator current) can be increased, which might increase the magnetic saturation of the motor [12]. Thus, the designer has to take into account such an effect, and based on the design objective one might choose to skew the rotor or not.

Consider the transformer at the n^{th} order harmonic in the general equivalent circuit (3-1). As mentioned before this circuit represents the per phase equivalent circuit with the rotor parameters referred to the stator side. The skew effect can be incorporated in the equivalent circuit by adding an ideal transformer between the stator and the rotor circuits (Fig. 3-5a) with a turns ratio $1 : k_{sk}$, where k_{sk} is the skew factor.

The skew factor k_{sk} in Fig. 3-5 can be expressed as:

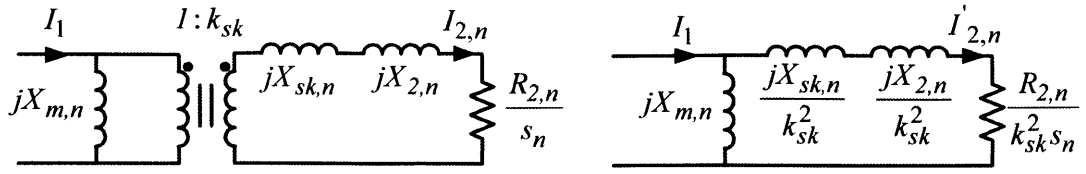

(a) Skew factor seen as a transformer's turns ratio

(b) Rotor circuit referred to stator by $1/k_{sk}^2$

Figure 3-5: The n^{th} order transformer element of the per phase equivalent circuit including the skew effect

$$k_{sk,n} = \frac{sin(n\frac{\theta_{sk}}{2})}{n\frac{\theta_{sk}}{2}} \tag{3.58}$$

It is mathematically easier to analyze the per-phase equivalent circuit with the rotor circuit referred to the stator side, as shown in Fig. 3-5b. By the circuit referral operation, the rotor circuit parameters are multiplied $1/k_{sk}^2$. Thus, in later subsections we will see this factor in the final expressions for the rotor leakage reactance elements. Also, it can be seen from Figs. 3-5a & 3-5b that there is an extra rotor leakage element due to the skew effect ($X_{sk,n}$); this element can be absorbed in the total leakage reactance X_2.

3.3.2 Rotor Resistances $R_{2,n}$

In squirrel cage induction motors, the rotor consists of shorted bars through end-rings from both ends, rather than discrete coils. Thus, unlike wound rotors whose resistance can be calculated analytically from Ohms law similar to that of the stator windings shown in Subsection 3.2.1, cage rotor resistance is different and depends on both the rotor bars and end-rings.

The rotor resistance consists of the slot (bar) resistance, and end-ring resistance. First we will provide an expression for the rotor bar resistance R_b, then for the end-ring resistance R_{er}, then add them to form the equivalent bar resistance, coined as the rotor resistance R_r. Finally we will multiply it with the appropriate factor (which also accounts for space harmonics of the airgap field) to get per-phase rotor resistance R_{2n} referred to the stator side.

1 Rotor Bar Resistance (R_b)

In this work, a low speed, small three phase induction motor is designed. The skin depth in such motors is much larger than the rotor slot depth, i.e, the skin depth can be in the order of $5-6$ times the rotor slot depth at unity slip, and > 15 times the rotor slot depth at rated speed ($\sim 8-12\%$ slip). Therefore, in this work, skin effect or what is known as deep rotor bar effect is ignored in the rotor slot impedance calculation. Furthermore, since we are designing a motor for appliances with rated power $< 30W$, the required starting torque is not particularly high. This means the high resistance due to deep bar effect at locked rotor condition is not needed, and thus we do not require an advanced rotor slot shape or so deep of a rotor slot to achieve to high starting torque. For this reason, the typical semi-closed, rectangular slot shape (Fig. 3-6) is considered for this motor design. As shown in the figure, w_r is rotor slot width, h_r is the slot depth, and finally u_r and d_r are the associated depression width and depth, respectively.

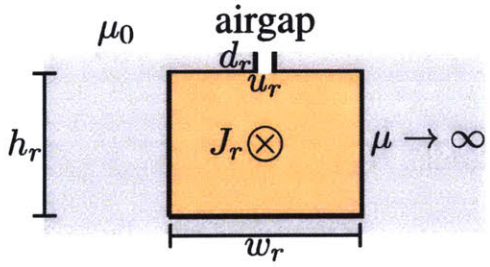

Figure 3-6: Rectangular rotor slot

It is worthy to note that the cage rotor will be made of cast aluminum bars and connected to end-rings from both ends. The casting process will be easier with closed rotor slots as opposed to opened ones. Later, we will modify the rotor slot impedance to consider closed slots as opposed to open ones, with tapered top edges to reduce core saturation near the edges.

The rotor bar resistance or equivalently known as rotor slot resistance can be be simply calculated from Ohms law as:

$$R_b = \frac{l}{\sigma_{Al} A_{rslot}} \tag{3.59}$$

where σ_{Al} is the electrical conductivity of Aluminum ($3.5 \times 10^7 S/m$ at $20\,^\circ C$). In this work, a lower conductivity of Aluminum corresponding to $150°C$ will be taken into account in the analytical and FEA models: $\sigma_{Al}^{150^\circ C} = 2.3 \times 10^7 S/m$.

In case of the rotor slot, with the depression region filled with air (Fig. 3-6) the rotor bar resistance can be approximated as:

$$R_b = \frac{l}{\sigma_{Al}\, w_r h_r} \tag{3.60}$$

2 Rotor end-ring Resistance (R_{er})

We start by defining the element end-ring resistance (r_{er}). As the name suggests it is the resistance of the end-ring portion between any two adjacent bars. Taking a cross section of the end-ring with radial depth of h_{er} and axial length of l_{er}, and considering the length of one end-ring element to be equivalent to one rotor slot pitch ($\tau_{\gamma,r}$), the element end-ring resistance can be expressed as:

$$\begin{aligned} r_{er} &= \frac{\tau_{\gamma,r}}{\sigma_{Al}\, h_{er} l_{er}} \\ &= \frac{\frac{2\pi D_{rg}/2}{Nr}}{\sigma_{Al}\, h_{er} l_{er}} \\ &= \frac{\pi D_{rg}}{\sigma_{Al}\, N_r h_{er} l_{er}} \end{aligned} \tag{3.61}$$

Note that the expression in (3.61) does not represent the resistance of an end-ring, rather the resistance of the portion of the end-ring connecting two adjacent rotor bars. We cannot simply multiply the end-ring resistance of one element by number of rotor bars to get the end-ring resistance, because they are not connected in series as there is a bar between any two end-ring elements. Here, the rotor end-ring resistance is derived based on two approaches, one is presented by Lippo and Williamson [38] & [65], and another by Alger

[3]. Although they take different approaches both methods lead to the same result.

Derivation of Rotor End-ring Resistance: Cage Equivalent Circuit Approach

Let us start with the first approach [38] & [65]. Consider the planer circuit of a cut made to a cage rotor as shown in Fig. 3-7. In this circuit, each bar (say the k^{th} element for example) is represented by an impedance consisting of a resistance (R_b) and inductance (L_b). Similarly, each end-ring element connecting two bars is also modeled as a resistor (r_{er}) and inductance (ℓ_{er}). r_{re} is as given per (3.61), and ℓ_{er} will be provided later in the rotor leakage reactance section (Section 3.3.3). Accounting for only the fundamental-frequency component of

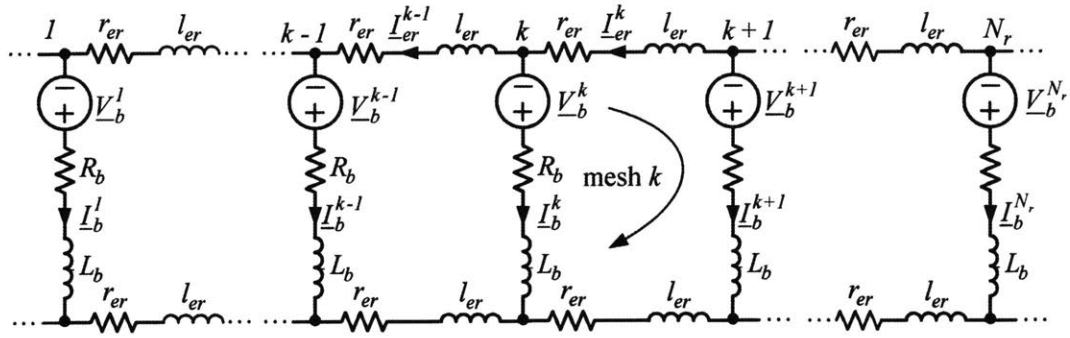

Figure 3-7: Planer circuit representing cage of an induction motor

the airgap flux density, this rotating wave will induce currents in the bars that are also sinusoidal and with electrical frequency equal to the slip (rotor) frequency $\omega_r = s\omega$. Since the rotating airgap flux has constant amplitude (assuming only fundamental flux sinusoidal wave) it induces currents in the rotor bars of the same magnitude, and since the rotor bars are placed uniformly in space (by symmetry) around the periphery, the rotor currents are induced in a progressive fashion as the flux wave rotates and crosses them one after the other. This means that the rotor currents are balanced: have equal magnitude and phase displaced by an angle equal to the rotor slot pitch angle.

In the phasor domain, the rotor current at the k^{th} bar ($\underline{I_b}^k$) can be expressed in steady-state as:

$$\underline{I_b}^{k+1} = \underline{I_b}^k e^{-jp\frac{2\pi}{N_r}} \tag{3.62}$$

Similarly, the voltage induced in the k^{th} bar ($\underline{V_b}^k$) and the current in the k^{th} end-ring element ($\underline{I_{er}}^k$) can be expressed as:

$$\underline{V_b}^{k+1} = \underline{V_b}^k e^{-jp\frac{2\pi}{N_r}} \tag{3.63}$$

$$\underline{I_{er}}^{k+1} = \underline{I_{er}}^k e^{-jp\frac{2\pi}{N_r}} \tag{3.64}$$

Applying Kirchhoff Voltage Law (KVL) at mesh k (see Fig. 3-7):

$$\begin{aligned} \underline{V_b}^{k+1} - \underline{V_b}^k &= Z_b\left(\underline{I_b}^k - \underline{I_b}^{k+1}\right) + 2z_{er}\underline{I_{er}}^k \\ \underline{V_b}^k\left(1 - e^{-jp\frac{2\pi}{N_r}}\right) &= Z_b\underline{I_b}^k\left(1 - e^{-jp\frac{2\pi}{N_r}}\right) + 2z_{er}\underline{I_{er}}^k \\ \underline{V_b}^k &= Z_b I_b{}^k + 2z_{er}\frac{\underline{I_{er}}^k}{\left(1 - e^{-jp\frac{2\pi}{N_r}}\right)} \end{aligned} \tag{3.65}$$

where, the bar and end-ring impedances can be expressed in terms of their resistance and inductance counter parts as:

$$Z_b = \left(R_b + j\omega_r L_b\right) \tag{3.66}$$

$$z_{er} = \left(r_{er} + j\omega_r \ell_{er}\right) \tag{3.67}$$

To get the equivalent rotor bar impedance, we can write the induced bar voltage at node k in terms of the bar current. From Kirchhoff Current Law (KCL) at node $k+1$ (refer to Fig. 3-7), we can express the end-ring current at the k^{th} node in terms of the bar current at the same node as:

$$\begin{aligned} \underline{I_{er}}^k &= \underline{I_{er}}^{k+1} - \underline{I_b}^{k+1} \\ \underline{I_{er}}^k\left(e^{-jp\frac{2\pi}{N_r}} - 1\right) &= \underline{I_b}^k e^{-jp\frac{2\pi}{N_r}} \\ \underline{I_{er}}^k &= \frac{I_b^k}{1 - e^{jp\frac{2\pi}{N_r}}} \end{aligned} \tag{3.68}$$

Substituting (3.68) in (3.65):

$$\underline{V_b}^k = \left(Z_b + 2\frac{z_{er}}{\left(1 - e^{-jp\frac{2\pi}{Nr}}\right)\left(1 - e^{jp\frac{2\pi}{Nr}}\right)}\right) {I_b}^k$$
$$\underline{V_b}^k = \left(Z_b + 2\frac{z_{er}}{4\sin^2\left(\frac{p\pi}{N_r}\right)}\right) {I_b}^k \tag{3.69}$$

Thus, the equivalent bar impedance can be expressed as:

$$\begin{aligned} Z_r &= Z_b + Z_{er} \\ &= Z_b + \frac{z_{er}}{2\ sin^2\left(\frac{p\pi}{N_r}\right)} \end{aligned} \tag{3.70}$$

From (3.70) the equivalent bar impedance or rotor impedance can be expressed as:

$$\begin{aligned} R_r &= R_b + R_{er} \\ &= R_b + \frac{r_{er}}{2\ sin^2\left(\frac{p\pi}{N_r}\right)} \end{aligned} \tag{3.71}$$

$$\begin{aligned} L_r &= L_b + L_{er} \\ &= L_b + \frac{\ell_{er}}{2\ sin^2\left(\frac{p\pi}{N_r}\right)} \end{aligned} \tag{3.72}$$

where R_{er} & L_{er} are the equivalent resistance and inductance of each of the two end-rings, respectively.

Refer to the stator side, the per phase rotor resistance will be:

$$\begin{aligned} R_{2,n} &= R_{2b,n} + R_{2er,n} \\ &= 12\frac{(N_a k_{w,n})^2}{N_r}/k_{sk,n}^2 R_b + 12\frac{(N_a k_{w,n})^2}{N_r}/k_{sk,n}^2 R_{er} \\ &= 12\frac{(N_a k_{w,n})^2}{N_r}/k_{sk,n}^2 \left(R_b + \frac{r_{er}}{2\ sin^2\left(\frac{p\pi}{N_r}\right)}\right) \end{aligned} \tag{3.73}$$

Derivation of Rotor End-ring Resistance: Current Density Approach

This method was presented by P. Alger in [3]. As in the rotor cage equivalent circuit approach, we start by assuming the currents in the bars and end rings to be sinusoidally

distributed around the periphery (see Fig. 3-8). Thus, each bar current can be expressed as:

$$i_b = \frac{I_{b,pk}}{2p} sin(p\theta) \tag{3.74}$$

where p is the number of pole pairs.

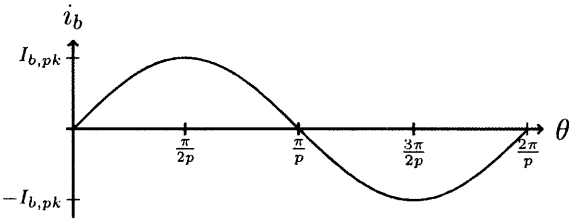

Figure 3-8: Rotor bar current assumed to be sinusoidally distributed around periphery

The peak current of each end-ring can be approximated by taking the average of the total bar currents over a half pole pitch:

$$\begin{aligned} I_{er,pk} &= \frac{2p}{\pi} \int_0^{\frac{1}{2}\frac{\pi}{p}} \frac{1}{2} I_{b,pk} \frac{N_r}{2p} sin(p\theta)\, d\theta \\ &= \frac{N_r I_{b,pk}}{2\pi} \frac{cos(p\theta)}{p} \Big|_{\frac{\pi}{2p}}^{0} \\ \frac{I_{er,pk}}{I_{b,pk}} &= \frac{N_r}{2\pi p} \end{aligned} \tag{3.75}$$

The ratio of current densities are thus:

$$\begin{aligned} \frac{J_{er,pk}}{J_{b,pk}} &= \frac{I_{er,pk}/A_{er}}{I_{b,pk}/A_b} \\ &= \frac{N_r}{2\pi p} \frac{A_b}{A_{er}} \\ &= \frac{N_r}{2\pi p} \frac{w_r h_r}{l_{er} h_{er}} \end{aligned} \tag{3.76}$$

Usually it is practical to design the end-rings such that its radial extent is equal to the rotor slot height ($h_{er} = h_r$) so that the end-ring covers the slot completely. The ratio of current densities becomes:

$$\frac{J_{er,pk}}{J_{b,pk}} = \frac{N_r}{2\pi p}\frac{w_r}{l_{er}} \tag{3.77}$$

Since both the end-ring and bar currents vary sinusoidally around the periphery, the power loss in the end-rings, and bars can be found knowing their geometry and current densities. From Poynting's theorem, real power per unit volume can be expressed as:

$$\begin{aligned} P_v &= \frac{1}{2}\Re(EJ^*) = \frac{1}{2}\Re(\frac{J}{\sigma}J^*) \\ &= \frac{1}{2}\frac{|J|^2}{\sigma} \end{aligned} \tag{3.78}$$

Using (3.78), the end-ring loss to bar loss can be expressed as as the ratio of current densities multiplied by the ratio of end-rings volume (volume of two end-rings) to the total bar volume:

$$\begin{aligned} \frac{P_{er}}{P_b} &= \frac{\frac{1}{2}\frac{|J_{er,pk}|^2}{\sigma_{Al}}}{\frac{1}{2}\frac{|J_{b,pk}|^2}{\sigma_{Al}}}\frac{2\times V_{er}}{N_r \times V_b} \\ &= \frac{|J_{er,pk}|^2}{|J_{b,pk}|^2}\frac{2\times V_{er}}{N_r \times V_b} \\ &= \left[\frac{N_r}{2\pi p}\frac{w_r}{l_{er}}\right]^2 \frac{2\times \pi D_{rg} l_{er} h_{er}}{N_r \times w_r h_r l} \\ &= \frac{N_r w_r D_{rg}}{2\pi p^2 l_{er} l} \end{aligned} \tag{3.79}$$

where V_{er} is the volume of one end-ring and V_b is the volume of one rotor bar.
It is also can be shown that:

$$\frac{P_{er}}{P_b} = \frac{1/2 R_{er} I_{er}^2}{1/2 R_b \sum I_b^2} \tag{3.80}$$

In (3.80), each end-ring can can be thought of one big node, or:

$$I_{er} = \sum I_b \tag{3.81}$$

Using equation (3.81) and equating equations (3.79) & (3.80), the ratio of the end-ring resistance to the bar resistance can be written as:

$$\frac{R_{er}}{R_b} = \frac{N_r w_r D_{rg}}{2\pi p^2 l_{er} l} \tag{3.82}$$

Substituting the expression for R_b as per (3.60) in (3.82), the end-ring resistance can be expressed as:

$$\begin{aligned} R_{er} &= \frac{N_r w_r D_{rg}}{2\pi p^2 l_{er} l} \frac{l}{\sigma_{Al}\, w_r h_r} \\ &= \frac{N_r D_{rg}}{2\pi p^2\, \sigma_{Al}\, l_{er} h_{er}} \end{aligned} \tag{3.83}$$

The end-ring resistance expression (R_{er}) in equation (3.83) is given for the case that $h_{er} = h_r$ as mentioned earlier.

It is worthy to note that the expression derived by the cage rotor equivalent circuit method given in (3.71) approaches the expression derived by the current density method (3.83) as the angle of the sine term becomes small enough that it can be represented by the first term of its Taylor series expansion.

Expand the sine term of R_{er} in (3.71) to its first order Tylor series expansion ($sin(x) \simeq x$, x is small and in radians), and substitute for the element end-ring resistance r_{er} as per (3.61):

$$
\begin{aligned}
R_{er} &= \frac{r_{er}}{2\ sin^2\left(\frac{p\pi}{N_r}\right)} \\
&\simeq \frac{r_{er}}{2\left(\frac{p\pi}{N_r}\right)^2} \\
&= \frac{\pi D_{rg}}{\sigma_{Al}\ N_r h_{er} l_{er}}\ \frac{1}{2\left(\frac{p\pi}{N_r}\right)^2} \\
&= \frac{N_r D_{rg}}{2\pi p^2 \sigma_{Al}\ h_{er} l_{er}}
\end{aligned} \tag{3.84}
$$

It is evident by equations (3.83) & (3.84) that both derivation methods of the end-ring resistance lead to the same result. Therefore, the per-phase rotor resistance $R_{2,n}$, referred to primary, in (3.85) is alternatively written as:

$$
\begin{aligned}
R_{2,n} &= 12\frac{(N_a k_{w,n})^2}{N_r}/k_{sk,n}^2\left(R_b + \frac{r_{er}}{2\ sin^2\left(\frac{p\pi}{N_r}\right)}\right) \\
&= 12\frac{(N_a k_{w,n})^2}{N_r}/k_{sk,n}^2\left(R_b + \frac{N_r D_{rg}}{2\pi p^2 \sigma_{Al}\ h_{er} l_{er}}\right)
\end{aligned} \tag{3.85}
$$

Similar approximation can be applied to the end-ring inductance when calculating the end-ring leakage reactance as will be shown later in Section (3.3.3.3).

3.3.3 Rotor Leakage Reactances $\mathbf{X}_{2n}$

The rotor leakage reactance of the squirrel cage induction motor consists of: (1) slot leakage, (2) zigzag leakage, (3) end-ring leakage, and (4) skew leakage.

1 Rotor Bar (Slot) Leakage $X_{2s,n}$

As mentioned earlier in the rotor bar resistance Section 1, the skin depth in this design is much larger than the rotor depth, and thus filed diffusion effect (deep rotor bar effect) is ignored.

The rotor bar self- permeance and inductance are equivalent in the case of cage rotors since there is no discrete coils as in wound rotors (no number of turns). Thus, similar to

the stator slot permeance of a full-pitch stator winding of a rectangular shape of equation (3.40) the rotor slot self-permeance (and self-inductance) can be expressed as:

$$\mathcal{P}_b = L_b = \mu_0 l\left(\frac{1}{3}\frac{h_r}{w_r} + \frac{d_r}{u_r}\right) \tag{3.86}$$

Note that there is no mutual inductance associated with the the rotor slot since each bar carries a current of the same phase. Thus, the leakage inductance of every bar and end-ring segment can be approximated by its self-inductance. The referred rotor bar leakage reactance ($X_{2s,l}$) corresponding to the n^{th} space harmonic airgap flux wave can be expressed as:

$$\begin{aligned} X_{2sl,n} &= 12\frac{(N_a k_{w,n})^2}{N_r}/k_{sk,n}^2 \cdot X_b \\ &= 12\frac{(N_a k_{w,n})^2}{N_r}/k_{sk,n}^2 \cdot \omega L_b \qquad\qquad n = 1,5,7,\frac{N_s}{p} \mp 1 \end{aligned} \tag{3.87}$$

where, N_r is th number of rotor slots/bars.

Note that the $1/k_{sk,n}^2$ factor in equation (3.87) is a result of accounting for the skew effect through $1 : k_{sk,n}$ transformer ratio as was shown in Section 3.3.1. Details on the derivation of rotor slot leakage can be found in [31], [38] [3].

2 Rotor Zigzag Leakage Reactances $X_{2z,n}$

As described in [31], the voltage induced in a rotor slot is due to (1) the space fundamental of rotor current plus space fundamental of stator current, (2) and additional voltage due to the zigzag order harmonics of the rotor current. This additional voltage is contributed to an additional leakage reactance of the rotor circuit called the rotor zigzag leakage reactance. The rotor leakage reactance can be expressed as:

$$X_{2z} = p^2\left(\frac{1}{(N_r+p)^2} + \frac{1}{(N_r-p)^2}\right) X_{m,n}\Big/k_{sk,n}^2 \tag{3.88}$$

Further details on the derivation of the rotor leakage reactance can be found in [31].

3 End-Ring Leakage X_{2e}

The end-ring leakage is very small, especially for small induction motors such as the one being designed in this work, and thus one may argue to that it can be ignored. However, for a more accurate analytical model, it will be considered nonetheless.

As presented in [65] & [38], a good start for the end-ring leakage inductance approximation is based on Grover's formula [25] for the self inductance of a circular loop with a square cross section. Assuming a rectangular cross section of the end-ring of mean radius of $D_{er}/2$, the self inductance of the k^{th} end-ring element between two rotor bars can be expressed as:

$$\frac{D_{er}}{2} = \frac{D_{rg}}{2} + \frac{h_{er}}{2} \tag{3.89}$$

$$\ell_{er} = \mu_0 \frac{D_{er}}{2N_r}\left[\frac{1}{2}\left(1 + \frac{h_{er}l_{er}}{6D_{er}^2}\right) ln\left(8\frac{D_{er}^2}{h_{er}l_{er}}\right) - 0.8434 + 0.2041\frac{h_{er}l_{er}}{D_{er}^2}\right] \tag{3.90}$$

where ℓ_{er} refers to the end-ring inductance of one element connecting two adjacent rotor bars. The end-ring cross section has an area of $h_{er} \times l_{er}$, wherein h_{er} & l_{er} are the radial and axial length of the end-ring, respectively, and D_{rg} is the airgap (inner) rotor diameter.

From equation (3.72), the leakage inductance of one of the two end-rings can be expressed as:

$$L_{er} = \frac{\ell_{er}}{2sin^2\frac{p\pi}{N_r}} \tag{3.91}$$

When the angle $\frac{p\pi}{N_r}$ of the sine term in the denominator of equation (3.91) is small, it is reasonable to approximate the sine squared term to its first order Tylor series expansion. Thus, the expression becomes:

$$L_{er} \approx \frac{\ell_{er}}{2\left(\frac{p\pi}{Nr}\right)^2} \tag{3.92}$$

Referring the end-ring leakage inductance to the stator side, the per-phase end-ring leakage reactance corresponding to the n^{th} space harmonic airgap flux wave can be ex-

pressed as:

$$X_{2er,n} = 12\frac{(N_a k_{w,n})^2}{N_r}/k_{sk,n}^2 \cdot X_{er}$$
$$= 12\frac{(N_a k_{w,n})^2}{N_r}/k_{sk,n}^2 \cdot 2\pi f L_{er} \qquad n = 1, 5, 7, z_-, z_+ \tag{3.93}$$

4 Skew Leakage $X_{sk,n}$

The skew leakage inductance ($L_{sk,n}$) and reactance ($X_{sk,n}$) at the n^{th} harmonic can be expressed as:

$$L_{sk,n} = L_{m,n}(1 - k_{sk,n}^2) \qquad n = 1, 5, 7, z_-, z_+ \tag{3.94}$$

$$X_{sk,n} = \omega L_{m,n}(1 - k_{sk,n}^2)/k_{sk,n}^2 \qquad n = 1, 5, 7, \frac{N_s}{p} \mp 1 \tag{3.95}$$

As noted previously, the $1/k_{sk,n}^2$ factor in (3.95) is due to the referral of the rotor quantities to the primary side, accounting for the skew effect through the transformer ratio $1 : k_{sk}^2$.

3.4 Core Branch

3.4.1 Steinmetz Equation

Core loss in electric machines is the total power loss in the core material of the stator and rotor. There are two main mechanism for loss in the core of magnetic materials: eddy-current loss and hysteresis loss. In general, the eddy-current loss can be considerably reduced by laminating the core material; however, the core loss depends on the properties of the ferromagnetic material and the operating frequency. In reality, the simple core loss model that accounts only for eddy-current and hysteresis loss is not sufficient, and the experimental core loss will be higher than the theoretical one. The difference between the theoretical loss (eddy-current & hysteresis) and experimental loss is accounted for what is called excess or anomalous loss. The total core loss (P_c) per unit volume (W/m^3) can be generally expressed as,

$$P_{core} = P_{eddy} + P_{hys} + P_{excess}$$
$$= (K_{eddy} f^2 + K_{hys} f) B_{pk}^2 + K_{exc} (B_{pk} f)^{1.5} \tag{3.96}$$

where f is the drive frequency in Hz, B_{pk} is the peak flux density in Tesla or Gauss (based on the manufacturer's datasheet), K_{eddy}, K_{hys} and K_{exc} and are the eddy, hysteresis, and excess loss coefficients in W/cm^3, respectively.

The equation as per (3.96) can be curve fitted into a model expressed in terms of frequency and flux density, each raised to a exponent unique and multiplied by a loss coefficient. The result is an empirical formula traced back to Steinmetz. Steinmetz equation can estimate core loss with reasonable accuracy for sinusoidal drive input, and thus is extensively used in literature. It can be expressed as:

$$P_{core} = K_S f^{e_f} B_{pk}^{e_B} \tag{3.97}$$

where K_S is the Steinmetz coefficient and e_f, e_B are the frequency and flux exponents, respectively.

It is worthy to note that equation (3.97) is valid only under sinusoidal drive conditions and a modified Steinmetz equation ought to be used in case of distorted drive input as proposed by J. Li et al. [37]. From [31], an alternative form of core loss widely used in electric machine design is expressed in Watts per unit mass as,

$$P_{core} = P_b \left(\frac{f}{f_b}\right)^{\varepsilon_f} \left(\frac{B}{B_b}\right)^{\varepsilon_B} \tag{3.98}$$

where P_b is the base power in W/Kg, f is the drive frequency in Hz, f_b is the base frequency and is usually 50 or 60 Hz, B_b is the base flux density in 'rms' is usually equal to 1 Tesla.

The Steinmetz parameters which includes the base power P_b and the exponents e_f, e_B, are provided by the manufacturer directly or can be extracted from the datasheet loss

density plots ($P_v - f$ or/and $P_v - B$ curves) in cases where the Steinmetz parameters are not provided explicitly. For example, M19-26G non-oriented electrical steel material is used in this design, and the corresponding Steinmetz parameters are: $P_b = 1.3$, $e_f = 1.88$ and $e_B = 1.53$. Typical values for Steinmetz coefficients for different grades of electrical steel are: $e_f \sim 1.3 - 1.6$ and $e_B \sim 1.9 - 2.4$ [31].

Similarly, the volt-amp drop in the core can be modeled by a similar Steinmetz relation as follows:

$$Q_{core} = \left\{ Q_{b1} \left(\frac{B}{B_b} \right)^{\varepsilon_1} + Q_{b2} \left(\frac{B}{B_b} \right)^{\varepsilon_2} \right\} \frac{f}{f_b} \tag{3.99}$$

where Q_{b1} & Q_{b1} are empirical Steinmetz coefficients in VAR/Kg, and ε_1 & ε_2 are the corresponding exponents for the first and second term, respectively. For M19-26G, $\varepsilon_1 = 1.7$ $\varepsilon_1 = 16.1$ and $Q_{b1} = 1.08$, $Q_{b1} = 0.0144$.

3.4.2 Core Elements Calculation

The core branch impedance consists of a resistive element R_c in parallel with a reactive element X_c as shown in Fig.3-1. The resistive element represents the real power consumption in the core sections in Watts, whereas the reactive element represents the reactive power drop in the core in VARs. The core loss (P_{core}) (in W/Kg) is calculated at the teeth and back-iron of the stator as per (3.98), whereas the volt-amp consumption (Q_{core}) is calculated at the teeth, back-iron of the stator and at the rotor teeth as per (3.99). Furthermore, another resistor $R_{rt,snl}$ connected in parallel with fundamental magnetizing branch to model the no-load stray loss in the rotor teeth (discussed in detail in Section 3.5). The losses in Watts are then found by multiplying the per unit mass loss quantities (P_{core}, Q_{core}) with the active weight ($inKg$) of stator, and multiplying $P_{rt,snl}$ with the the active weight of the rotor teeth. Finally, the core branch elements are found as:

$$R_c = 3\frac{V_{ag}^2}{P_{core}}$$
$$\simeq 3\frac{V_a^2}{P_{core}} \tag{3.100}$$
$$X_c = 3\frac{V_a^2}{Q_{core}} \tag{3.101}$$
$$R_{rt,snl} = 3\frac{V_a^2}{P_{rt,snl}} \tag{3.102}$$

In (3.100)-(3.101), the airgap voltage is assumed to be equal to the terminal voltage ($V_{ag} = V_a$) in the core branch parameter calculations assuming a small drop across the armature (stator) resistor. An iterative approach may be adopted to achieve more accurate estimate of the core branch. At every iteration the equivalent circuit is solved and the core branch elements are updated until a convergence value is reached as suggested in [31]. In this work, however, the simple model is found to be sufficient for estimating the core loss.

To calculate P_{core}, Q_{core} and $P_{rt,snl}$ from Steinmetz law, we need to first estimate the airgap flux density, and flux density at each portion of the core, including the stator back-iron, teeth and rotor teeth. We are going to only consider the fundamental component of each flux density. From (3.15), the peak of the fundamental airgap flux density at unity slip can be written as:

$$B_{r,1} = \frac{pV_{ag,1}}{2R_g\, l\, \omega\, N_a k_{w,1}} \tag{3.103}$$

where R_g is the airgap radius at the airgap midpoint: $R_g = D_{rg}/2 - g_e/2$.

The airgap flux per pole crosses the airgap and splits into the back-iron of the stator and

rotor. Thus, half of the peak airgap flux per pole is equal to the peak flux in the core:

$$\begin{aligned}
\frac{1}{2}\phi_{g,pk} &= \phi_{c,pk} \\
\frac{1}{2}\frac{2}{\pi}B_{r,1}\frac{A_g}{2p} &= B_{c,\{s,r\}}A_{c,\{s,r\}} \\
\frac{1}{2}\frac{2}{\pi}B_{r,1}\frac{2\pi R_g l}{2p} &= B_{c,\{s,r\}}d_{c,\{s,r\}}\, l \\
B_{c,\{s,r\}} &= B_{r,1}\frac{R_g}{p\, d_{c,\{s,r\}}}
\end{aligned} \tag{3.104}$$

where $B_{c,\{s,r\}}$ is the 'core' flux density behind the stator or rotor slots (back-iron).

For more accurate calculation of the flux density, the lamination stacking factor (κ_{stack}) should be taken into account. In practice, the lamination stacking factor is in the range of: $\kappa_{stack} \sim 0.9 - 0.98$. Also note that same stacking factor is assumed for both the stator and the rotor (not necessarily the case in general).

Thus, the back-iron flux density becomes:

$$\begin{aligned}
B_{c,\{s,r\}} &= B_{r,1}\frac{R_g}{p\, d_{c,\{s,r\}}/\kappa_{stack}} \\
&= B_{r,1}\frac{D_g}{2p\, d_{c,\{s,r\}}} \times \kappa_{stack}
\end{aligned} \tag{3.105}$$

And, the back-iron depth of the stator ($d_{c,s}$) and the rotor ($d_{c,r}$) in inner-stator, outer-rotor machines are:

$$d_{c,s} = \frac{D_{sg}}{2} - h_s \tag{3.106}$$

$$d_{c,r} = \frac{D_{ry}}{2} - \frac{D_{rg}}{2} - h_r \tag{3.107}$$

The airgap flux enters the core from teeth as it have the minimum reluctance and thus, naturally, the flux lines are condensed in the teeth area. A reasonable approximation of the flux density at the stator or rotor tooth ($B_{t,\{s,r\}}$) is to multiply the airgap density by the slot pitch to tooth width ratio, or equivalently divide it by the tooth width to slot pitch ratio

($K_{t\tau,\{s,r\}}$):

$$K_{t\tau} = \frac{t_{\{s,r\}}}{\tau_{\gamma,\{s,r\}}} \tag{3.108}$$

$$B_{t,\{s,r\}} = \frac{B_{ag}}{K_{t\tau,\{s,r\}}} \times \kappa_{stack} \tag{3.109}$$

where $t_{0,\{s,r\}}$ and $\tau_{\gamma,\{s,r\}}$ are the corresponding tooth width and slot pitch of the stator and rotor, respectively. The slot pitch of the stator and rotor in (3.108) are found from the motor dimensions as:

$$\tau_{\gamma,s} = \frac{2\pi(D_{sg}/2 - d_s)}{N_s} \tag{3.110}$$

$$\tau_{\gamma,r} = \frac{2\pi(D_{rg}/2 + d_r)}{N_s} \tag{3.111}$$

And, the tooth width is simply:

$$t_{0,s} = \tau_{\gamma,s} - w_{s,top} \tag{3.112}$$

$$t_{0,r} = \tau_{\gamma,s} - w_r \tag{3.113}$$

where $t_{0,s}$ & $t_{0,r}$ are the corresponding stator and rotor tooth width, respectively, assuming a trapezoidal stator slot and rectangular rotor slot.

3.5 Performance Evaluation

The strength of the analytical model is that it provides a simple way to evaluate the performance of a motor by solving a relatively simple circuit (Fig. 3-1). At start, some initial motor design data is fed to the analytical model program which outputs the the equivalent circuit model with all elements calculated. The circuit is then solved for all the currents, including the terminal stator current I_t, rotor currents referred to the stator $I_{2,n}$, and the resistive core branch current I_c. The input power, mechanical (output) power, electromagnetic and mechanical torque, efficiency and power factor are then easily calculated given the currents and the terminal voltage applied at the terminals of the motor. In this section,

the equivalent circuit is first solved for stator, core, and rotor currents, then the performance metric quantities including power, torque, and power factor are calculated. We describe the steps to solve the circuit and evaluate the performance of the motor in Matlab as follows:

(1) Define slip vectors for the rotor circuits: s_n

The slip due to the fundamental component of the airgap flux density wave is the difference between the fundamental synchronous speed and rotor speed with respect to the fundamental synchronous speed as defined in (3.16). In this section, we are going to denote the slip in (3.16) as s_1 to indicate the corresponding space harmonic flux wave component being the fundamental.

The slip is s_1 is 0 at when the rotor approaches synchronous speed, and 1 at standstill. A vector of M points from 0 (synchronous) and 1 (locked rotor) is defined over which the circuit currents and voltages will be solved. In Matlab, the slip vector can be defined as:

$$\boldsymbol{s_1} \leftarrow logspace(-4, 0, M) \tag{3.114}$$

In (3.114), $\boldsymbol{s_1}$ is defined as an M logarithmically equally spaced points between the $10^{-4} \sim 0$ and $10^0 = 1$ decades. Note that throughout this section the boldface font indicates vector notation.

Since space harmonics travels at a speed equals a $1/n$ the synchronous speed of the fundamental component of the airgap flux wave in the forward/positive or backward/negative directions (depending on the harmonic order number), the slip at the n^{th} space harmonic can be expressed as:

$$\begin{aligned} s_n &= \frac{\omega_n - p\omega_m}{\omega_n} \\ &= \frac{\mp\frac{\omega}{n} - p\omega_m}{\mp\frac{\omega}{n}} \\ &= 1 \pm n\frac{p\omega_m}{\omega} \end{aligned} \tag{3.115}$$

where the '$-$' in $\omega_n = \mp\omega/n$ refers to backward rotating and '$+$' sign refers to forward rotating space harmonics.

From (3.16):

$$p\omega_m = (1 - s_1)\omega \tag{3.116}$$

Substituting (3.116) in (3.115), yields:

$$\begin{aligned} s_n &= 1 \pm n(1 - s_1) \\ &= \begin{cases} 1 + n_-(1 - s_1) & n_- = 5, 11, 17, ... \\ 1 - n_+(1 - s_1) & n_+ = 7, 13, 19, ... \end{cases} \end{aligned} \tag{3.117}$$

In this model, the most significant stator space harmonics for performance evaluation and loss prediction are belt and zigzag, thus $n_- = 5, z_-$, and $n_+ = 7, z_+$ harmonic numbers are of most significance. The harmonic slip vectors associated with the belt harmonics are defined as:

$$\begin{aligned} \boldsymbol{s}_5 &\leftarrow 6 - 5 \cdot \boldsymbol{s_1} \\ \boldsymbol{s}_7 &\leftarrow -6 + 7 \cdot \boldsymbol{s_1} \end{aligned} \tag{3.118}$$

And for three phase distributed windings ($m > 1$), we define another two slip vectors corresponding to the zigzag harmonics as:

$$\begin{aligned} \boldsymbol{s}_z &\leftarrow (1 + z_-) - z_- \cdot \boldsymbol{s_1} \\ \boldsymbol{s}_{z_+} &\leftarrow (1 - z_+) + z_+ \cdot \boldsymbol{s_1} \end{aligned} \tag{3.119}$$

where $\boldsymbol{s_1}$ is as defined in (3.114) and $z_\mp = 6m \mp 1$ (3.20).

(2) Find the input impedance (per phase) at the input terminals (Fig. 3-1)

First, let us find the stator impedance:

$$Z_1 = R_1 + jX_1 \tag{3.120}$$

(Note that Z_1 becomes a vector of M points when added or subtracted from another vector of length M in Matlab by default, so it is not necessary to convert to a vector by multiplying it with ones for example. If using another program this step might be necessary). The rotor impedences can be defined as:

$$\boldsymbol{Z_{2,n}} = R_{2,n}./\boldsymbol{s_n} + jX_{2,n} n = 1, 5, 7, z_{\mp} \tag{3.121}$$

where './' stands for element-wise division operator.

For every transformer circuit in Fig. 3-1 (fundamental airgap flux transformer + smaller transformers corresponding to higher order space harmonics), let's define the impedance which is in parallel with the rotor impedance harmonic as $Z_{m,n}$, and we are going to call them the magnetizing impedances for convenience as they contain the magnetizing reactances $X_{m,n}$. By inspecting Fig. (3-1), we can express the fundamental magnetizing impedance $Z_{m,1}$ as the parallel combination of the magnetizing reactance with the core branch:

$$\begin{aligned} Z_{m,1} &= jX_{m,1} // \underbrace{(R_c // jX_c // R_{rt})}_{Z_c} \\ &= \frac{1}{\frac{1}{jX_{m,1}} + \frac{1}{R_c} + \frac{1}{jX_c} + \frac{1}{R_{rt}}} \end{aligned} \tag{3.122}$$

The fundamental airgap impedance is thus:

$$\begin{aligned} \boldsymbol{Z_{ag,1}} &= \boldsymbol{Z_{2,1}} // Z_{m,1} \\ &= 1./(1./\boldsymbol{Z_{2,1}} + 1/Z_{m,1}) \end{aligned} \tag{3.123}$$

The airgap impedance at the n^{th} space harmonic of the airgap flux wave can be found as:

$$\begin{aligned} \boldsymbol{Z_{ag,n}} &= \boldsymbol{Z_{2,n}} // Z_{m,n} \\ &= 1./(1./\boldsymbol{Z_{2,n}} + 1/Z_{m,n}) \end{aligned} \tag{3.124}$$

The total airgap impedance is the series of all individual airgap impedences, and thus can be found as:

$$\boldsymbol{Z_{ag}} = \begin{cases} \sum\limits_{n=1,5,7} \boldsymbol{Z_{ag,n}} & = \boldsymbol{Z_{ag,1}} + \boldsymbol{Z_{ag,5}} + \boldsymbol{Z_{ag,7}} \quad m = 1 \\ \sum\limits_{1,5,7,z_{\mp}} \boldsymbol{Z_{ag,n}} & = \boldsymbol{Z_{ag,1}} + \boldsymbol{Z_{ag,5}} + \boldsymbol{Z_{ag,7}} + \boldsymbol{Z_{ag,z_{\mp}}} m > 1 \end{cases} \tag{3.125}$$

Now we can define the input terminal impedance as:

$$\boldsymbol{Z_a} = Z_1 + \boldsymbol{Z_{ag}} \tag{3.126}$$

(3) Solve for the currents: I_a, $I_{2,n}$ **and** I_c

Now the circuit is simply as shown in Fig. 3-9

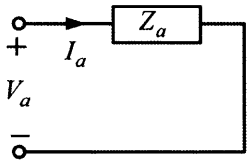

Figure 3-9: Equivalent circuit reduced to the terminal voltage in series with terminal impedance only

The per phase terminal (stator) current is simply found as:

$$\boldsymbol{I_a} = V_a \,./\, \boldsymbol{Z_a} \tag{3.127}$$

where V_a is the terminal voltage in Volts rms.

And the rotor currents can be calculated as:

$$\boldsymbol{I_{2,n}} = \boldsymbol{I_a} .* \ Z_{m,n} ./ \left(Z_{m,n} + \boldsymbol{Z_{2,n}}\right) \tag{3.128}$$

where '.*' stands for element-wise multiplication.

To find the current flowing through the resistive element in the core branch (R_c), let us first lump all other elements other than R_c in one impedance Z_x:

$$\boldsymbol{Z_x} = 1 ./ \left(1/R_{rt} - j/X_c - j/X_m + 1./\boldsymbol{Z_{21}}\right) \tag{3.129}$$

Thus, the current flowing through R_c can be expressed as:

$$I_c = I_a .* \ \boldsymbol{Z_x} ./ \left(\boldsymbol{Z_x} + R_c\right) \tag{3.130}$$

(4) Calculate Input Power, Airgap Power, and Electromagnetic Torque

Now that the currents are calculated from the equivalent circuit, the input P_a power, airgap P_{ag} power, and electromagnetic torque T_e can be found as:

$$P_a = 3\Re(V_a I_a^*) \tag{3.131}$$

$$P_{ag} = \sum_{n=1,5,7,zp,zn} P_{ag}^n = \sum_{n=1,5,7,zp,,zn} 3I_{2,n}^2 \frac{R_{2,n}}{s_n} \tag{3.132}$$

$$\begin{aligned} T_e &= \sum_{n=1,5,7,z_-,z_+} \frac{P_{ag}^n}{\Omega_n} \\ &= \sum_{n=1,5,7,z_-,z_+} \frac{P_{ag}^n}{\pm\omega/(np)} \\ &= \frac{p}{\omega_d}(P_{ag}^1 - 5P_{ag}^5 + 7P_{ag}^7 - zn \cdot P_{ag}^{zn} + zp \cdot P_{ag}^{zp}) \end{aligned} \tag{3.133}$$

(5) Estimate losses: stray and windage-&-friction losses

After calculating the airgap power, we would like to calculate the actual converted mechanical power of the motor. Two main losses are imposed on the the airgap power: stray (load and no-load) losses and bearings friction-&-windage losses.

Stray load loss

The stay load losses have two main components: (i) slip loss and (ii) load loss in the rotor teeth due to the stator zigzag mmf [31].

(i) Slip loss

Slip loss is the loss across the rotor resistances. Traditionally, it is the loss across $R_{2,1}$, and is extended to the harmonic rotor resistances $R_{2,n}$ in the general equivalent circuit model (Fig. (3-1)). Slip loss can thus be defined as:

$$P_{slip} = s_n \sum_{n=1,5,7,zp,zn} P_{ag} \tag{3.134}$$

$$= \sum_{n=1,5,7,zp,,zn} 3I_{2,n}^2 R_{2,n} \tag{3.135}$$

(ii) Load loss in the rotor teeth due to stator zigzag mmf

The zigzag components of the airgap flux density produced by the stator will drive magnetic losses in the core material of the rotor teeth. These losses are accounted for stray load losses and will be substantial only for the zigzag order harmonics (see [31], [3]). Similar to the approach of calculating the magnetic losses in the core due to the fundamental airgap flux in Section (3.4), first we define the amplitude of the airgap flux corresponding to the zigzag order harmonics:

$$B_{ag,z_{\mp}} = \frac{pV_{ag,z_{\mp}}}{D_g\, l\, \omega\, N_a k_{w,z_{\mp}}} = \frac{p|I_{2,z_{\mp}}\, Z_{2,z_{\mp}}|}{D_g\, l\, \omega\, N_a k_{w,z_{\mp}}} \tag{3.136}$$

Using (3.136) for zigzag airgap flux density:

$$P_{rt,load} = m_{rt}\left\{P_b\left(\frac{s_{z_-}\,\omega}{\omega_b}\right)^{\varepsilon_f}\left(\frac{B_{ag,z_-}}{B_b}\right)^{\varepsilon_B} + P_b\left(\frac{s_{z_+}\,\omega}{\omega_b}\right)^{\varepsilon_f}\left(\frac{B_{ag,z_+}}{B_b}\right)^{\varepsilon_B}\right\} \tag{3.137}$$

Stray no-load loss

As discussed in Section 3.4, the stator slot openings modulate the space fundamental of the airgap flux density wave [31]. This modulated flux wave in turns corresponds to loss in the rotor teeth. The amplitude of this modulated fundamental flux wave is:

$$B_H = \frac{2}{\pi} B_{ag} sin\left(\frac{1}{2}\,\theta_u\right) \tag{3.138}$$

where B_{ag} is as defined in (3.103), and θ_{u_s} is the normalized angular slot opening angle with respect to the stator slot pitch ($\tau_{\gamma,s}$) defined as:

$$\theta_{u_s} = \frac{2\pi u_s}{\tau_{\gamma,s}} = \frac{2\pi u_s}{2\pi R_{sg}/N_s} = N_s\,\frac{u_s}{R_{sg}} \tag{3.139}$$

where u is the stator slot opening width, R_{sg} is the stator gap radius, and N_s number of stator slots.

As was shown in Section 3.4, the no-load stray loss in the rotor teeth ($P_{rt,nl}$) to the modulated fundamental airgap flux density can be estimated from Steinmetz equation as:

$$P_{rt,snl} = P_0\left(\frac{N_s f}{f_b}\right)^{\varepsilon_f}\left(\frac{B_Z}{B_0}\right)^{\varepsilon_B} \tag{3.140}$$

where P_0 is the nominal output power of the motor in Watts, f is input (drive) electrical frequency in Hz, f_b is the base frequency (50 or 60 Hz), and B_b is the nominal flux density (usually 1 Tesla).

One can use the loss expression in (3.140) without significant error. But the more accurate loss is the one updated after solving the circuit. As shown before, we can model the no-load stray loss in the rotor teeth as a resistance in parallel the fundamental magnetizing reactance and core branch, and the resistance can be estimated as:

$$R_{rt,snl} = 3\frac{V_a^2}{P_{rt,snl}} \tag{3.141}$$

After solving the circuit, the no-load stray loss due can be updated as:

$$P'_{rt,snl} = 3|I_{rt}|^2 R_{rt,snl} \text{ or } 3|V_a - R_1 I_a|^2 / R_{rt,snl} \tag{3.142}$$

Friction-&-windage loss

From [31], the friction-&-windage loss can approximated as:

$$P_{f\&w} = 2\pi R_g^4 \Omega_m^3 l \rho_{air} b \tag{3.143}$$

where $\rho_{air} = 1.225 kg/m^3$ is the air density, Ω is the mechanical speed of the rotor in rad/s and can be expressed as (from 3.16):

$$\Omega_m = \frac{(1-s)\omega}{p} \tag{3.144}$$

And b in (3.143) is the rotor viscous friction factor in N.m/(Rad/s) and can be calculated as:

$$\begin{aligned} b &= \frac{0.0076}{R_n^{1/4}} \\ &= 0.0076\left(\frac{\Omega R_g g}{\nu_{air}}\right)^{-1/4} \end{aligned} \tag{3.145}$$

where $R_n = \frac{\Omega R_g g}{\nu_{air}}$ is Reynold's number and $\nu_{air} = 1.56 \times 10^{-5} m^2/s$ is the kinematic viscosity of air.

(6) Evaluate performance metrics: efficiency and power factor

Now that we have calculated the losses in step 5, the converted mechanical power can be calculated by subtracting the stray and friction-&-windage losses from the airgap power:

$$P_{mech} = P_{ag} - P_{stray} - P_{f\&w} \tag{3.146}$$

Note that this is equivalent to subtracting all the losses included the core loss (P_c), loss across the armature (P_{R_1}) form the input power (P_a):

$$P_{mech} = P_a - P_{R_1} - P_c - P_{stray} - P_{f\&w} \tag{3.147}$$

The mechanical torque from the output power as:

$$T_{mech} = \frac{P_{mech}}{\Omega} \tag{3.148}$$

$$= p\frac{P_{mech}}{\omega} \tag{3.149}$$

The efficiency can be calculated as:

$$\eta\% = \frac{P_{mech}}{P_a} \times 100 \tag{3.150}$$

And the power factor can be calculated as:

$$PF = \frac{P_a}{S_a} \tag{3.151}$$

where S_a is the apparent power and can be calculated as:

$$S_a = 3\,|V_a|\,|I_a| \tag{3.152}$$

Chapter 4

Verification of Analytical Model using Finite-Element Analysis and Design Optimization

4.1 Motor Configuration

Typically, ceiling fan motors can be of outer-stator inner-rotor configuration or vice versa. However, the latter is more commonly used in household ceiling fans. In this work, an outside-rotor inner-stator squirrel cage three phase induction motor is designed for ceiling fans. A two dimensional picture of the squirrel cage motor configuration adopted in this work is shown in Fig. 4-1.

4.2 Design Philosophy

The design approach of the three phase induction motor starts with some fixed parameters such as, fixed number of stator slots per pole per phase, number of pole pairs, number of rotor slots, and some stator and rotor slot dimensions that are proportionate in size to a typical ceiling fan geometry. These parameters are chosen initially such that the highest peak flux density in the machine is below a saturation limit (typically $< 1.8\ T$) that depends on the ferromagnetic lamination material chosen for the stator and rotor. Next, the motor

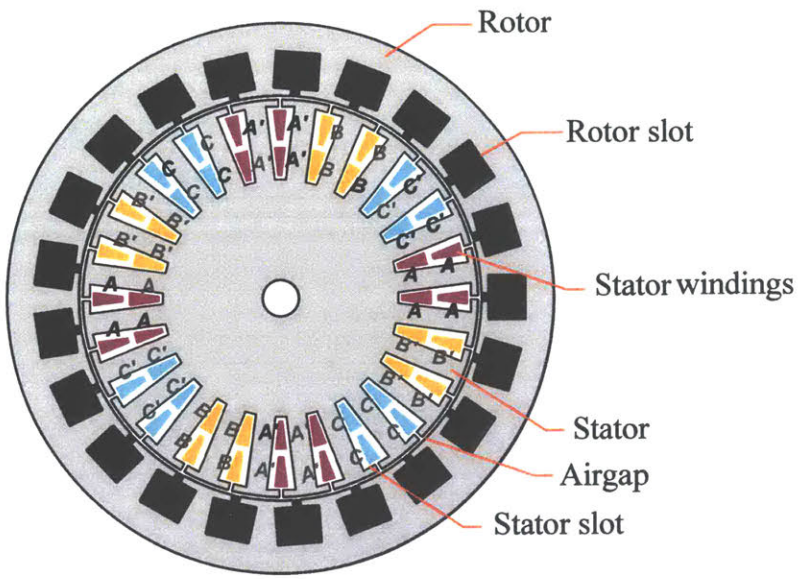

Figure 4-1: Outer-rotor, inner-stator three phase squirrel cage induction motor proposed for ceiling fans application

data are fed to the analytical model developed in Chapter 3 to analyze the behaviour of the motor by examining the torque speed curve, input power, output power, efficiency and power factor. Then, the initial design data are given to a finite element (FE) model as means to verify the analytical model developed earlier in Chapter 3. Finally, the model is verified, the design is optimized to meet certain design requirements as will be shown later (Section 4.5).

4.3 Initial Design

The goal of starting with an initial design is to validate the analytical model developed in Chapter 3 in finite element analysis (FEA). Thus, we do not set any design requirements on the initial design. Furthermore, the stator and rotor slot shapes are of typical rectangular shape, since we are not trying yet to optimize the performance. More advanced rotor and stator slots will be used in the optimized motor design. We start with some initial design with geometry proportional to a typical ceiling fan. The motor data of the initial design is provided in Table 4.1.

Using the analytical model developed in Chapter 3, the circuit parameters of the general

Table 4.1: Motor data of the initial design

parameter	*value*	*parameter*	*value*
Number of stator slots/pole/phase, m	2	Number of rotor Slots, N_r	18
No of pole pairs, p	2	Rotor slot width, w_r	$5mm$
Winding configuration	Distributed, 2-Layer	Rotor slot height, h_r	$6mm$
Number of slots short pitched,N_{sp}	2	Rotor slot opening (depression) width, depth, u_r, d_r	$2mm, 2mm$
Motor terminal voltage,V_a	$57.5V_{rms}$	Rotor end-ring radial height, h_{er}	$7mm$
Drive frequency, f	$12Hz$	Rotor end-ring axial length, l_{er}	$2mm$
Number of turns per coil, N_c	200	stator tooth to slot-pitch ratio, $K_{t\tau,s}$	0.5
Physical airgap, g	$0.5mm$	Tooth width, t_w	$6.9mm$
Packing factor, κ_{cu}	0.45	Stator slot top width, w_{st}	$6.9mm$
Synchronous Speed, n_s	$360rpm$	Stator slot bottom width, w_{sb}	$1.6mm$
Active length, l	$20mm$	Stator slot height, h_s	$20mm$
Rotor yoke diameter, D_{ry}	$150mm$	Stator depression width, depth, u_s, d_s	$2mm$,$2mm$
Rotor gap diameter, D_{rg}	$110mm$	Number of stator Slots, N_s	24
Stator yoke diameter (shaft diameter), D_{sy}	$15mm$	Stator and rotor Core	M19-26G

equivalent circuit (3-1) are calculated as provided in Table. 4.2. Note that the backward and forward zigzag order harmonics in Table. 4.2 are of order $N_s/p \mp 1 = 11, 13$, respectively. Using the equivalent circuit model, the motor performance can be evaluated as described in Section 3.5. The performance of the initial three phase induction motor design evaluated by the analytical model and FEA will be discussed in the following Section.

4.4 Validation of the Analytical Model in 2D and 3D Finite-element Analysis

The initial motor design is evaluated by the analytical model in MATLAB and simulated in ANSYS Maxwell 2D and 3D FEA transient simulation environment [5, 6, 47]. This

Table 4.2: Three phase induction motor equivalent circuit parameters of the initial design

Circuit element	Value (Ω)	Circuit parameter	Value (Ω)
R_1	50	$X_{2,7}$	4.35
X_1	18.5	X_{m,z_-}	1.75
$X_{m,1}$	211.5	R_{2,z_-}	446.5
$R_{2,1}$	446.5	X_{2,z_-}	60.32
$X_{2,1}$	12.3	X_{m,z_+}	1.25
$X_{m,5}$	0.61	R_{2,z_+}	446.5
$R_{2,5}$	32.06	X_{2,z_+}	20.58
$X_{2,5}$	1.52	R_c	$111.12k$
$X_{m,7}$	0.61	X_c	$49.36k$
$R_{2,7}$	32.1	$R_{rt,snl}$	$17.54k$

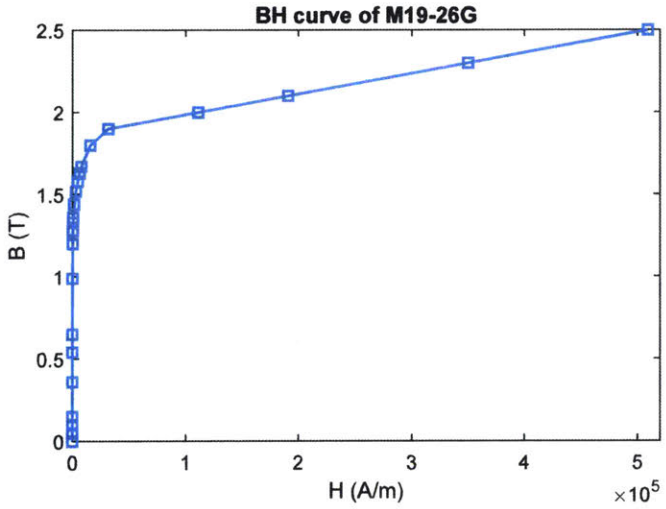

Figure 4-2: B-H curve of M19-26G electrical steel showing saturation characteristics of the stator and rotor core

step is carried out to verify the accuracy of the analytical model regardless of the motor performance. As indicated in Chapter 3, M19-26G non-oriented electrical steel is used in this design. The Steinmetz coefficients are extracted by curve fitting to use the core loss model in equations (3.98) & (3.99). The B-H curve of M19-26G is shown in Fig. 4-2.

4.4.1 2D Finite-Element Model of the Initial Motor Design

The initial design motor FE Model created in ANSYS Maxwell 2D is shown in Fig. 4-3. Since this is a 2D model, it does not account for stator end-winding effect (since it is in

the third dimension). Therefore, the end-winding leakage inductance (L_{1e}) must be fed into the 2D FE model before running the simulation. Furthermore, the end-ring impedance elements (r_{er}, ℓ_{er}) are also fed to the FE 2D model. It is worthy to note that the the 2D and 3D FE models do not calculate the armature resistance (R_1) and must be given as input to the excitation settings in the FE simulations as well.

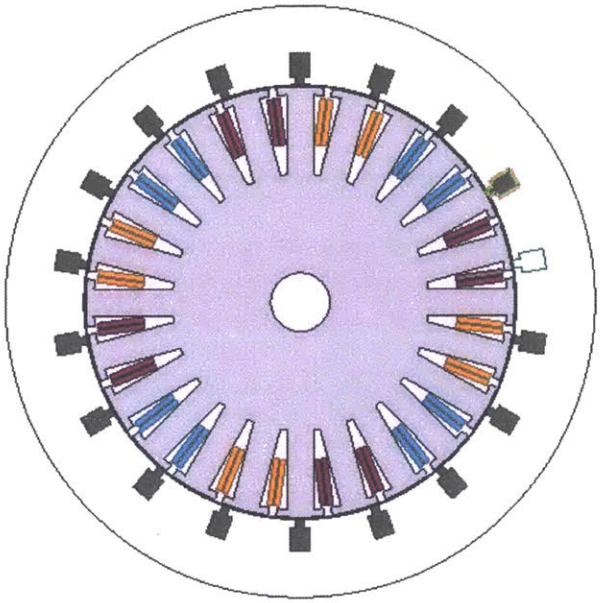

Figure 4-3: 2D image of the initial design motor (unoptimized)

The magnetic field density distribution (in $Tesla$) in the 2D FE model is shown in Fig. 4-4 at speeds 0 RPM and 300 RPM. The peak amplitude of the magnetic flux density across the different parts of the machine are also calculated by the analytical model as per equations (3.103), (3.105), (3.108) {Table. 4.3}. It can be seen in Table. 4.3 that peak flux densities of the analytical model approximately matches that of the FE model (compared at 0 RPM).

4.4.2 Three Dimensional Finite-element Model of the Initial Motor Design

The initial design of the three phase induction motor is also simulated in 3D FEA. A picture of the 3D FE model and the flux distribution are shown in Figs. 4-5 & 4-6. Similar to the

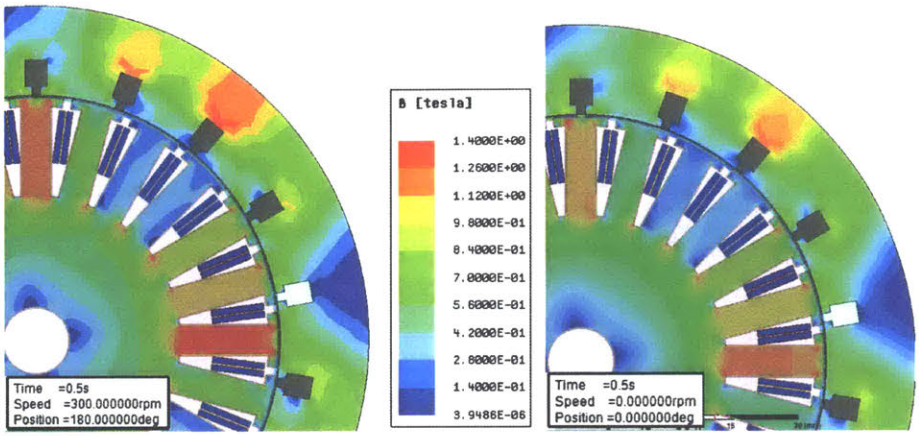

Figure 4-4: Flux density distribution at speeds (a) 300 RPM (left) and (b) 0 RPM (right)

Table 4.3: Flux densities in the rotor and stator at 0 RPM

Flux Density (T)	Analytical	ANSYS 2D
Airgap ($B_{r,1}$)	0.640223	0.6182
Stator teeth ($B_{t,s}$)	1.21642	1.24
Stator back iron ($B_{c,s}$)	0.482866	0.55
Rotor tooth ($B_{t,r}$)	0.85511	0.9
Rotor back iron ($B_{c,r}$)	1.18862	1.3

2D FE model, a fine mesh must be applied at the airgap, rotor bars and endrings, in addition to a small time step in the transient FE analysis, to obtain high accuracy field and torque calculations. A picture of the meshed 3D FE model of the initial design is shown in Fig. 4-7

4.4.3 Validation Results

The analytical model is compared with the 2D and 3D FE models in Fig. 4-8. The electromagnetic torque of the motor, input power, converted mechanical power, efficiency, power factor, and terminal current are plotted against speed in RPM as shown in Figs. 4-8a–4-8f. It can be seen that the analytical model matches closely with the 2D and 3D FEA models as the percentage error does not exceed 9% in all plots with the exception of the power factor. This implies that we can, to a certain extent, rely on the analytical model to optimize the design. Needless to say, the close match between the analytical and FEA models does not necessarily guarantee as similar performance with the real experimental motor.

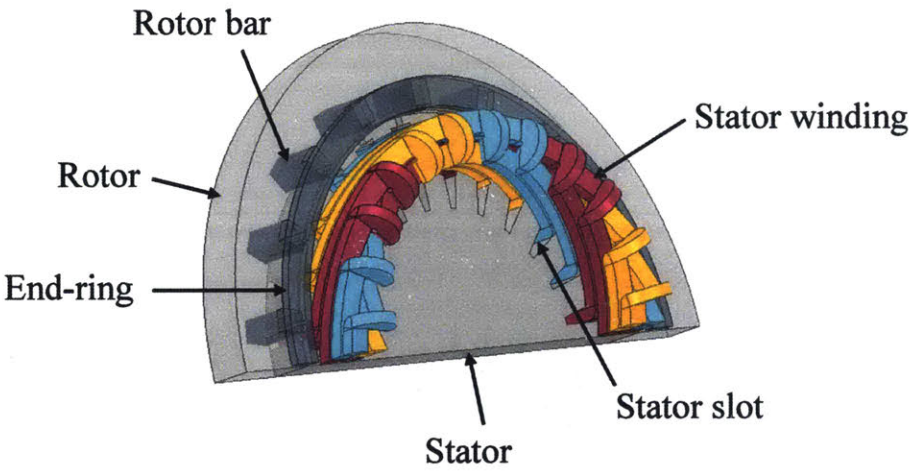

Figure 4-5: A picture showing the 3D FE model of the initial design simulated in ANSYS Maxwell 3D transient analysis

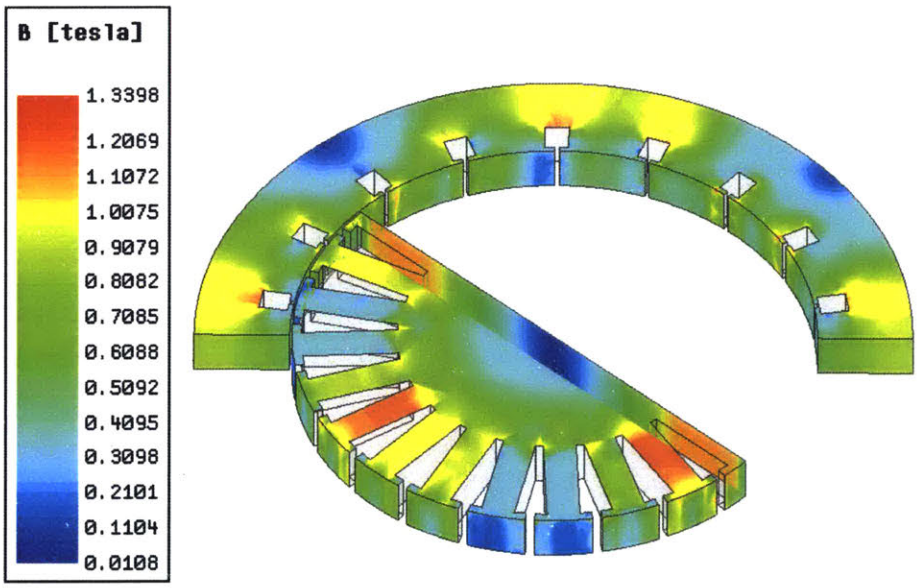

Figure 4-6: Magnetic flux density distribution in the 3D FE model of the initial motor design

There is approximately 15% difference between the 3D FE model and both the analytical model & FE 2D model in the power factor curve (Fig. 4-8e). This might be due to an overestimation of the end-winding leakage inductance which is estimated by Alger's formula [3] as per expression (3.57). More precise estimation of the stator end-winding leakage can yield to better matching of the power factor between the analytical and the 3D model. Note that this does not affect the torque, efficiency, input power and converted

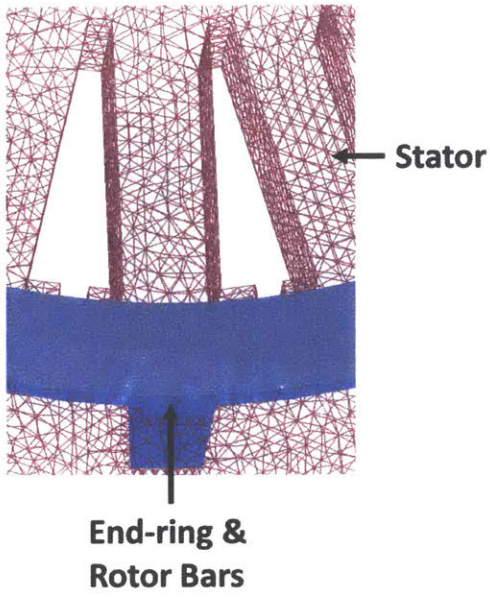

Figure 4-7: Meshed 3D FE model of the initial motor design

power, and therefore, we can still rely on the analytical model to perform optimization.

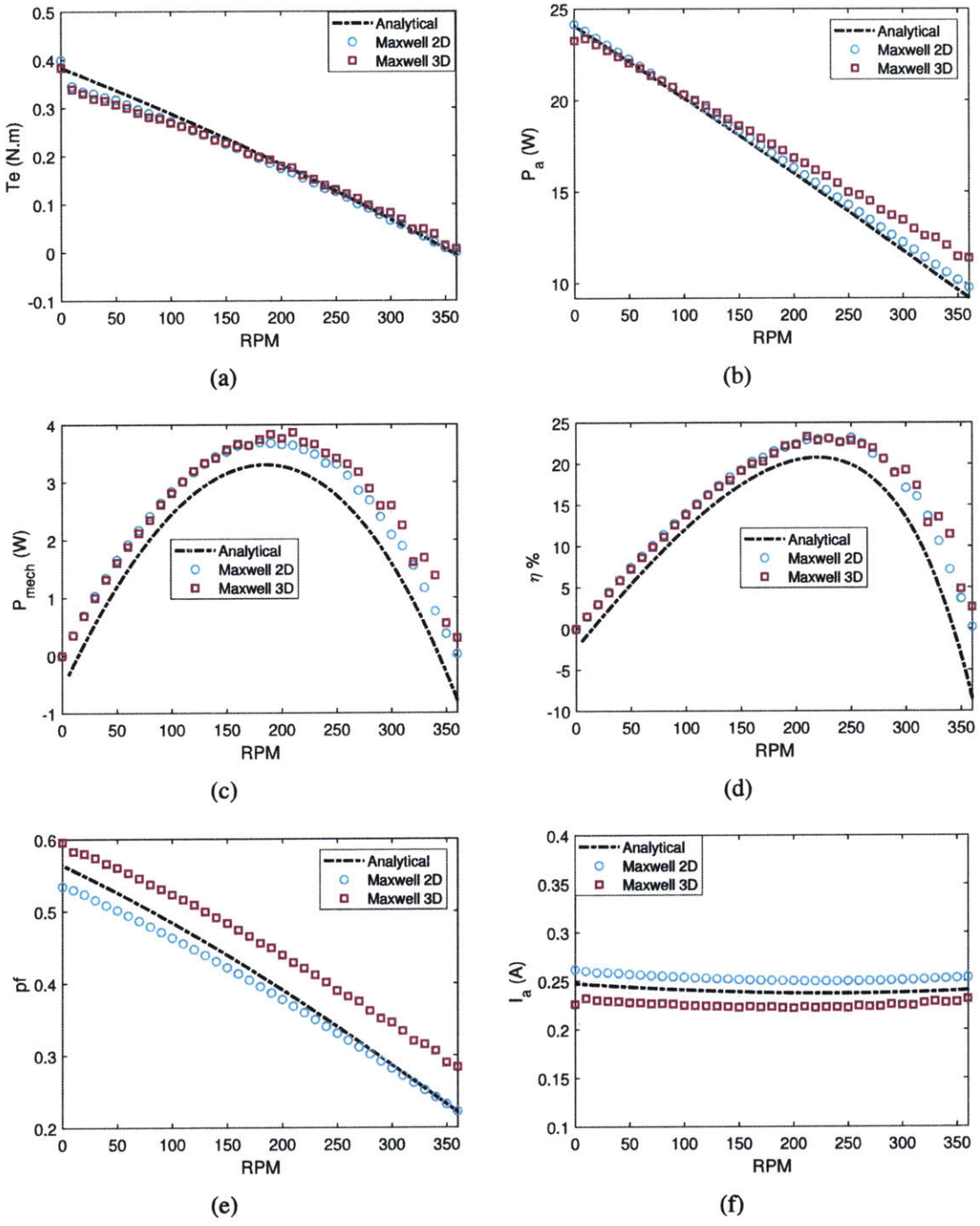

Figure 4-8: Evaluation of initial design by the analytical Model and 2D FEA model in ANSYS: (a) torque (T_e), (b) input power (P_a), (c) mechanical power (P_{mech}), (d) efficiency ($\eta\%$), (e) power factor (pf), and (f) terminal current (I_a) vs speed in RPM

4.5 Design Optimization Using Genetic Algorithm

The objective of electric machine optimization is to find the dimensions, materials, and/or methods of assembly that will result in a relatively optimum machine design with respect to two or more optimization targets called attributes [31]. In electric machine design, attributes can be efficiency, cost, active weight, output power, torque, torque ripple, etc. These attributes are often affected by the optimization variables in a contradictory way. In this section, genetic algorithm (GA) metaheuristic optimization is applied to the analytical model developed in Chapter 3 to assist in finding an optimum (or nearly optimum) design for three phase induction motors intended for ceiling fans application. The optimization setup details are described in the following subsections.

4.5.1 Design Requirements

The desired specifications at rated speed of the ceiling fan motor are summarized in Table. 4.4. Ceiling fans in India are required to deliver an airflow rate of $220m^3/min$ at rated speed, which requires $15W$ of mechanical power exerted on the fan blades. This is based on real measurements of a typical ceiling fan in the lab and surveying commercial ceiling fans in the Indian market. Furthermore, the drive frequency is selected as 12 Hz to be able to run at a rated speed in the range of $300 - 360$ RPM which is average full speed of ceiling fans in India.

Moreover, the drive voltage in this design problem is considered as a design requirement rather than an optimization variable. It is chosen to ensure that a simple, cost effective power electronic drive can be realized to drive the motor. A low voltage (as low as 6 V) can also be used to drive the motor with corresponding larger wire gauge. Although lower voltage may appear advantageous at first due to the lower armature losses and mechanically stronger wire, this imposes extra requirement on the power electronic drive circuit (Fig. 1-1). Specifically, the rectified voltage of the outlet supply in India is $325V$ peak, and if the motor is rated at lower voltage (e.g. $12V$ peak), and given that we are driving the inverter with sinusoidal pulse-width-modulation (PWM) or space vector modulation (SVM) as shown in Fig. 1-1, a small modulation index (m_a) is required to run the motor at full

speed. And in case of slower speed settings, even a lower m_a would be required. Inverters driven with sinusoidal PWM or SVM with low modulation index tend to have higher losses, and in cases where the modulation index is extremely low, it is not even feasible. To overcome this problem, an additional power electronic device is required (for example Flyback converter) to step up the dc link voltage of the inverter to a reasonable level to drive the motor with a higher modulation index ($m_a \sim 0.5 - 1$) at all speed settings. This adds to the cost of the power electronic drive circuit.

Table 4.4: Design requirements

Spec	Value	Spec	Value
Converted Power P_{mech}	$15W$	Line voltage, frequency	$230V_{rms}$, $50Hz$
Active Weight M	$< 10kg$	Synchronous Speed n_s	360 RPM
Maximum Flux Density	$< 1.8T$	Drive Frequency f	$pn_s/60 = 12Hz$
Wire Gauge	$> 0.321mm$ diameter ($>$ 28 AWG)	Drive Voltage	$115V_{rms}$
Rated Speed n_{rated}	> 250 RPM	Power factor	> 0.4

It is worthy to note that the requirement on the motor power factor is not very high ($pf > 0.4$) since the input power factor (at the input terminals of the power electronic package) can be easily corrected by provision of a power-factor-correcter (PFC) circuit without adding significant cost to the power electronic circuit.

4.5.2 Cost Function

Since the goal here is to see whether three phase induction motors – potentially those which can power home appliances – can be made efficient yet cost effective, efficiency and active weight of the motor are chosen as the optimization attributes.

Efficiency of the motor is an important attribute as it indicates how much power a consumer can save by replacing their typical ceiling fan ($70W$ consumption) with the proposed optimized induction motor. However, there is a trade-off between cost and efficiency. If efficiency was the only attribute to be optimized, it would be possible to achieve high efficiency ($\sim 82 - 85\%$) but at the expense of bulkier, heavier, and more expensive motor. Furthermore, we enforce a maximum limit on the weight of a typical household ceiling

fan as shown Table. 4.4. This limit is chosen based on surveying the average weight of a typical ceiling fan in India. It was found the average weight of the typical $70W$ household ceiling fan in India is around $3.5kg$ and the maximum weight does not exceed $10kg$.

In this optimization task, a scalar cost function formed by the product of inverse of efficiency and active weight is considered:

$$f = \frac{1}{\eta^{\alpha_\eta}} M^{\alpha_m} \tag{4.1}$$

where η refers to efficiency in percents, refers to the active weight of the motor in kg, and α_η and α_m are their corresponding exponents, respectively.

4.5.3 Genetic Algorithm

Genetic algorithm is a meta-heuristic optimization technique that is used for objective functions with multiple local minimums. Depending on the multi-optimization problem at hand, genetic algorithm is generally used to reach to the global optimum point. A genetic algorithm, referred as 'ga'in MATLAB, is used to optimize the motor design. The algorithm starts with a population of motor specifications called individual solutions or genes at which it evaluates the fitness function as per equation (4.1). Based on the score, it randomly selects individuals from the current population and uses them as parents to produce new specifications called children for the next generation. The new generation or so called evolution is generated through series of genetic operators, such as selection, crossover and mutation. A small portion of the fittest candidates called elites may be sent directly into the next generation. Over many iterations, the population evolves toward an optimal solution [43]. The GA settings used in the optimization are listed in Table. 4.5. Other settings of the MATLAB 'ga'optimization algorithm remains as default. It is worthy to note that studying genetic algorithms and enhancing its performance is out of the scope of this work, and for more details about the algorithm we strongly recommend the reader to refer to [43].

Table 4.5: GA settings

Setting	Value	Setting	Value
Population size	100	Fitness Scaling	Proportional
Number generations	150	Elite Count	5
Selection function	Rank	Crossover fraction	0.8

4.5.4 Optimization Variables and Fixed Parameters

The optimization variables are tabulated in Table. 4.6. They are chosen based on the designer engineering knowledge of machine design and experimenting with various combinations of optimization variables. For example, the stator slot opening width (u_s) is made to be at least $1mm$ to ensure that a an average gauge wire (e.g. AWG 27) can be physically inserted in the slot. Furthermore, the maximum limit on the rotor slot height was chosen based on experience to be not larger than $10mm$ (or appropriate depending on design goal whether it is favouring efficiency or active weight) to ensure that peak flux density in the rotor back-iron does not exceed $1.8T$ (another design requirement).

Table 4.6: Motor design optimization variables

Variable	Symbol	Bound $[min\ max]$	Variable	Symbol	Bound $[min\ max]$
Number of turns per coil	N_c	[1 300]	Rotor tooth to slot-pitch ratio	$K_{t\tau,r}$	[0.3 0.7]
Rotor yoke diameter	D_{ry}	[100 200]mm	Rotor end-ring radial height	h_{er}	[1 10]mm
Rotor core depth	$d_{c,r}$	[20 25]mm	Rotor end-ring axial length	l_{er}	[1 15]mm
Physical airgap	g	[0.5 1]mm	Stator slot opening width	u_s	[1 3]mm
Active length	l	[10 40]mm	Stator slot opening depth	d_s	[0.5 3]mm
Rotor slot opening width	u_r	[0.5 3]mm	Stator tooth to slot-pitch ratio	$K_{t\tau,s}$	[0.3 0.7]
Rotor slot opening depth	d_r	[0.5 3]mm	Stator slot height	h_s	[1 35]mm
Rotor slot height	h_r	[1 8]mm	Number of slots short pitched	N_{sp}	$\{0, 1\}$

All the other parameters are fixed during optimization. From experimenting with differ-

ent number of pole pairs it was noticed that two or three pole pairs are ideal for optimizing performance of small induction motors. In this work, the pole pairs is fixed to two. Furthermore, the number of stator slots is chosen to be 24 (proportionate to small motors) and rotor slots to be 18. Note that it is recommended to use odd number of rotor slots, such as 21, to avoid even vibration, noise and cogging torque (see [38] Chapter 6.11.1 for further details). However, the number of rotor slots in this work is chosen as an even number ($N_r = 18$) to take advantage of the field symmetry which can reduce the computation time of FE simulations considerably. After the motor design is optimized and if we wish to use an odd number of rotor slots, we can change the number of rotor slots to 21 for example without significantly affecting the performance of the motor, or rerun the optimization routine with only one optimization variable (N_r) while all other variables fixed to the optimized values from the previous run. The fixed parameters of the motor design for three phase induction motors for ceiling fans in India is summarized in Table. 4.7.

Table 4.7: Fixed parameters in the motor design

Fixed parameters	Value	Constants
Number of pole pairs, p	2	$\sigma_{Al} = 2.3 \times 10^7\ S/m$
Number of stator slots N_s	24	$\sigma_{Cu} = 5.84 \times 10^7\ S/m$
Number of rotor slots N_r	18	$\rho_{Cu} = 8400 kg/m^3$
Packing factor κ_{cu}	0.45	$\rho_{Al} = 2800 kg/m^3$
Stacking factor κ_{stack}	0.95	$\rho_{air} = 1.225 kg/m^3$
		$\nu_{air} = 1.56 \times 10^{-5} kg/m^3$

4.5.5 Optimization Results

Based on the different design requirements, motor application and cost constraints, the attributes exponents of cost function (equation 4.1) may be of different power according to the attribute importance. In this design, since we want high efficiency with a relatively low weight (hence cost), it is likely that we require the efficiency attribute exponent (α_η) to be higher than the active weight exponent (α_m). To reach to a satisfactory trade-off between efficiency and active weight, we try different combination of their corresponding exponents in the objective function. Not only this ensures that we reach to the 'best 'optimized design

for a balance between efficiency and weight, but also does assist us to survey different designs that may be suitable for other design targets such as high efficiency requirement with no cost constraint or very light motor with no emphasis on efficiency. A total of seven optimized designs are produced by selecting different combination of the exponents of the objective function attributes (α_η & α_m). Table. 4.8 summarizes the eight different optimization runs (schemes) with their corresponding attribute exponents (α_η & α_m).

Table 4.8: Exponents of the optimization attributes of the eight different optimization schemes

Attribute exponent	f_1	f_2	f_3	f_4	f_5	f_6	f_7
α_η	1	1	0	4	2	4	3
α_m	1	0	1	2	4	1	4

One of the best ways to visualize the tradeoffs between the optimization attributes and facilitate the process of selecting the best compromise between them is the Pareto frontier. Fig. 4-9 shows a two-dimensional Pareto frontier of the seven optimization functions indicating active weight versus efficiency of all the feasible solutions (given in Table. 4.8). The feasible solutions meet the design requirements in Table. 4.4. The best fit (optimal solution) reached by the GA for each optimization objective is indicated by the red dot in each of the sub-figures in Fig. 4-9. The corresponding motor data (optimized variables, calculated dimensions and calculated flux densities) of the seven optimized designs is provided in Table. 4.9. The equivalent circuit parameters evaluated by the analytical model for the optimized designs are also provided in Table. 4.10.

In Fig. 4-9, each Pareto frontier figure shows the feasible solution space. The minimum active weight and maximum efficiency achieved is represented by a solid black line to represent the optimal Pareto line. Among the feasible solutions, the genetic algorithm selects an optimal point indicated by red dot on the line. The optimal Pareto line can be fitted with a polynomial curve (convex) that pass through the optimal point. For the purpose of this analysis the optimal Pareto line shown in Figs. 4-9a - 4-9g is sufficient to explore the different designs.

By examining the Pareto frontiers in Fig. 4-9, a lot of insight can be gained from the location of feasible solutions and the trend they follow. For example, it can be observed that

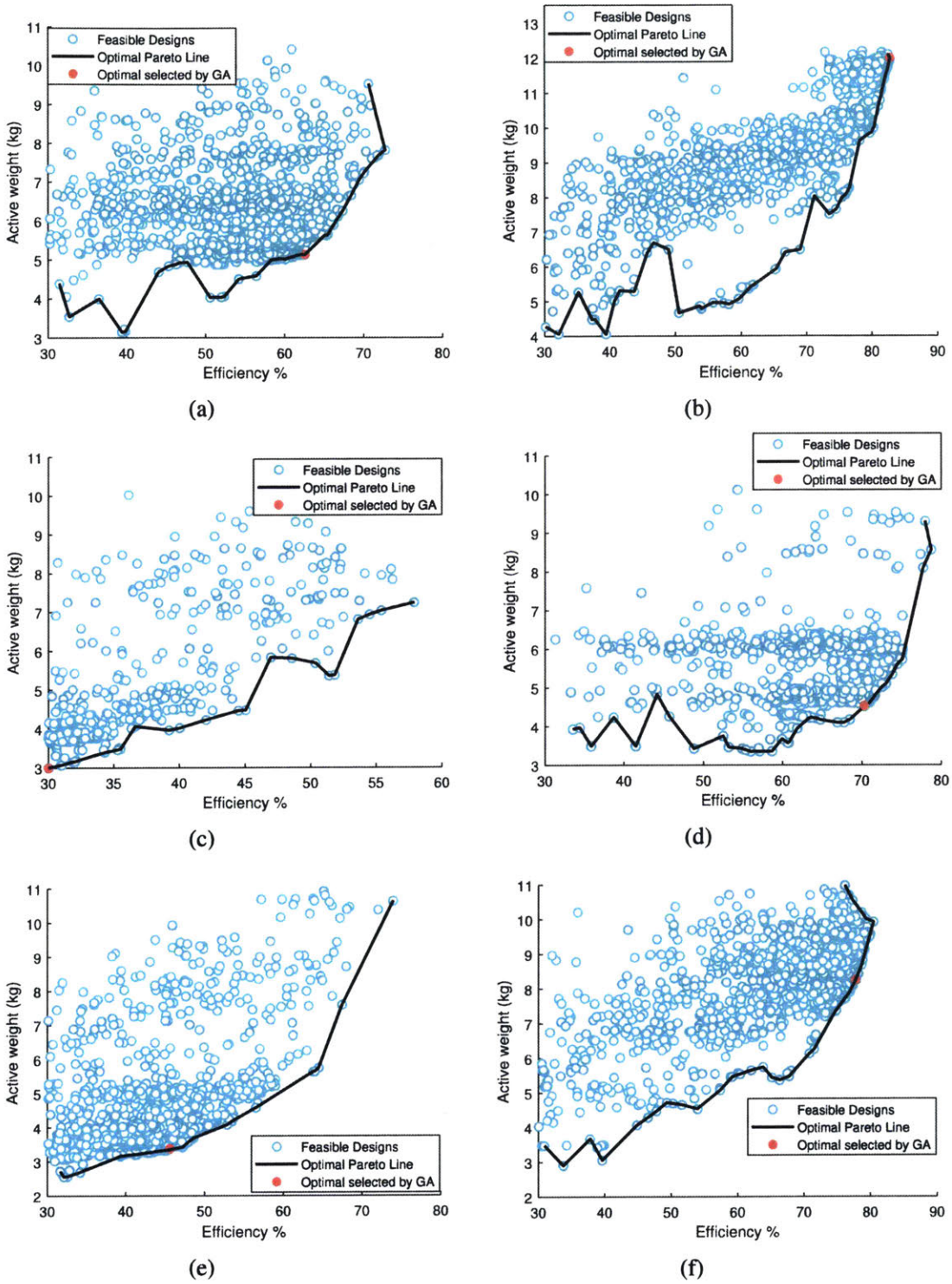

when only efficiency is considered in the cost function (design 2) where $\alpha_\eta = 1$ &$\alpha_m = 0$ as shown in 4-9b, the feasible solutions found almost follow a trend that approximates

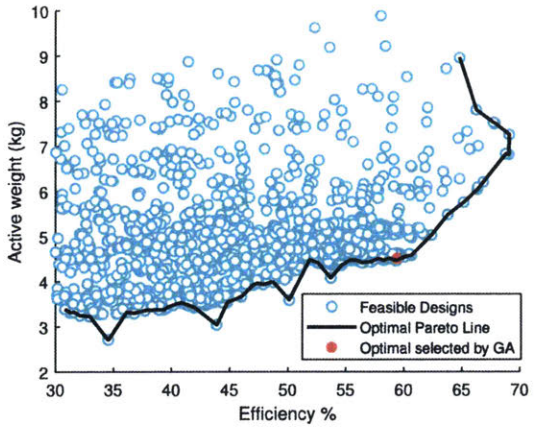

(g)

Figure 4-9: Dominating designs reached by GA illustrating efficiency versus active weight for the different optimization objectives: (a) $\alpha_\eta = 1$ $\alpha_m = 1$, (b) $\alpha_\eta = 1$ $\alpha_m = 0$, (c) $\alpha_\eta = 0$ $\alpha_m = 1$, (d) $\alpha_\eta = 4$ $\alpha_m = 2$, (e) $\alpha_\eta = 2$ $\alpha_m = 4$, (f) $\alpha_\eta = 4$ $\alpha_m = 1$, (g) $\alpha_\eta = 3$ $\alpha_m = 4$

a linear curve indicating that higher efficiency can be achieved at the expense of higher weight (except for few outliers). On the other hand, when only weight is optimized such as in design 3 where $\alpha_\eta = 0$ & $\alpha_m = 1$, most feasible solutions are concentrated in at the bottom left corner of the plot suggesting lighter designs at the expense of lower efficiency (4-9c). Equal importance given to efficiency and active weight attributes in design 1 Pareto frontier ($\alpha_\eta = 1$ & $\alpha_m = 1$) as shown in Fig. 4-9a. In this optimized design, most feasible solutions concentrated in center of the plot as the GA tries to find feasible solutions that satisfies a balance between active weight and efficiency. This can be also observed by noting that the optimal solution indicated by the red dot on the optimal Pareto line is located at the middle. More combinations of attribute exponents are tried in Figs. 4-9d - 4-9g by either giving more importance to efficiency or to active weight. This provides the designer of a larger spectrum to choose from when designing a motor, and to better reach to a compromise between all the contradicting attributes. Figs. 4-9d & 4-9e ($\alpha_\eta = 4, 2$ & $\alpha_m = 2, 4$, respectively), for example, shows a better compromise between efficiency and active weight with emphasis on either one of them. That is, if the designer cares more about efficiency but also require a reasonable weight, they may want to select design 4 over design 5, and vice versa. Similar insights can be drawn from design 6 & 7 (Figs.4-9f &

Table 4.9: Optimized motor data found by the GA for the different optimized designs

Optim. Variable	$\alpha_{\eta,m} = 1,1$	1,0	0,1	4,2	2,4	4,1	3,4
N_c	290	278	293	288	289	300	294
$D_{ry}(mm)$	158.3	199.4	149.85	160	139.5	180.6	155.2
$d_{c,r}(mm)$	21.2	20.6	20.3	20	20.6	20.95	20
$g(mm)$	0.51	0.56	0.6	0.5	0.51	0.5	0.52
$l(mm)$	30.2	40	19.6	29.5	26.34	0.034	26.7
$d_r(mm)$	2.95	2.95	3	3	2.75	2.66	2.96
$u_r(mm)$	1.7	0.8	0.93	0.54	0.66	0.74	0.89
$h_r(mm)$	5.8	5.9	6	5.7	5.93	5.56	5.95
$K_{tr,r}$	0.35	0.3	0.53	0.41	0.45	0.31	0.39
$h_{er}(mm)$	9.1	9.9	8	9.2	7.4	9.5	6.8
$l_{er}(mm)$	12.5	15	11.22	10	11.3	4.4	13.85
$d_s(mm)$	2.7	0.66	2.99	1.6	2.54	2.81	2.24
$u_s(mm)$	1.12	1.12	1.22	1.1	1.01	1.12	1.01
$K_{tr,s}$	0.33	0.3	0.55	0.31	0.43	0.3	0.37
$h_s(mm)$	19.7	34.8	8.66	25.7	17.7	31.2	21.3
N_{sp}	0	0	0	0	0	0	0
Calc. dimensions (mm)							
D_{rg}	115.9	158.2	109.2	120	98.2	138.7	115.1
t_r	7.9	8.9	11.3	9.4	8.7	7.9	8.7
w_r	14.4	20.7	9.9	13.6	10.5	18.2	13.4
t_s	4.8	6.1	7.3	4.7	5.2	5.2	5.3
$w_{s,top}$	9.6	14.3	6	10.5	6.9	12.1	9.1
$w_{s,bot}$	4.4	5.2	3.8	3.8	2.2	3.9	3.5
wire diameter	0.59	0.368	0.204	0.427	0.283	0.349	0.361
Calc. $B(T)$							
$B_{r,1}$	0.55	0.32	0.91	0.55	0.75	0.4	0.62
$B_{c,s}$	0.4	0.27	0.51	0.46	0.56	0.35	0.47
$B_{t,s}$	1.59	1.02	1.57	1.69	1.67	1.26	1.61
$B_{c,r}$	0.99	0.82	1.64	1.1	1.19	0.85	1.21
$B_{t,r}$	1.57	1.07	1.7	1.35	1.66	1.31	1.58

4-9g).

Furthermore, each optimized motor design is evaluated by the analytical model as shown in Fig. 4-10. The electromagnetic torque of the motor (T_e), input power (P_a), converted mechanical power (P_{mech}), efficiency (η), power factor (pf), and terminal current (I_a) of the optimization schemes are compared as shown in Figs. 4-10a–4-10f. From Fig. 4-10a it can be noticed that the electromagnetic torque, and converted mechanical power,

Table 4.10: Equivalent circuit parameters for the different optimized designs

Circuit element (Ω)	$\alpha_{\eta,m} = 1,1$	$1,0$	$0,1$	$4,2$	$2,4$	$4,1$	$3,4$
R_1	73.11	36.6	222.6	53.98	104.29	48.35	73.57
X_1	52.81	44.39	37.1	47.64	48.5	62.9	50.85
$X_{m,1}$	730.7	1.127k	389.63	1.09k	556.66	1.1K	671.5
$R_{2,1}$	161	146.6	179.42	193.25	187.59	167.57	184.49
$X_{2,1}$	41.8	78.35	36.36	85.85	54.58	76.76	52.34
$X_{m,5}$	2.1	2.12	0.84	3.14	1.6	2.44	1.93
$R_{2,5}$	11.5	6.89	9.7	13.88	13.47	9.29	13.23
$X_{2,5}$	5.2	5.9	2.85	9.46	5.6	6.82	5.77
$X_{m,7}$	2.1	2.12	0.84	3.14	1.6	2.44	1.93
$R_{2,7}$	11.5	4.18	7.09	13.88	13.47	7	13.21
$X_{2,7}$	14.97	9.57	4.95	24.07	13.04	13.68	14.73
X_{m,z_-}	6	0.25	0.51	9.03	4.6	1.78	5.51
R_{2,z_-}	160.77	3.94	28.3	193.25	187.59	32.84	183.29
X_{2,z_-}	207.39	8.96	19.65	333.76	180.87	63.91	203.36
X_{m,z_+}	4.32	0.06	0.09	6.47	3.29	0.41	3.94
R_{2,z_+}	160.72	1.28	6.73	193.25	187.59	10.64	182.82
X_{2,z_+}	70.16	1.07	1.93	128.4	76.25	7.59	77.78
R_c	205.5k	168.9k	448k	148.2k	235.9k	153.94k	200.25k
X_c	87.4k	768.6k	141.4k	64.3k	91.29k	73.4k	84.42k
$R_{rt,snl}$	38.5k	190.8k	11.62k	43.2k	19.34k	1.01k	36.84k

(I_a) of the optimization schemes are compared as shown in Figs. 4-10a–4-10f. From Fig. 4-10a it can be noticed that the electromagnetic torque, and converted mechanical power, and efficiency for $\alpha_{\eta,m} = 1,0$ is the highest as compared to all other designs while it is the lowest for $\alpha_{\eta,m} = 0,1$. This is not the case, however, for the power factor where the light weight design $\alpha_{\eta,m} = 0,1$ has the the highest power factor from locked rotor condition to $230RPM$ and starts declining pass afterwards. In general, these analytical results further help the designer to select the optimal design for their application based on other design requirements and performance metrics, such as torque, converted power, power factor and input current.

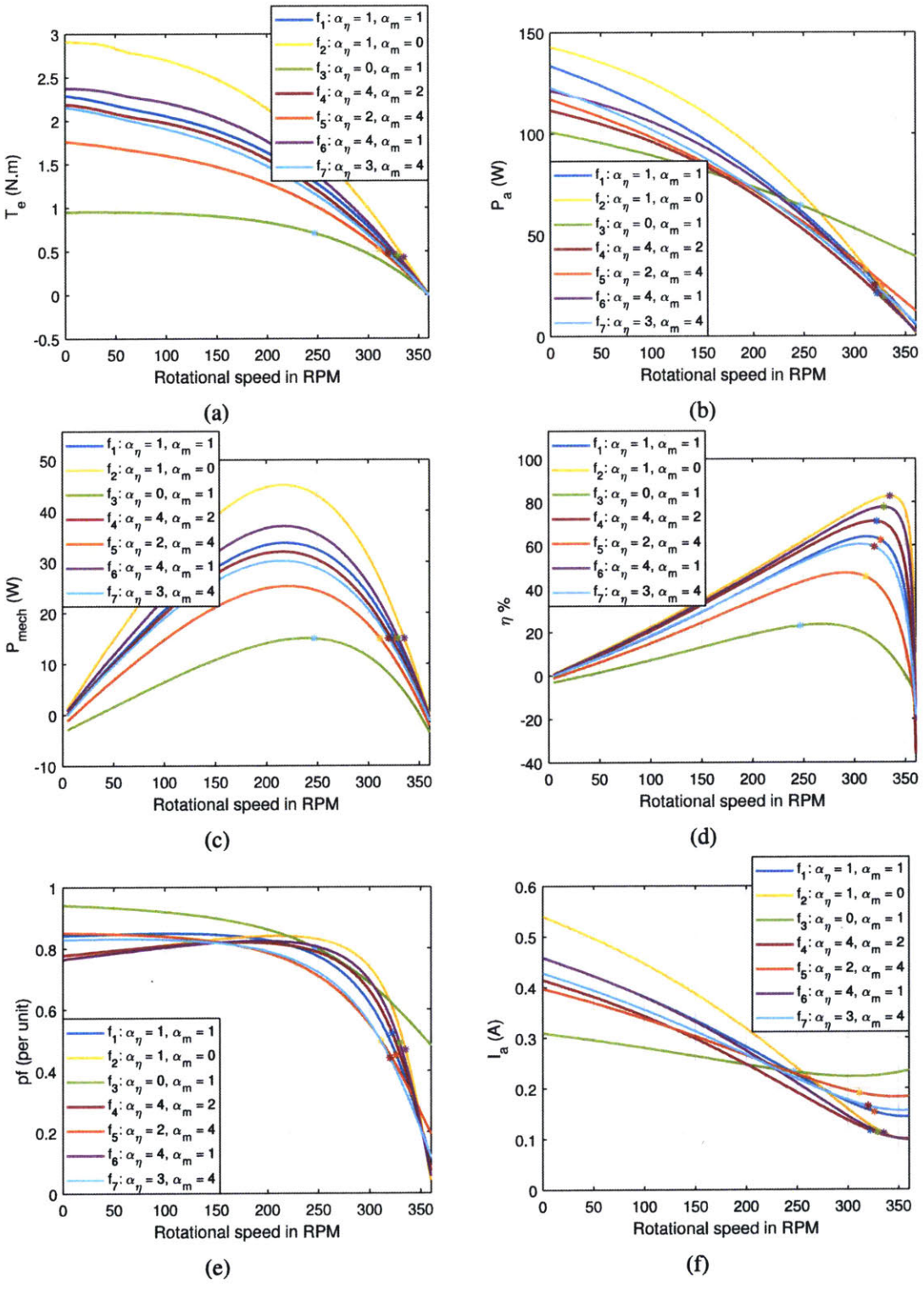

Figure 4-10: Evaluation of each optimized motor design by the analytical model: (a) torque (T_e), (b) input power (P_a), (c) converted mechanical power (P_{mech}), (d) efficiency ($\eta\%$), (e) power factor (pf), and (f) terminal current (I_a) vs speed in RPM

4.6 Optimized Motor Design for Ceiling Fans

To further assist in selecting the 'best 'motor design for ceiling fans, the optimal points evaluated for efficiency and weight of each optimization run are compared in the bar graph of Fig. 4-11. It can be seen from the bar graph that the optimized design with attribute exponents of $\alpha_{\eta,m} = 4, 2$ (design 4) gives the best trade off between efficiency and active weight which best satisfies the design objective of ceiling fan motors in India. Therefore, it is selected as the 'best 'design for three phase squirrel cage induction motor to drive ceiling fans that satisfy the requirements given in Table 4.4. The corresponding efficiency for the selected optimized motor at rated speed of 321.7 RPM is $\eta = 70.31\%$ and active weight of $M = 4.53kg$. Note that we do not claim that this design is the 'global'optimum design, rather we suggest it is superior to the other six optimized designs in terms of satisfying a balance between efficiency and active weight.

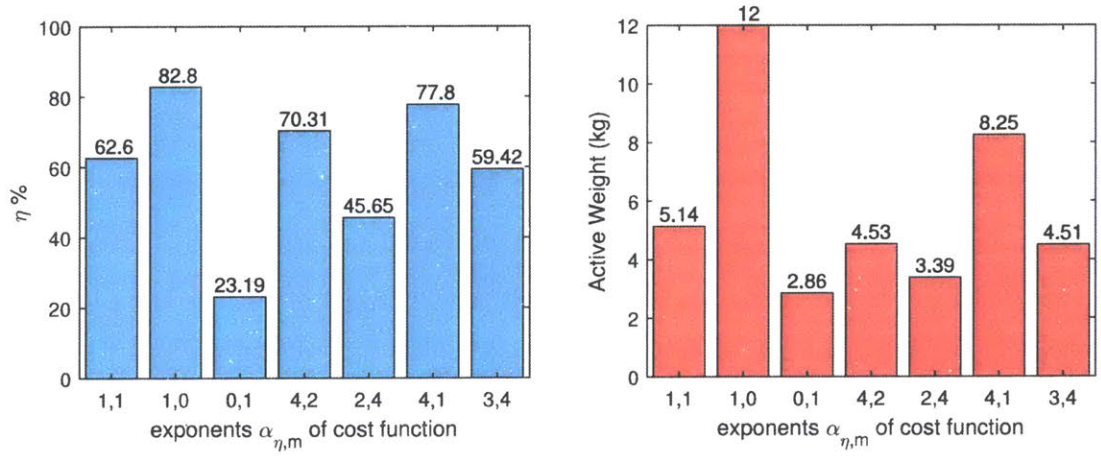

Figure 4-11: Optimal solution found by GA corresponding to each optimization run objective function: (a) efficiency (b) active weight

The selected optimized design (f_4, $\alpha_{\eta,m} = 4, 2$) is simulated in Maxwell 2D FE transient analysis (Fig. 4-12). Unlike the iron regions where a relatively coarse mesh may be sufficient for accuracy, a fine mesh at the rotor bars and airgap is required to attain high accuracy. This along with sufficiently small time step, high accuracy of the FEA solutions can be attained. Fig.4-13 shows the mesh of the 2D FE model of the optimized motor

design obtained from the optimization results in Section 4.5.5.

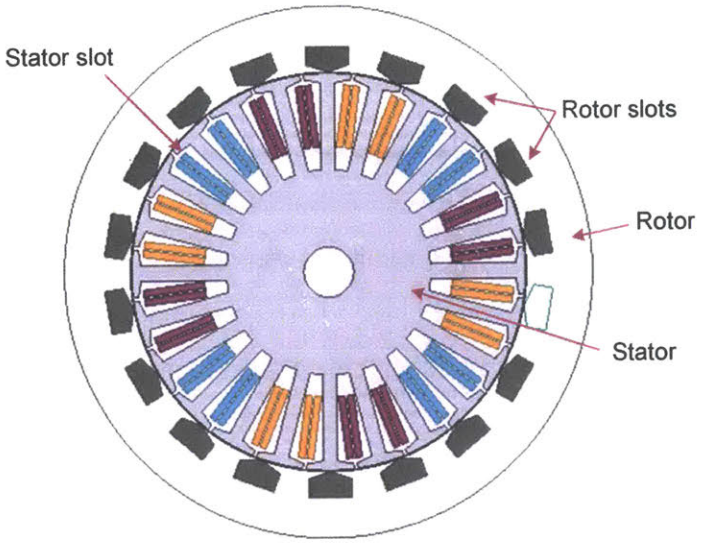

Figure 4-12: 2D FE model of optimized motor design

In the manufacturing process, casting aluminum bars in closed slot is easier than semi closed slots. Therefore, the rotor slot is made with no slot opening (closed slot) as shown in Fig. 4-13b. In addition, slightly tapered rotor slots are used to help reduce flux saturation at the corner regions of the rotor teeth (Fig. 4-13b). Similarly, stator slots are drawn in the FE 2D model slightly tapered from the top to reduce flux saturation in the teeth. Furthermore, trapezoidal shape stator slots are adopted in optimized design (as well as the analytical model) to ensure a uniform teeth width, and thus reduce flux saturation along the stator teeth.

The optimized motor parameters are fed to both the analytical and FE models, and the performance metrics are compared as shown in Fig. 4-14. The electromagnetic torque of the motor, input power, converted mechanical power, efficiency, power factor, and terminal current are plotted against speed as shown in Figs. 4-14a–4-14f. A red dashed line plotted for each curve indicates the rated speed of 321.7 RPM of the optimized motor satisfying the $15W$ converted mechanical power design requirement.

From Fig. 4-14, it can be seen that the analytical model closely matches with the FE 2D model (> 150 RPM) for almost the whole speed range. The following observations are made based on the performance plots:

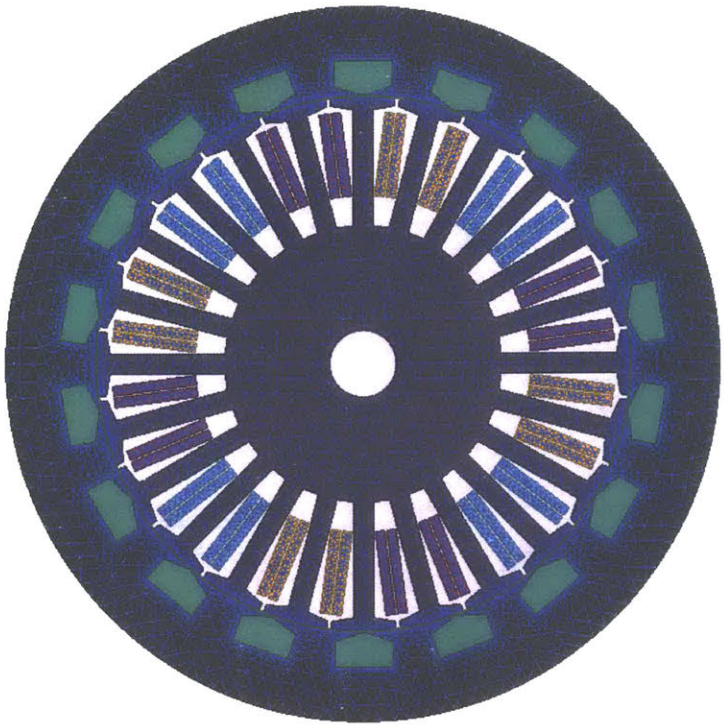

(a)

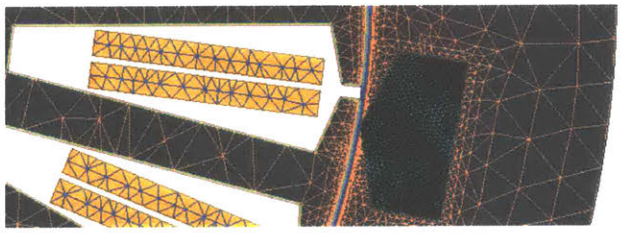

(b)

Figure 4-13: Mesh at different regions of the 2D FE model of the optimized motor design

(1) The electromagnetic torque, motor input power, converted power, efficiency (Fig. 4-14a, 4-14d) closely match with the analytical model for the entire speed range with percentage error of less than 5%. The slight mismatch (within 5%) is in the lower speed range ($0 - 150$ RPM).

(2) A slight dip in the electromagnetic torque at speed $360/7 = 51.4$ RPM can be seen due to the 7th harmonic forward wave. It is clear that this dip is very mild that it does not affect the starting of the motor. This dip can be easily mitigated, if desired, by skewing the rotor bars by one rotor slot pitch with only slight reduction in efficiency.

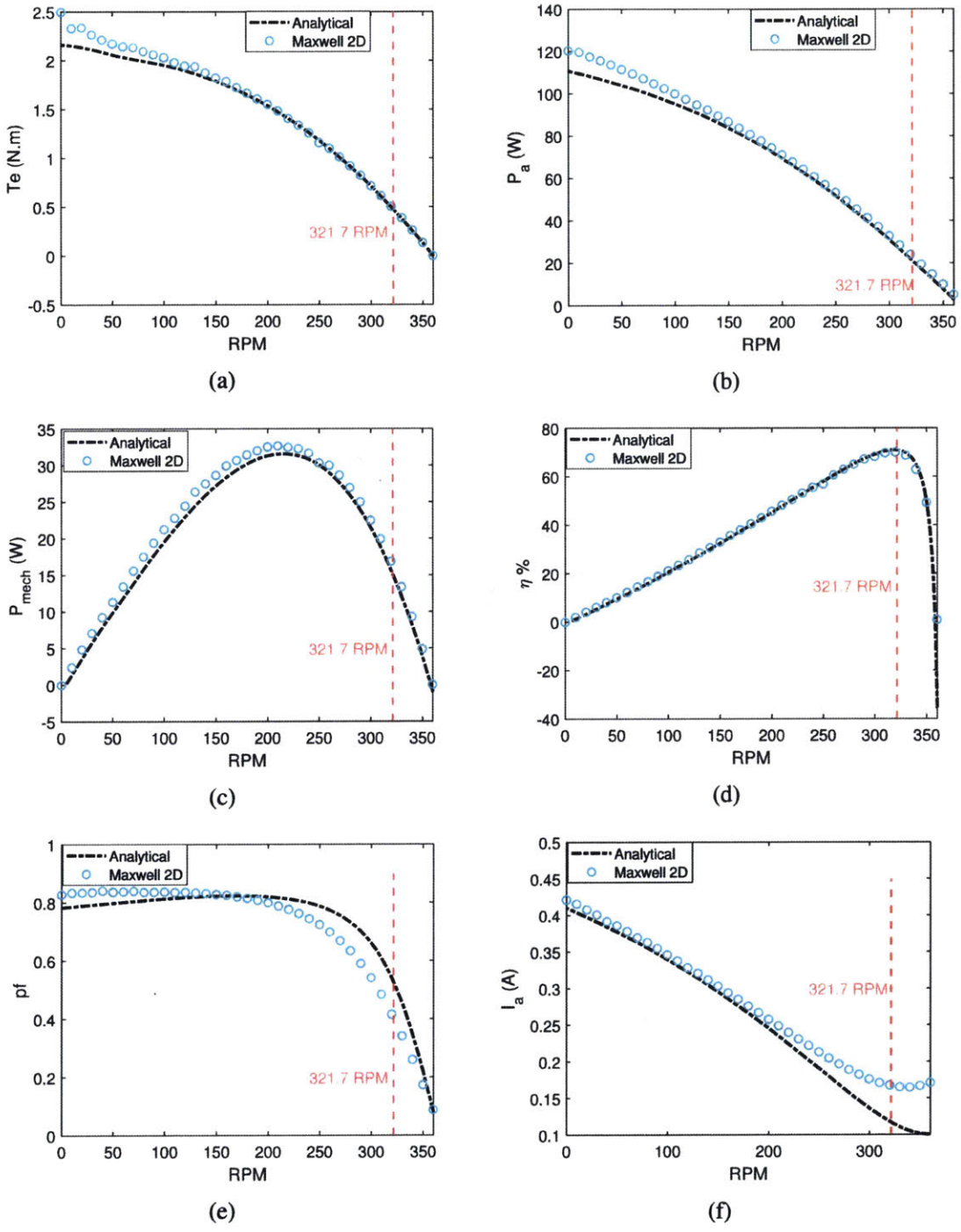

Figure 4-14: Verification of analytical optimized design ($\alpha_\eta = 4, \alpha_m = 2$) using Maxwell 2D FEA: (a) torque (T_e), (b) input power (P_a), (c) converted mechanical power (P_{mech}), (d) efficiency ($\eta\%$), (e) power factor (pf), and (f) terminal current (I_a) vs speed in RPM

(3) Examining the power factor curves in Fig. 4-14e, there is a percentage error of $0 - 12\%$ across the full speed range between the analytical model and FE 2D model.

(4) The stator current of the analytical model closely matches with that of the FE model from standstill to 200 RPM. After 200 RPM, the two curves start deviating from each other. A maximum difference of 50% is noticed at synchronous speed.

In conclusion, with the exception of the stator current, all the performance metrics including torque, mechanical power, power factor and efficiency are matched between the analytical and FE 2D model. The FE model predicts higher stator current at rated speed than that of the analytical model. We anticipate that this can be due to the two main reasons. First, the stator and rotor teeth are observed to slightly saturate ($B \sim 1.9T$) near synchronous speed. The second reason might be due to the fact that the loss elements calculated by the analytical model does not exactly match with that calculated by the FE model in spite of the match between the total losses (the powers {input and mechanical} are similar and thus the efficiency).

4.7 Sensitivity Analysis

The main goal of the sensitivity analysis is to understand which optimization variables most affect the optimization attributes and how they affect them. It provides the designer a great tool to visualize the prime design factors that they can control to meet the design requirement and most importantly optimize their motor design.

4.7.1 Sensitivity Analysis Setup

In this section, we perform the sensitivity analysis on the optimized design (Design 4) selected in Section 4.6. The sensitivity analysis is performed on the analytical model by varying the two optimization variables while all other variables are held constant at the optimized values. The objective attributes (efficiency and active weight), electromagnetic torque and converted power are evaluated in the sensitivity analysis at rated speed (321.7 RPM) as shown in Figs. 4-15, 4-16. The range at which the optimization variables are

varied is as chosen in the optimization exercise (Table. 4.6). From the sensitivity analysis, we wish to accomplish the following:

(1) Verify if the GA provided the optimal solution

(2) Observe how efficiency, active weight, converted power, and torque vary against the optimization variables.

(3) Zoom in around the optimal solution found by GA (design 4) and search in the nearby region. Find out, if exists, a nearby solution that that may achieve a 'better 'compromise between efficiency and active weight.

4.7.2 Sensitivity Analysis Results

Let us examine the sensitivity results in Figs. 4-15, 4-16. From Fig. 4-15a it can be noticed that the maximum efficiency can be obtained by minimizing the airgap and maximizing the active length which is a natural effect of increased torque that we know from electric machine theory. On the other hand the active weight increases with increased active length and minimized airgap as can be observed from Fig. 4-15b. That is why the GA performed on the optimization scheme (f_4,$\alpha_{\eta,m} = 4, 2$) gives us a compromise of efficiency and active weight as seen in the orange region of Figs. 4-15a, 4-15b. Furthermore, this suggests that if a physical airgap of less than $0.5mm$ can be realized by the motor manufacturer, a more efficient motor may be obtained without affecting the active weight. Note that the dark blue region to the most right of Figs. 4-15a, 4-15b represent areas where the requirement of mechanical power of $15W$ was not met (the algorithm returns zero if power constraint is not met).

It can learned from Figs.4-15c, 4-15d that the active weight does not change significantly with rotor slot height (h_r) and rotor tooth to slot ratio ($K_{t\gamma,r}$). However, there is an optimum range of h_r & $K_{t\gamma,r}$ at which an optimum efficiency can be attained as seen by the yellow region wherein the optimized design (design 4) lies within. This verifies that the GA reached to an optimal solution in terms of both efficiency and active weight.

Furthermore, it is evident from Figs. 4-16a, 4-16b that there is a trade off between efficiency and active weight as the stator slot height (h_s) and stator tooth to slot ratio ($K_{t,s}$)

varies. However, the reduction in active weight as $K_{t\gamma,s}$ increases is not significant, and consequently the GA converges in the yellow region to satisfy both high efficiency and acceptable active weight. We can deduce from this analysis that the efficiency can be improved by using a deeper stator slot (higher h_s) with larger stator slot top width (lower $K_{t\gamma,s}$). As mentioned earlier, the blue areas are regions where the mechanical power requirement is not met.

Finally, as expected the active weight does not depend much on the stator slot depression dimensions (d_s, u_s) as seen in Fig. 4-16d. On the other hand, the efficiency tends to depend only on the depression depth d_s. It can be noticed a higher efficiency up to 75% can be attained for example if d_s is increased to $3mm$ with a slight increase in active weight from $4.5kg$ (selected optimized design) to $5.42Kg$. This is powerful since it provides the designer with an insight on how to easily improve efficiency without redoing the optimization if they can tolerate the slight increase in active weight.

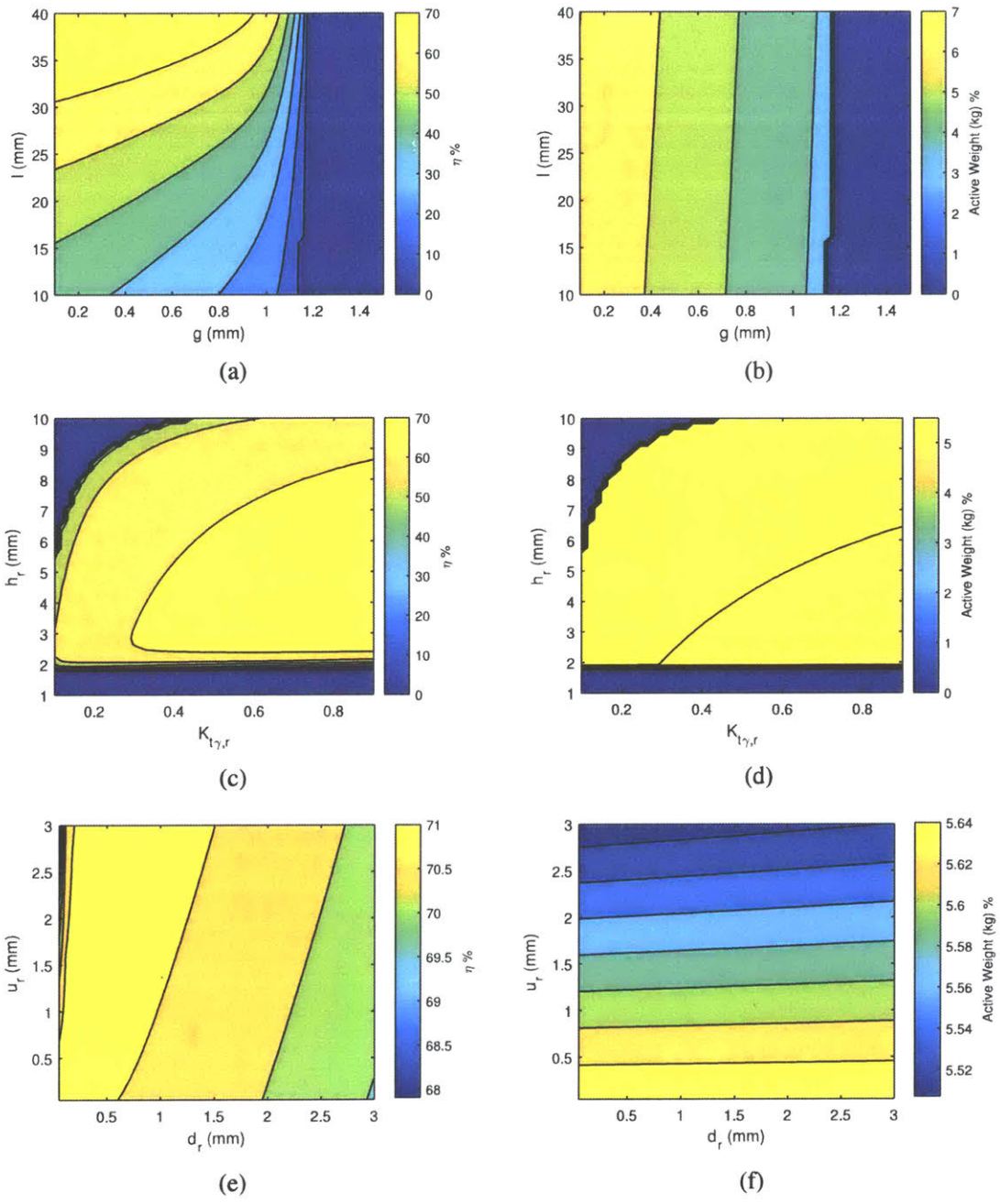

Figure 4-15: Contour maps showing the sensitivity of efficiency and active weight against two optimization variables around the optimal solution at rated speed (design 4): (a) g and l versus $\eta\%$ and (b) g and l versus M, (c) $K_{t\gamma,r}$ and h_r versus $\eta\%$ and (d) $K_{t\gamma,r}$ and h_r versus M (e) d_r and u_r versus $\eta\%$, (f) d_r and u_r versus M

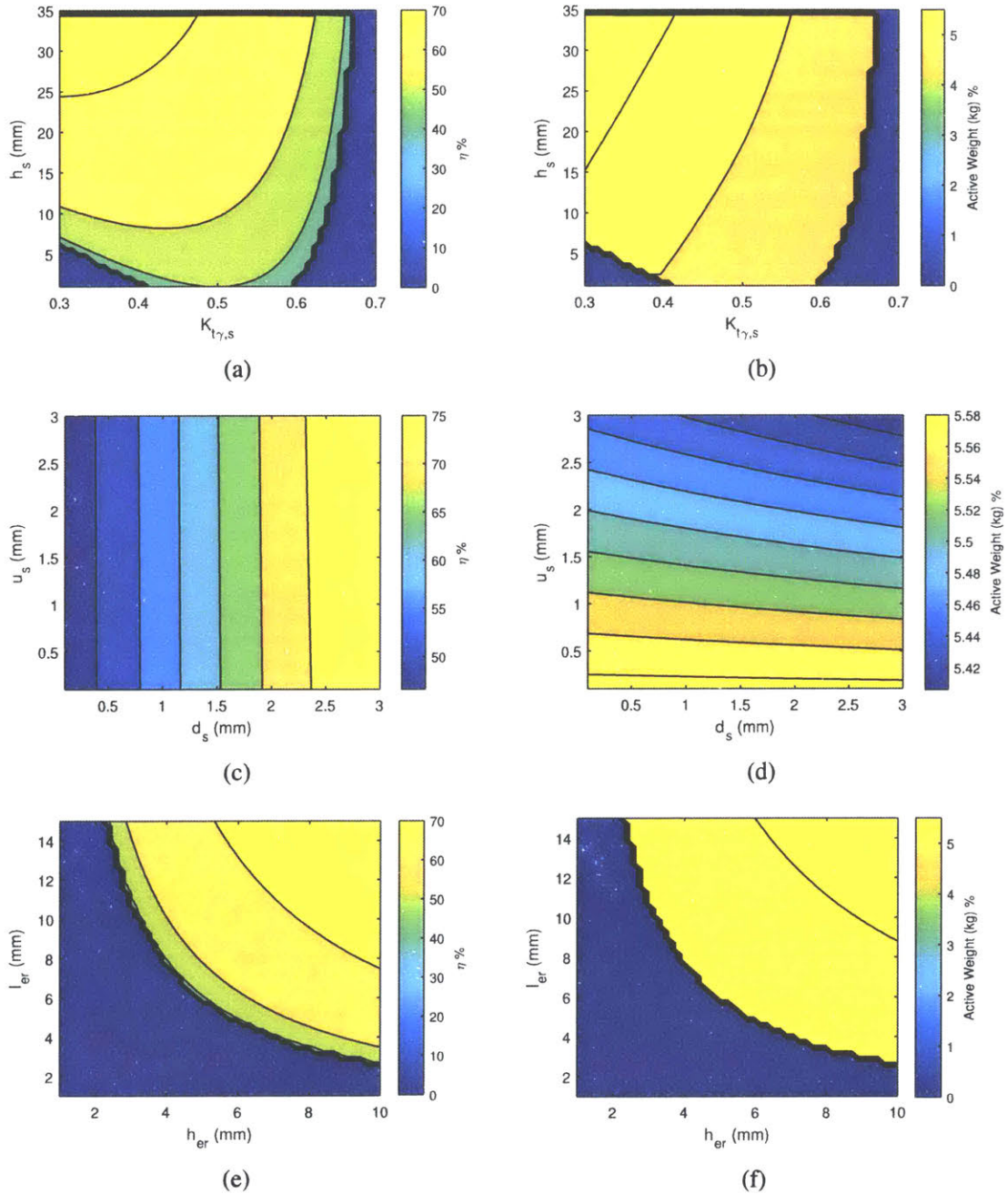

Figure 4-16: Contour maps showing the sensitivity of efficiency and active weight against two optimization variables around the optimal solution at rated speed (design 4): (a) $K_{t\gamma,s}$ and h_s versus $\eta\%$, (b) $K_{t\gamma,s}$ and h_s versus M, (c) d_s and u_s versus $\eta\%$, (d) d_s and u_s versus M(e) h_{er} and l_{er} versus $\eta\%$, (f) h_{er} and l_{er} versus M

Chapter 5

Evaluation of the Optimized Three Phase Induction Motor with the Adjustable Speed Drive

The main objective of this chapter is to validate the performance of the optimized three phase induction motor design (obtained in Chapter 4) driven by a power electronic drive circuit commonly known as adjustable speed drive. This provides the designer with a more practical view on the performance of the motor when driven by pulse-width-modulation (pwm) inverter. In this chapter, we will first describe the drive circuit along with its control scheme, then we will validate the performance of the motor with simulation results in Matlab/Simulink. It is worthy to note that it is not the focus of this thesis to propose a new drive topology nor control strategy for the power electronic drive circuit, rather evaluate the performance of the proposed optimized design with the power electronic drive and verify that it behaves as predicted in Chapter 4.

5.1 Three Phase Induction Motor Drive Circuit and Volt-Hz Speed Control

Fig. 5-2 shows the overall motor system adopted for ceiling fans along with the adopted control strategy for variable speed drive. The overall motor system (Fig. 5-2a) has two parts: the drive circuit and the optimized three phase squirrel cage induction motor. The drive circuit consists of a diode bridge rectifier (DBR), dc link capacitor, and a three leg inverter realized by MOSFET switching devices. The diode bridge rectifier converts the grid voltage from AC to DC, and the transformed electric energy is stored in the dc link capacitor. The dc link capacitor acts as an input dc voltage source to the inverter. volt-Hz (v/f) control is implemented to generate the unit reference voltage. Sinusoidal pwm scheme is implemented generate the gate signals relayed to the inverter to drive the motor at different speed settings. The volt-Hz controller is illustrated in the block diagram shown in Fig. 5-2b.

5.2 Motor Simulation Model

The rotor reference frame d-q model of the squirrel cage induction motor is adopted for the motor simulations. The d-q model uses only the fundamental component equivalent circuit elements, and thus it ignores the core loss branch, and higher order harmonic effects. Luckily, the core losses and slip losses of the optimized design is low, and thus the d-q model is sufficient to evaluate the performance of the motor against the drive circuit. We refer to [30, 32] to provide the d-q simulation model.

With the rotor quantities referred to the stator, the terminal behaviour of the machine can be described by its flux linkages in the d-q reference frame as:

$$\begin{aligned} \lambda_{ds} &= L_s i_{ds} + L_m i_{dr} \\ \lambda_{dr} &= L_m i_{ds} + L_r i_{dr} \\ \lambda_{qs} &= L_s i_{qs} + L_m i_{qr} \\ \lambda_{qr} &= L_m i_{qs} + L_r i_{qr} \end{aligned} \tag{5.1}$$

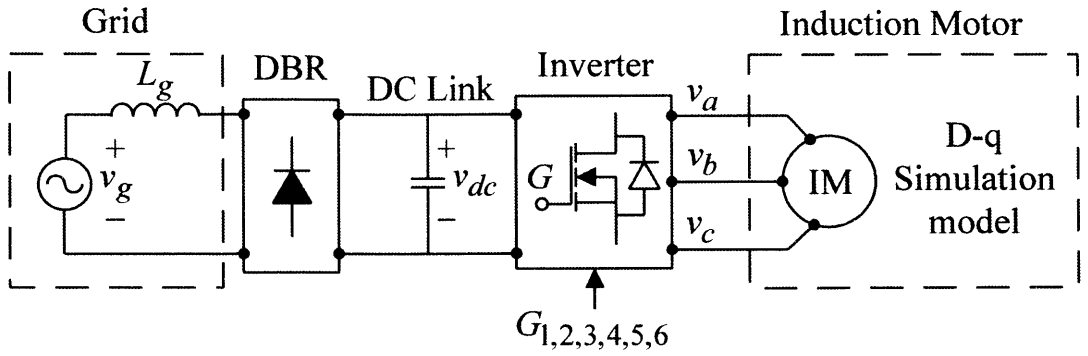

(a) Overall motor system consisting of the power electronic drive and the optimized three phase squirrel cage induction motor

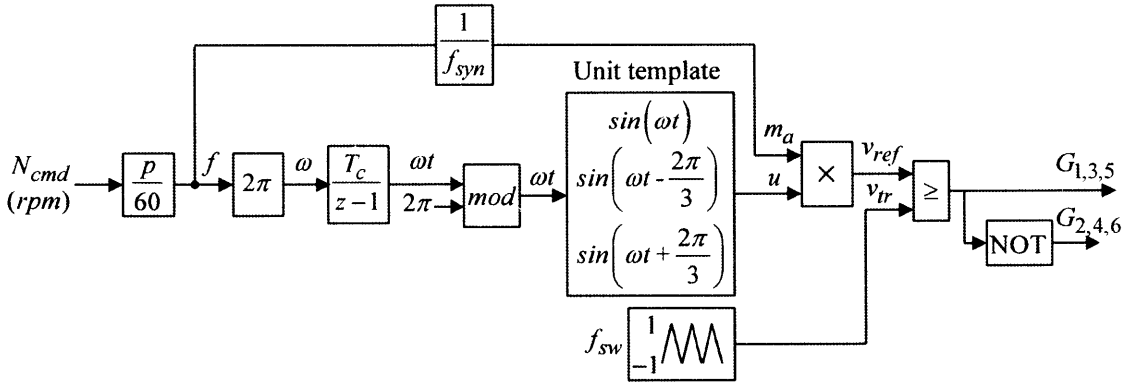

(b) Open loop volt-Hz speed control

Figure 5-1: Proposed three phase induction motor system to drive ceiling fans: (a) overall motor system, (b) volt-Hz speed control and pwm generation

where L_s, L_r are the stator and rotor self inductances respectively, L_m is the fundamental magnetizing inductance (same as $L_{m,1}$ defined as per equation 3.18).

And the stator and rotor voltage equations are:

$$\begin{aligned} v_{ds} &= \frac{d\lambda_{ds}}{dt} - \omega\lambda_{qs} + R_1 i_{ds} \\ v_{qs} &= \frac{d\lambda_{qs}}{dt} + \omega\lambda_{ds} + R_1 i_{qs} \\ 0 &= \frac{d\lambda_{dr}}{dt} - \omega_r\lambda_{qr} + R_2 i_{dr} \\ 0 &= \frac{d\lambda_{qr}}{dt} + \omega_r\lambda_{dr} + R_2 i_{qr} \end{aligned} \tag{5.2}$$

where, ω_r is the rotor electrical frequency in rad/sec:

$$\omega_r = \omega - p\omega_m = s\omega \tag{5.3}$$

In (5.3), ω and ω_m are the synchronous speed and rotor physical speed in electrical rad/s.

Note that $v_{dr} = 0 = v_{qr}$ for squirrel cage rotors in which the rotor bars are short circuited by end-rings from both sides. Since the rotor is round (no saliency) and the rotor is referred to the stator, the self inductances can be expressed as:

$$\begin{aligned} L_s &= L_m + L_1 \\ L_r &= L_m + L_2 \end{aligned} \tag{5.4}$$

where, L_1 and L_2 are the stator and rotor leakage inductances, respectively, as previously defined in Chapter 3.

Substituting (5.4) in (5.1), the d-axis and q-axis voltages can be rewritten as:

$$\begin{aligned} v_{ds} &= L_1\frac{di_{ds}}{dt} + L_m\frac{d(i_{ds}+i_{dr})}{dt} - \omega\lambda_{qs} + R_1 i_{ds} \\ v_{qs} &= L_1\frac{di_{qs}}{dt} + L_m\frac{d(i_{qs}+i_{qr})}{dt} + \omega\lambda_{ds} + R_1 i_{qs} \\ 0 &= L_2\frac{di_{dr}}{dt} + L_m\frac{d(i_{ds}+i_{dr})}{dt} - \omega_r\lambda_{qr} + R_2 i_{dr} \\ 0 &= L_2\frac{di_{qr}}{dt} + L_m\frac{d(i_{qs}+i_{qr})}{dt} + \omega_r\lambda_{dr} + R_2 i_{qr} \end{aligned} \tag{5.5}$$

From equation (5.5), the d-axis and q-axis equivalent circuits of dynamic simulation model of the squirrel cage induction motor can be deduced as shown in Fig. **??**.

The electromagnetic torque (in peak values) can be calculated in the d-q reference frame as:

$$T_e = \frac{3}{2}p\big(\lambda_{ds}i_{qs} - \lambda_{qs}i_{ds}\big) \tag{5.6}$$

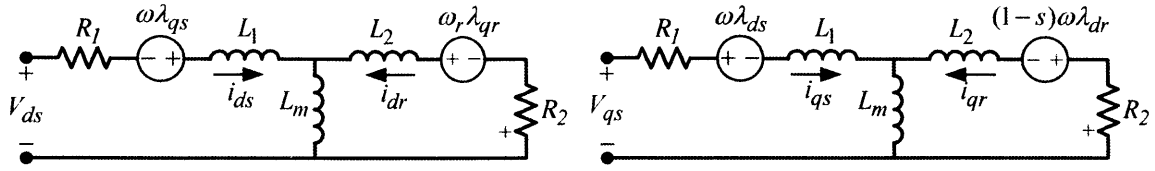

(a) d-axis (b) q-axis

Figure 5-2: D-q simulation model of squirrel cage induction motor: (a) d-axis equivalent circuit, (b) q-axis equivalent circuit

And the mechanical system is described by:

$$\frac{d\omega_m}{dt} = \frac{1}{J}(T_e - T_m - b\omega_m) \tag{5.7}$$

where T_m is the shaft mechanical torque in $N.m$, J is the rotor inertia in $kg.m^2$, b (can be estimated from equation 3.143) is the viscous friction coefficient in N.m/(Rad/s).

5.3 Simulation Results

The optimized three phase induction motor with the power electronic drive circuit (Fig. 5-2) is simulated in Matlab/Simulink to evaluate its performance. The optimized motor data is given to the d-q simulation model. A mechanical torque T_m is applied to the motor to simulate the mechanical load at a given speed. The motor system is simulated (motor and drive) at $0.5\mu s$, while the volt-Hz control is implemented at $50\mu s$. The motor and inverter data along with the simulation settings are provided in Table. 5.1.

To emulate a mechanical load of $15W$ at rated speed (321.7 RPM), the mechanical torque T_m is set in the simulation to the electromagnetic torque value of the analytical and FEA of the optimized motor obtained at the rated speed, defined as T_{ref}. At the rated load, $T_{ref} = 0.472N.m$ as obtained in Chapter 4.

Fig. 5-3 depicts the simulation results at rated torque (thus rated speed). The figure shows the electromagnetic torque (Fig. 5-3a), rotor speed (Fig. 5-3b), stator currents (Fig. 5-3c), input power to the drive circuit (Fig. 5-3d), mechanical power (Fig. 5-3e), and dc link voltage (Fig. 5-3f). From Fig. 5-3a, the inverter adds switching ripple on the electromagnetic torque but has no effect on its average value. It is also evident that the

rotor speed (322.5 RPM) is close to the reference value (321.7 RPM), and has insignificant fluctuations.

The stator currents have a peak value of $0.16A$ which is close to that obtained from the analytical model ($0.164A$) in Chapter 4. Note the switching ripple seen at the stator currents. Furthermore, the average input power to the drive is $23W$ (Fig. 4-8b). The added losses ($1.5W$) are due to the power electronic drive circuit. It can be noticed from Fig. 5-3e that the average mechanical power is around $16W$ as opposed to $15W$ in the analytical and FE models. This is due to the fact that the d-q simulation model does not model the core loss and slip loss due to the higher order space harmonics of airgap flux density. The dc link voltage ripple in Fig. 5-3f does not exceed $4V$ due to the large size of dc link capacitor.

It is worth noting that detailed analysis of the power electronics loss was ignored in this simulation study as it is not scope of this thesis. The main objective of this study is verify that the overall performance of the optimized motor remains approximately the same with the power electronic drive circuit as was shown in Fig. 5-3.

Table 5.1: System data

Grid	$f_g = 50\ Hz$ $V_g = 230\ V, rms$
Optimized motor data (d-q model)	Stator resistance, $R_1 = 53.98\ \Omega$ Stator leakage inductance, $L_1 = 0.632\ H$ Rotor resistance $R_2 = 193.25\ \Omega$ Rotor leakage inductance $L_2 = 1.14\ H$ Magnetizing inductance, $L_m = 14.45\ H$ Number of pole pairs, $p = 2$ Friction coefficient, $b = 0.0029\ N.m.s/Rad$ Motor Inertia, $J = 0.0122 kg.m^2$
Inverter	Dc link Capacitor, $C_{dc} = 200\ \mu F$ Voltage, $V_{dc} = 325\ V, pk$ Switching frequency, $f_{sw} = 1kHz$
Simulation sampling time	Plant (motor & drive), $T_s = 0.5\ \mu s$ V/F control, $T_c = 50\ \mu s$

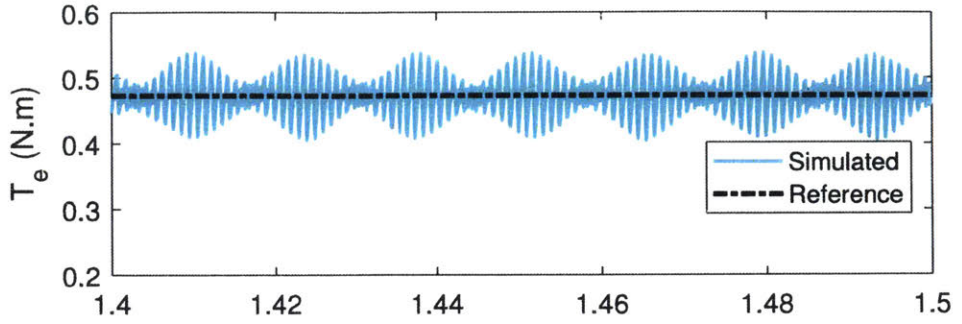
0.6
0.5
0.4
0.3
0.2
T_e (N.m)
Simulated
Reference
1.4
1.42
1.44
1.46
1.48
1.5

(a)

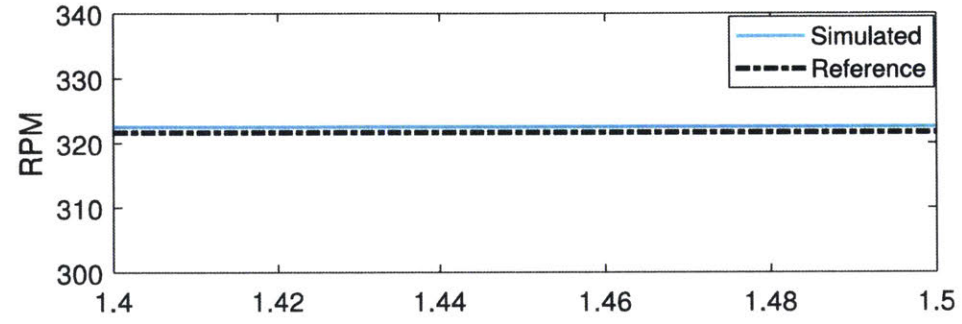
340
330
320
310
300
RPM
Simulated
Reference
1.4
1.42
1.44
1.46
1.48
1.5

(b)

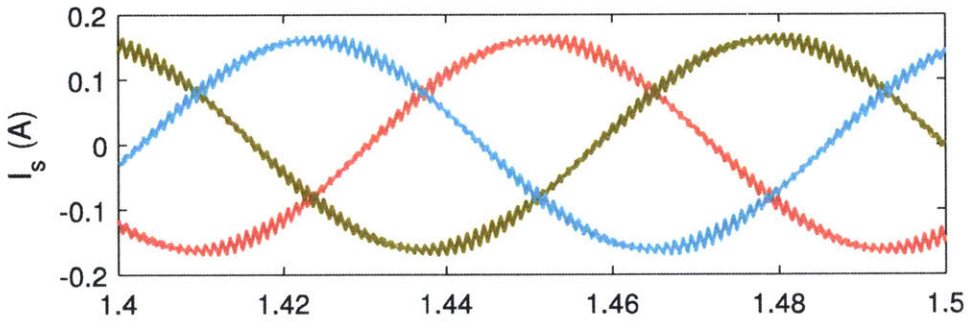
0.2
0.1
0
-0.1
-0.2
I_s (A)
1.4
1.42
1.44
1.46
1.48
1.5

(c)

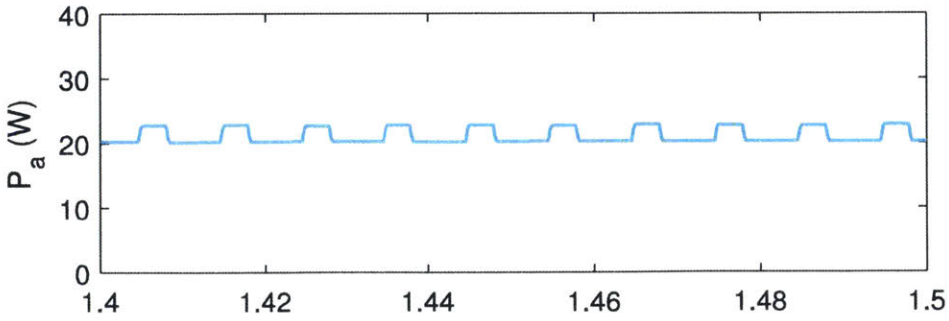
40
30
20
10
0
P_a (W)
1.4
1.42
1.44
1.46
1.48
1.5

(d)

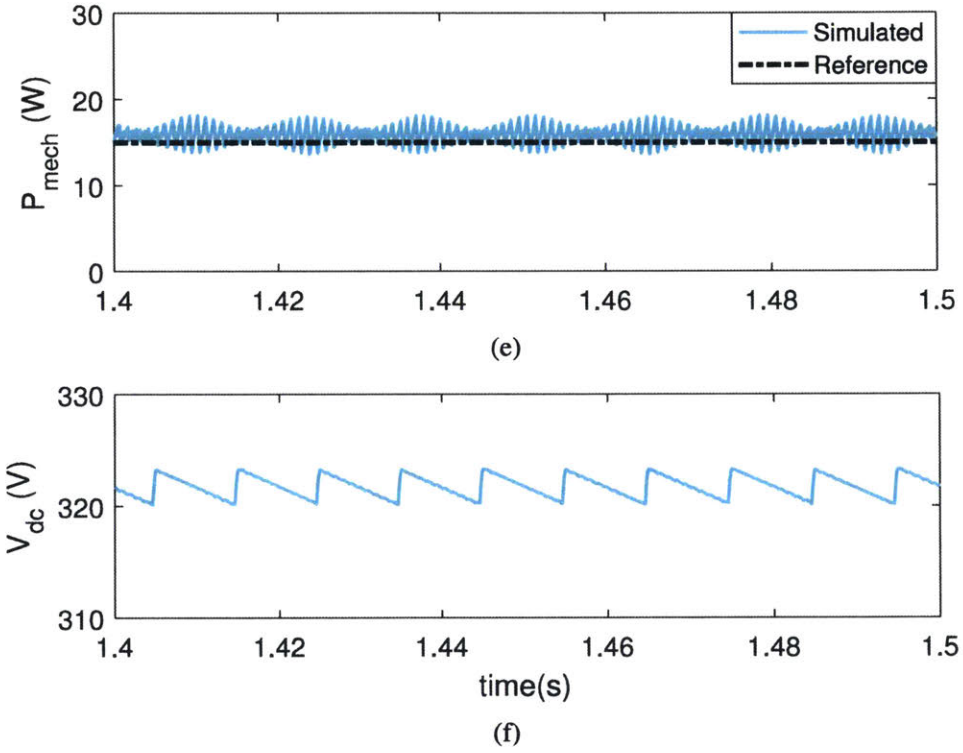

Figure 5-3: Steady state simulation results of the optimized three phase induction motor driven by a three leg inverter using volt-Hz control: (a) electromagnetic torque, T_e $(N.m)$, (b) rotor speed, N (rpm), (c) stator currents, I_s (A), (d) drive input power P_a (W), (e) mechanical power, P_{mech} (W) and (f) dc link voltage, V_{dc} (V)

Chapter 6

Summary and Conclusions

6.1 Thesis Summary

This thesis explores the design and optimization of three phase squirrel cage induction motors for the application of ceiling fans in India, with the objective of achieving a balance between efficiency and cost. A detailed analytical model for low speed, low power three phase squirrel cage induction motor is developed. The analysis to derive, calculate, and solve the extended equivalent circuit to evaluate the performance of the motor design is provided. The analytical model is validated using finite-element transient analysis. This thesis also optimize the design of three phase induction motor using genetic algorithms which rely on the validated analytical model for objective function evaluation. Several optimization objective functions were explored to reach to the optimal design that achieve improvements in efficiency and cost. The selected optimized design weighs $4.5kg$, draws $21.4W$ input power and delivers $15W$ mechanical power at a rated speed of $321rpm$, resulting in 70% efficiency, which proves more efficient than existing household ceiling fan motors in India. The optimized design is also validated in finite-element transient analysis. Finally, this thesis presents the power electronic drive implementation for the proposed, optimized motor for ceiling fans using MATLAB/Simulink simulations. The drive implements volt-hertz control to achieve variable speed settings without deteriorating the overall performance.

6.2 Thesis Conclusions

Thesis conclusions can be summarized in threefold. First, although unconventional in home appliances, three phase induction motors can be designed to be efficient and affordable due to the reduced cost of power electronics. In this thesis, a 21.4 W, 4.5 kg three phase induction motor ceiling fan motor was designed as compared to the $70W$ conventional single phase induction motor ceiling fan in India.

Second, optimizing the performance of three phase induction motor is a trade-off between efficiency and weight (and thus cost). By experimenting with different optimization objective functions a satisfactory balance between these two attributes can be achieved. The third conclusion that can be drawn from this thesis is that, while the torque, input power and mechanical power evaluated by the analytical model and finite element analysis closely match, the stator current tend to deviate near synchronous speed. This shows a limitation to the analytical model in modeling the saturation effect for the entire speed range.

6.3 Recommendations for Future Work

There are several recommendations for future work. Although the optimized motor design has achieved satisfactory efficiency and weight with ordinary rectangular rotor slot shapes, experimenting with other slot shapes may be worthwhile to further improve the efficiency.

To get higher degree of validation of the performance of the optimized motor with its drive, it is recommended to co-simulate the drive circuit along with transient finite-element model. This can be done in ANSYS/Simplorer environment.

While finite-element models validated the analytical model, the real experimental motor may perform perhaps (slightly) differently. Therefore, another future work is to build the optimized motor along with its power electronic drive circuit to validate the optimized design experimentally.

Although preliminary results has shown that the losses of power electronic drive are not major, a more detailed loss analysis of the power electronic drive should be pursued for a more precise prediction of the overall efficiency of the motor system.

Finally, a detailed comparison (cost and performance) between the optimized squirrel cage induction motor and a benchmark, super efficient brushless dc motor ceiling fan is recommended to identify the advantages and disadvantages of each motor, with special focus on cost of drive, complexity of controller, active weight and performance metrics such as efficiency and power factor.

Appendix

The appendix contains the Matlab routines used for analysis and design of three phase squirrel cage induction motors. Specifically, the analytical model, optimization routines, and sensitivity analysis are implemented by the following functions and scripts:

Optimized_Motor.m	This is the main script of the optimized motor analysis. It uses the optimized motor dimensions and variables obtained from the optimization script, RunOptim.m
carterf.m	Calculates the carter factor given the slot opening, stator or rotor core radius, number of slots, and airgap depth
wf.m	Takes number of slots short pitched, number of stator slots per pole per phase, and harmonic order as inputs and calculates the winding factor
skewf.m	Calculates the skew factor in the rotor bars
dispmotordata.m	Displays the motor data
performance_eval.m	Solves the equivalent circuit and evaluate the performance of the motor
dispresults.m	prints the performance results
RunOptim.m	Runs genetic algorithms to optimize the motor design. Returns the optimized motor dimensions and parameters.
costfunc.m	Cost function defined for the optimization routine, RunOptim.m
run_sensitivity.m	Runs a sensitivity analysis between two variables. Calls sensitivity_analysis_var1_var2.m function to perform sensitivity of efficiency and active weight against var1 and var2
sensitivity_analysis_dr_ur.m	Sensitivity function of rotor slot depth and width
sensitivity_analysis_ds_us.m	Sensitivity function of stator slot depth and width
sensitivity_analysis_her_ler.m	Sensitivity function of the endring height and axial length
sensitivity_analysis_rtsp_hr.m	Sensitivity function of rotor-tooth-slot-pitch and rotor slot height
sensitivity_analysis_stsp_hs.m	Sensitivity function of stator-slot-stator-pitch and stator slot height
sensitivity_analysis_g_l.m	Sensitivity function of airgap depth and axial length

- **Optimized_Motor.m**

```
% This is main script to run the evaluation of the optimized motor design
% The script uses the optimized dimensions and parameters obtained by the
% optimization routine.


% Define some global vars (later pass these as local vars)
global m p omega R1 X1 Xm Xm5 Xm7 Xmm Xmp X2 X25 X27 X2m X2p R2 R25 R27...
R2m R2p Rc Xc nm np V P0 nuair peB pef Rrtnls l g Rsg Na kwm kwp mteethr...
B0 omega0 rhoair Pbase

% Constants
sigAlum   = 2.3e7;      % Alum conductivity (S/m) (at 150 Deg C)
sigCopper = 5.8e7;      % stator conductor cond (S/m)
rhocopper = 8400;       % copper density in (kg/m^3)
rhoalum   = 2800;       % rotor bars mass density (kg/m^3)
rhofe     = 7650;       % steel density (kg/m^3)
u0        = 4*pi*1e-7; % permeability of air (H/m)
rhoair    = 1.225;      % air density kg/m^3
nuair     = 1.56e-5;    % kinematic viscosity of air (m^2/s)

%=========================================================================
                                % Design data
%=========================================================================

p     = 2;                      % pole pairs
m     = 2;                      % number of slots/pole/phase
Ns    = 6*p*m;                  % number of stator slots

% (1) Winding data
Nc    = 288; %                  % number of turns per coil
Na    = 2*p*m*Nc;               % Armature # turns per phase
nsp   = 0;                      % # slots short pitched
nct   = 3*m -nsp;               % # slots coil throw

% (2) Motor dimensions
Rry   = 160e-3/2; %150e-3/2;    % rotor yoke radius (outer radius) [m]
dcr   = 20e-3;                  % radial depth of rotor annulus
Rrg   = Rry - dcr;              % rotor airgap radius (inner radius)
g     = .35e-3; % 5e-3;        % physical airgap
Rsg   = Rry - dcr - g;          % stator airgap radius (outer)
Rsy = 15e-3;                    % yoke (inner) radius of stator
Dsy = 2*Rsy;
l     = 29.5e-3;                % active/axial length

% (3) Rotor slots
Nr = 18;                        % number of rotor slots (even is chosen for symmertry
     purposes)
dr    = 3e-3;                   % depression depth
ur    = 0.54e-3;                % depression width
hr    = 5.7e-3;                 % slot depth
wr    = 13e-3;                  % slot width
her = 9.2e-3;                   % end ring radial height
ler = 10e-3;                    % end ring axial height

rslotp = 2*pi*(Rrg+dr)/Nr;      % rotor slot pitch
rssp = wr/rslotp;               % rotorslotopening-slotpitch ratio
rtsp = 1 - rssp;                % rotor-tooth to slot-pitch ratio

gama = p*2*pi/Ns;               % stator slot pitch in elect.
sk    = 1e-17; %gama; %.        % rotor skew in elect. rad

% (4) Nominal and operating values
V0      = 230;                  % grid voltage rms
f0      = 50;                   % grid frequency (Hz)
omega0 = 2*pi*f0;               % grid frequency (r/s)
V       = V0/2;                 % drive voltage (V,rms)
fd       = 9; 360/60*p;         % drive frequency (Hz)
omega   = 2*pi*fd;              % drive frequency (r/s)
P0      = 15;                   % Desired output power at rated speed
% (6) Data for hysteresis core losses calculation
Pbase   = 1.3;                  % Core iron base dissp (W/kg)
B0      = 1;                    % for loss calculation
peB     = 1.88;                 % B power exponent of steel
```

```
pef     = 1.53;                 % f power exponent of steel
Q01     = 1.08;                 % core iron var base 1
Q02     = 0.0144;               % core iron var base 2
epq1    = 1.7;                  % core iron var expon 1
epq2    = 16.1;                 % core iron var expon 2

% (7) Stator slots

slotff = .45;                   % packing factor
stf    = 0.95;                  % steel laminations stacking factor
ds     = 1.6e-3;                % depression depth (m)
us     = 1.1e-3;                % depression width (m)
sslotp = 2*pi*(Rsg-ds)/Ns;      % stator slot pitch airgap (top) side
hsmax  = Rsg*0.8;               % maximum allowed stator slot height (m)

%% Correct airgap
ccs = carterf(us,Rsg,Ns,g);  % carter factor stator
ccr = carterf(ur,Rrg,Nr,g);  % carter factor rotor
ge  = ccs*ccr*g;
R   = Rsg + ge/2;            % mean airgap radius

%=========================================================================
                                % EQV CKT
%=========================================================================
% 1) Stator resitance

hs      = 25.7e-3;                      % slot height
stsp    = .31;                          % toothwidth-slotpitch ratio
t0      = stsp*sslotp;                  % tooth-width
wst     = sslotp - t0;                  % stator slot top width
wsb = 2*pi*(Rsg-ds-hs)/Ns-t0;
sarea                = 1/2*(wsb +wst)*hs;       % slot trapezodial area
Aw                   = slotff*sarea/(2*Nc);     % wire area per phase
wire_radius          = sqrt(Aw/pi);             % wire radius per phase
lw                   = 2*(1+pi*(Rsg-ds-hs/2)/p);% length of wire
lwt                  = lw*Na;                   % effective length per phase
R1 = lwt/sigCopper/Aw;                  % stator resistance

% print some warnings if dimensions voilate the physics
if hs>hsmax
    fprintf('warning: stator slot height is too large: max hs is %f mm \n',hsmax*1e3)
end

if wst<0 || wsb<0
    fprintf('Warning: Stator slot width bottom or top is negative\n');
end

if wsb < 2*pi*(Rsg-ds-hs)/Ns-t0
    fprintf('Warning: Stator slot width bottom or top is negative\n');
end

% Calculate winding factors needed later to calculate inductances

kw1 = wf(1,nsp,m);
kw5 = wf(5,nsp,m);
kw7 = wf(7,nsp,m);

% Zigzag order harmonics winding factors
% Note that zigzag and belt are the same if m = 1
np = Ns/p + 1; % or 6m + 1
nm = Ns/p - 1; % or 6m - 1

kwp = wf(np,nsp,m);
kwm = wf(nm,nsp,m);

% Stator
% =========================================================================

% 2) Airgap magnetizing inductance: fundamental magnetizing inductance

Lm = 3/2*4/pi*u0*R*l*(kw1*Na)^2/(p^2*ge);
Xm = omega*Lm;

% 3) Stator leakage inductance

% a) Airgap leakage inductance: Space harmonic leakage induct components
```

```
149
150 % Belt leakage
151 Lm5 = Lm*(kw5/kw1/5)^2;
152 Xm5 = omega*Lm5;
153 Lm7 = Lm*(kw7/kw1/7)^2;
154 Xm7 = omega*Lm5;
155
156 % Zigzag leakage
157 if m>1
158 Lmp = Lm*(kwp/kw1/np)^2;
159 Xmp = omega*Lmp;
160
161 Lmm = Lm*(kwm/kw1/nm)^2;
162 Xmm = omega*Lmm;
163 end
164
165 % b) Slot leakage
166
167 % slot leakage notes:
168 % number of slots per phase with two coils with the the same phase =
169 % = 2*p*(m-nsp).
170 % number of slots per phase sharing with another phase = 2*p*nsp
171 % number of mutual slots between each pair of phases = p*nsp
172 % slot leakage = self - mutual
173 % self          = 4*Lslot*2p(m-nsp) + Lslot*2*p*nsp
174 % where Lslot = Nc^2*u0*l*(hs/3ws + ds/us)
175 % mutual        = - Lslot*p*nsp
176 % The negative sign since the conductors have currents in oppos. directions
177 % OR interms of Nc:
178 % Lslot          = Nc^2*PermSlot;
179 % Lsslotleak2 = p*Lslot*(8*m - 5*nsp);
180
181 w_ave        = (wst+wsb)/2;
182 Psslot      = u0*l*(hs/3/w_ave + ds/us);
183 Lsslotleak = Na^2/p*Psslot*(2/m - 5/4*nsp/m^2);
184 Xsslot      = Lsslotleak*omega;
185
186 % c) End-winding leakage inductance
187
188 wp = nct/(3*m); % winding pitch as a ratio of coil throw to pole pitch
189 Xe = 7*fd*3*Na^2*(2*Rsg)/p^2*le-6*(wp - 0.3);
190 Le = Xe/omega;
191 % Xe = 14*3/2*(u0*10/4/pi^2)*omega*r*Na^2/p^2*(wp -0.3)
192
193 L1 = Lsslotleak + Le;
194 X1 = Xsslot + Xe;
195
196 % Rotor
197 % ========================================================================
198 % 1) Skew leakage (we are consider it on the rotor side)
199
200 ks1 = skedwf(1,sk);
201 ks5 = skewf(5,sk);
202 ks7 = skewf(7,sk);
203 ksp = skewf(np,sk);
204 ksm = skewf(nm,sk);
205
206 % Rotor skew leakage inductances reffered to stator
207 Lsk1 = Lm *(1 - ks1^2)/ks1^2 ; Xsk1 = omega*Lsk1;
208 Lsk5 = Lm5*(1 - ks5^2)/ks5^2 ; Xsk5 = omega*Lsk5;
209 Lsk7 = Lm7*(1 - ks7^2)/ks7^2 ; Xsk7 = omega*Lsk7;
210 if m>1
211     Lskp = Lmp*(1 - ksp^2)/ksp^2 ; Xskp = omega*Lskp;
212     Lskm = Lmm*(1 - ksm^2)/ksm^2 ; Xskm = omega*Lskm;
213 end
214
215 % 2) Rotor slot harmonics:
216
217 skin_depth = 1/sqrt(pi*fd*u0*sigAlum); % skin depth = 33mm >> hr
218
219 Lrslotleak  = u0*l*(hr/3/wr + dr/ur); % H
220 Lrslotleak5 = Lrslotleak*(kw5/kw1)^2;
221 Lrslotleak7 = Lrslotleak*(kw7/kw1)^2;
222 if m>1
223     Lrslotleakp = Lrslotleak*(kwp/kw1)^2;
224     Lrslotleakm = Lrslotleak*(kwm/kw1)^2;
```

```
225 end
226
227 % Fundamental:
228 X2slot      = (12*omega*Na^2*kw1^2/Nr*Lrslotleak)/ks1^2; % divide by ks1^2
229 % when referring to the stator side
230 % Belt:
231 X25slot     = (12*omega*Na^2*kw1^2/Nr*Lrslotleak5)/ks5^2;
232 X27slot     = (12*omega*Na^2*kw1^2/Nr*Lrslotleak7)/ks7^2;
233 % Zigzag:
234 if m>1
235     X2pslot = (12*omega*Na^2*kw1^2/Nr*Lrslotleakp)/ksp^2;
236     X2mslot = (12*omega*Na^2*kw1^2/Nr*Lrslotleakm)/ksm^2;
237 end
238
239 % 3) End ring leakage extended to slot/rotor bar leakage
240
241 % Based on Grover's formula for the self inductance of a circular ring
242 % with mean radius (Ri+her/2) with a sqaure cross section (ignore depression):
243 er_mean_radius = Rrg+her/2;
244 Ler = u0*er_mean_radius*1/2/Nr*...
245     ( 1/2*(1+wr*hr/er_mean_radius^2/6)*log(8*er_mean_radius^2/wr/hr)...
246       -.8434 + .2041*wr*hr/er_mean_radius^2 );
247
248 L2e  = Ler/2/(sin(p*pi/Nr))^2; % leakage inductance of one endring
249 L25e = L2e*(kw5/kw1)^2;
250 L27e = L2e*(kw7/kw1)^2;
251 if m>1
252     L2pe = L2e*(kwp/kw1)^2;
253     L2me = L2e*(kwm/kw1)^2;
254 end
255
256 % Fundamental:
257 X2e      = (12*omega*Na^2*kw1^2/Nr*L2e)/ks1^2; % divide by ks1^2
258 % when referring to the stator side
259 % Belt:
260 X25e     = (12*omega*Na^2*kw1^2/Nr*L25e)/ks5^2;
261 X27e     = (12*omega*Na^2*kw1^2/Nr*L27e)/ks7^2;
262 % Zigzag:
263 if m>1
264     X2pe = (12*omega*Na^2*kw1^2/Nr*L2pe)/ksp^2;
265     X2me = (12*omega*Na^2*kw1^2/Nr*L2me)/ksm^2;
266 end
267
268 % 4) Rotor zigzag harmonics
269
270 % Fundamental
271 X2z  = Xm*p^2*( 1/(Nr+p)^2 + 1/(Nr-p)^2 )/ks1^2;
272 % Belt
273 X25z = Xm*p^2*(kw5/kw1)^2*( 1/(Nr+5*p)^2 + 1/(Nr-5*p)^2 )/ks5^2;
274 X27z = Xm*p^2*(kw7/kw1)^2*( 1/(Nr+7*p)^2 + 1/(Nr-7*p)^2 )/ks7^2;
275 % Zigzag
276 X2pz = Xm*p^2*(kwp/kw1)^2*( 1/(Nr+np*p)^2 + 1/(Nr-np*p)^2 )/ksp^2;
277 X2mz = Xm*p^2*(kwm/kw1)^2*( 1/(Nr+nm*p)^2 + 1/(Nr-nm*p)^2 )/ksm^2;
278
279 % Compute Total leakage reactance
280 X2  = X2slot  + X2e + X2z + Xsk1;
281 X25 = X25slot + X25e + X25z + Xsk5;
282 X27 = X27slot + X27e + X27z + Xsk7;
283 if m>1
284 X2p = X2pslot + X2pe + X2pz + Xskp;
285 X2m = X2mslot + X2me + X2mz + Xskm;
286 end
287
288 % 5) Rotor resitance (reffered to stator)
289
290 % Alger's Method:
291
292 % R2b: resistance in one bar/rotorslot
293 % R2e: resistance in one endring
294 % Rer: bar bar endring resistance (ith  endring resitance element over a pitch
295 % of rotor slot)
296
297 % Ie,pk = integral of bar currents over half pole pitch
298 %       = integral(1/2*Nr*Ib,pk/2/p*sin(n*p*theta),0->pi/(2*p))
299 % Ie,pk = Nr*Ib,pk/(2*pi*p)
```

```
% Ploss_e/Ploss_b = Je^2/Jb^2 * 2*vol_one-endring/vol_bar = Rele_tot^2/Rblb_tot^2
% Ie_tot = Ib_tot (total endring current
% Je/Jb = Nr/2/pi/p*wr*hr/he*le = Nr/2/pi/p*wr/le (assuming hr = he)
% vol_e = pi*((Ri+he)^2 - Ri^2)*le = 2*pi*Ri*he*le + pi*he^2*le
% vol_b = wr*hr*l*Nr (ignoring the depression volume)
% R2e/R2b = Nr*wr*Ri/pi*p^2*le*l
% In Alger's 'he' is left out assuming that Ri>>he
% thus  R2e = (Nr*wr*Ri/pi*p^2*le*l) * (rho*l/wr/hr)
%       R2e = 1/2*(rho*2*pi*Ri/Nr/hr/le) / (pi*p/Nr)^2
%       R2e = 1/2* Rer / (pi*p/Nr)^2


% More detailed method (Lippo's Introduction to AC Machine Design)

% R2e = 1/2*Ree/sin^2(p*pi/Nr)
% if you take first order tylor series of sin^2(p*pi/Nr) = (pi*p/Nr)^2
% R2e = 1/2*R2ee/(pi*p/Nr)^2 which as the same as Alger's

R2b = 1/(sigAlum*(wr*hr + ur*dr));
Rer = 2*pi*Rrg/Nr/her/ler/sigAlum;
Re_method = 'detailed'; % choose between 'reduced_order' or 'detailed'

if(strcmp(Re_method,'reduced_order')) % (Alger's)
    R2e = R2b*Nr*Rrg*wr/(pi*l*ler*p^2);
else % detailed (Lippo's)
    R2e = Rer/2/(sin(p*pi/Nr))^2;
end


R2be = R2b + R2e;


R2  = 12*Na^2*kw1^2/Nr*R2be/ks1^2;
R25 = 12*Na^2*kw5^2/Nr*R2be/ks5^2;
R27 = 12*Na^2*kw7^2/Nr*R2be/ks7^2;
if nr>1
R2p = 12*Na^2*kwp^2/Nr*R2be/ksp^2;
R2m = 12*Na^2*kwm^2/Nr*R2be/ksm^2;
end

% Calculate Core elements
% ========================================================================

% (1) First calculate the stator core loss density (W/Kg)of
% (a) stator teeth, (b) stator back iron, (c) rotor teeth, (d) rotor back
% iron

Bg = p*V/(2*Rsg*l*Na*kw1*omega); % air gap flux density

% (a) Stator teeth

Bst  = Bg/stsp*stf; % stator tooth flux density;
Pst  = Pbase*abs(Bst/B0)^peB*abs(omega/omega0)^pef; % tooth loss density (W/kg)
Qst  = (Q01*abs(Bst/B0)^epq1 + Q02*abs(Bst/B0)^epq2)*abs(omega/omega0);

% (b) Stator back iron
dsc = (Rsg-hs); % depth of the core
Bcs = Bg*(Rsg+ge/2)/(p*dsc/stf); % stator back iron flux density

% Pdc = Pcloss(Keddy,Kh,Kex,f,Bcs); % W/Vol
Pdc = Pbase*abs(Bcs/B0)^peB*abs(omega/omega0)^pef; % back iron loss density
Qdc = (Q01*abs(Bcs/B0)^epq1 + Q02*abs(Bcs/B0)^epq2)*abs(omega/omega0);
% back iron VAR density

% (c) Rotor teeth
Brt = Bg/rtsp; % rotor tooth flux density
Qrt = (Q01*abs(Brt/B0)^epq1 + Q02*abs(Brt/B0)^epq2)*abs(omega/omega0);
% rotor teeth var density

% (d) Rotor back iron

Bcr = Bg*(Rrg-ge/2)/( p*(dcr-hr) )*stf; % rotor back iron flux density
Pdrc = Pbase*abs(Bcr/B0)^peB*abs(omega/omega0)^pef; % back iron loss density

% 2) calcualte the mass of (a) back iron , (b) teeth, and (c) conductor

% (a) Mass of back iron
```

```
mcores = pi*(Rsg-ds-hs - Dsy/2)^2*l*rhofe;
mcorer = pi*(Rry^2-(Rrg+dr+hr)^2)*l*rhofe;

% (b) Mass of tooth
mteeths =( ds*(sslotp-us) + hs*( sslotp-(wst+wsb)/2 ) )*l*Ns*rhofe; % my expr
mteethr = pi*((Rrg+dr+hr)^2-(Rrg)^2)*l*rhofe*rtsp;

% (c) Conductor mass
rslot_area  = wr*hr+ur*dr;
mconds = 3*lwt*Aw* rhocopper; % stator conductor mass
mcondr = Nr*rslot_area*l*rhoalum + 2*(pi*((Rrg+dr+her)^2-(Rrg+dr)^2)...
    *ler*rhoalum); % rotor conductor mass inculding end ring

mstator = mcores + mteeths + mconds; % total mass of stator
mrotor  = mcorer + mteethr + mcondr; % total mass of rotor
mtot    = mstator + mrotor; % total active mass of the IM

% Motor moment of inertia: (only for result display)
% stator
Ds = 2*Rsg;
Jsx = 1/8*mstator*Ds^2;
Jsy = 1/4*mstator*(Ds^2/4 + l^2/3);
Js = sqrt(Jsx^2+Jsy^2);
% rotor
D1 = 2*Rry;
D2 = 2*Rrg;
Jrx = 1/8*mrotor*(D1^2 + D2^2);
Jry = 1/4*mrotor*( (D1^2 + D2^2)/4 + l^2/3);
Jr = sqrt(Jrx^2+Jry^2);

J = sqrt(Js^2+Jr^2);

% total stator core loss at nominal flux density
Pc = Pst*mteeths + Pdc * mcores;
% Pc = Pst*pi*Rsg^2*l + Pdc * pi*(Rsg-hs)^2*l/p;

% total VAR loss (stator core + stator teeth + rotor teeth) at nominal B0
Qc = Qst*mteeths + Qdc*mcores + Qrt*mteethr;

% then core parallel resistance is %
Rc = 3*V^2/Pc;
% and parallel reactance is:
Xc = 3*V^2/Qc;

% Compute the no load loss in rotor teeth because of stator slot opening
% modulation of fundamental flux density:

% parallel resistance element for zigzag flux loss
% first, generate nominal zigzag flux variation:
% thetad is the normalized angular slot opening
thetad = Ns*us/Rsg;

% BH is the nominal flux variation
BH = Bg * (2/pi) * sin (0.5*thetad);
% Prtnls = Peloss(Keddy,Kh,Kex,f,BH); % W/Vol
Prtnls = P0*abs(BH/B0)^peB*abs(Ns*omega/omega0)^pef; % back iron loss density
% so then the equivalent resistance is:
Rrtnls = 3 * V^2 / Prtnls;

% Display Motor Data
dispmotordata

%=========================================================================
                                % Motor Analysis
%=========================================================================

% Motor analysis

s       = logspace(-6,0,1e3);
[y sp]  = performance_eval(s);
It      = y(1,:);
Pin     = y(2,:);
S       = y(3,:);
Pag1    = y(4,:);
Pag5    = y(5,:);
Pag7    = y(6,:);
```

```
453 Pagm     = y(7,:);
454 Pagp     = y(8,:);
455 Pag      = y(9,:);
456 Pslip1   = y(10,:);
457 Pslip5   = y(11,:);
458 Pslip7   = y(12,:);
459 Pslipm   = y(13,:);
460 Pslipp   = y(14,:);
461 Pslip    = y(15,:);
462 Pa       = y(16,:);
463 Pc       = y(17,:);
464 Prtnls   = y(18,:);
465 Prtls    = y(19,:);
466 Pwf      = y(20,:);
467 Ploss    = y(21,:);
468 Pmech    = y(22,:);
469 Te       = y(23,:);
470 Tm       = y(24,:);
471 eff      = y(25,:);
472 pf       = y(26,:);
473 I21      = y(27,:);
474 I25      = y(28,:);
475 I27      = y(29,:);
476 I2m      = y(30,:);
477 I2p      = y(31,:);
478 Ic       = y(32,:);
479 Vr       = y(33,:);
480 ff       = y(34,:);
481 %%
482 Tstarting = Te(end); % starting torque at slip = 1
483
484 if isempty(sp) % if power spec is not met
485     fprintf('Pconv,pk < Pout.rating \n');
486 else % evaluate when design meet power requirement
487     yp = performance_eval(sp);
488     It0       = yp(1);
489     Pin0      = yp(2);
490     S0        = yp(3);
491     Pag10     = yp(4);
492     Pag50     = yp(5);
493     Pag70     = yp(6);
494     Pagm0     = yp(7);
495     Pagp0     = yp(8);
496     Pag0      = yp(9);
497     Pslip10   = yp(10);
498     Pslip50   = yp(11);
499     Pslip70   = yp(12);
500     Pslipm0    = yp(13);
501     Pslipp0   = yp(14);
502     Pslip0    = yp(15);
503     Pa0       = yp(16);
504     Pc0       = yp(17);
505     Prtnls0   = yp(18);
506     Prtls0    = yp(19);
507     Pwf0      = yp(20);
508     Ploss0    = yp(21);
509     Pmech0    = yp(22);
510     Te0       = yp(23);
511     Tm0       = yp(24);
512     eff0      = yp(25);
513     pf0       = yp(26);
514     I210      = yp(27);
515     I250      = yp(28);
516     I270      = yp(29);
517     I2m0      = yp(30);
518     I2p0      = yp(31);
519     Ic0       = yp(32);
520     Vr0       = yp(33);
521     ff0       =  yp(34);
522
523     % calculate current densities:
524
525     % stator
526     Jslimit = 5; % Arms/mm^2 (based on Lippo's table6.6 for ODP motors chp 6 pg  285)
```

```
527
528     Js0RPM     = abs(It(end))/Aw*1e-6;
529     JsRated    = abs(It0)/Aw*1e-6;
530
531     % rotor
532
533     I20RPM = sqrt(abs(I21(end))^2+abs(I25(end))^2+abs(I27(end))^2+abs(I2m(end))^2+abs(I2p(
            end))^2);
534     I2Rated = sqrt(abs(I210)^2+abs(I250)^2+abs(I270)^2+abs(I2m0)^2+abs(I2p0)^2);
535
536     % bar current desnity
537     Ib0RPM  = 6*Na*kw1/Nr*I20RPM;
538     IbRated = 6*Na*kw1/Nr*I2Rated;
539
540     Jblimit = 7.75; %Arms/mm^2 or 5000 Arms/in^2 as indicated by Lippo chp6 pg 285
541
542     Jb0RPM      = Ib0RPM/rslot_area*1e-6;
543     JbRated     = IbRated/rslot_area*1e-6;
544
545     % end ring
546     endring_current = 'exact'; %1stOrderTylor
547     if(strcmp(endring_current,'exact'))
548         Ie0RPM = abs(Ib0RPM/(1-exp(j*2*pi*p/Nr)));
549         IeRated = abs(IbRated/(1-exp(j*2*pi*p/Nr)));
550     elseif(strcmp(endring_current,'1stOrderTylor'))
551         Ie0RPM = Ib0RPM*Nr/2/pi/p;
552         IeRated = IbRated*Nr/2/pi/p;
553     end
554
555     Je0RPM      = Ie0RPM/rslot_area*1e-6;
556     JeRated     = IeRated/rslot_area*1e-6;
557
558     % Calculate skin_depth at slip:
559     skin_depth_rated_speed = 1/sqrt(sp*pi*fd*u0*sigAlum);
560     skin_depth_rated_speed_to_hr = skin_depth_rated_speed/hr;
561
562     % plot results
563
564     omegam = omega/p*(1-s);
565     N = omegam*60/(2*pi);
566     N0 = omega/p*(1-sp)*60/2/pi;
567
568     figure(1);
569     plot(N,Te,'LineWidth',2);
570     hold on;
571     plot(N0,Te0,'*');
572     hold off;
573     grid on;
574     xlabel('Rotational speed in RPM')
575     ylabel('N.m')
576     title('Torque-speed curve');
577
578     figure(2);
579     plot(N,Tm,'LineWidth',1.5);
580     hold on;
581     plot(N0,Tm0,'*');
582     hold off;
583
584     grid on;
585     grid minor;
586     xlabel('Rotational speed in RPM')
587     ylabel('N.m')
588     title('Mechanical Torque-speed curve');
589
590     figure(3);
591     plot(N,Pmech,'LineWidth',1.5)
592     hold on;
593     plot(N0,Pmech0,'*');
594     hold off;
595
596     grid on;
597     grid minor;
598     xlabel('Rotational speed in RPM')
599     ylabel('W')
600     title('Converted mechanical power');
601
```

```
602     figure(4);
603
604     plot(N,Pin,'LineWidth',1.5)
605     hold on;
606     plot(N0,Pin0,'*');
607     hold off;
608
609     grid on;
610     grid minor;
611     xlabel('Rotational speed in RPM')
612     ylabel('W')
613     title('Input power');
614
615     figure(5);
616     plot(N,eff,'LineWidth',1.5)
617     hold on;
618     plot(N0,eff0,'*');
619     hold off;
620
621     grid on;
622     grid minor;
623     xlabel('Rotational speed in RPM')
624     ylabel('Percentage')
625     title('Efficiency versus speed');
626
627     figure(6);
628     plot(N,pf,'LineWidth',1.5)
629     hold on;
630     plot(N0,pf0,'*');
631     hold off;
632
633     grid on;
634     grid minor;
635     xlabel('Rotational speed in RPM')
636     ylabel('Per unit')
637     title('PF versus speed');
638
639     figure(7);
640     plot(N,Pc,'LineWidth',1.5)
641     hold on;
642     plot(N0,Pc0,'*');
643     hold off;
644
645     grid on;
646     grid minor;
647     xlabel('Rotational speed in RPM')
648     ylabel('Per unit')
649     title('Core Loss');
650
651     figure(7);
652     plot(N,abs(It),'LineWidth',1.5)
653     hold on;
654     plot(N0,abs(It0),'*');
655     hold off;
656
657     grid on;
658     grid minor;
659     xlabel('Rotational speed in RPM')
660     ylabel('Ia (A)')
661     title('Terminal current, RMS');
662
663     figure(8);
664     plot(N,abs(I21),'LineWidth',1.5)
665     hold on;
666     plot(N0,abs(I210),'*');
667     hold off;
668
669     grid on;
670     grid minor;
671     xlabel('Rotational speed in RPM')
672     ylabel('I21 (A)')
673     title('Fundamental rotor current, RMS');
674
675     figure(9);
676     plot(N,ff,'LineWidth',1.5)
```

```
677         hold on;
678         plot(N0,ff0,'*');
679         hold off;
680
681         grid on;
682         grid minor;
683         xlabel('Rotational speed in RPM')
684         ylabel('N.m.s/Rad')
685         title('Friction Factor versus speed');
686
687         % display results if the power requirement
688         dispresults
689     end
```

- carterf.m

```
1   function cc = carterf(u,Ri,Ns,g)
2   %CARTERF calculates the effective airgap using Carter Correction factor
3
4   %%%%% Input %%%%
5   % u  : slot opening width (depression width)
6   % Ri : stator inner radius
7   % Ns : number of stator slots
8   % g  : physical airgap
9
10  %%%%% Output %%%%
11  % cc: carter's coefficient
12
13  % ueff  :
14  % Background
15  % Account for effect of rotor and stator slot openings on airgap: Carter's
16  % airgap correction. For reference, look at "Design of Rotating Electrical
17  % Machines for Juha PyrhÃünen"
18
19  % Carter's factor:
20  % Kc = slot pitch/(slot pitch - equivalent slot opening) = Bmax/Bave
21  % Kc = spitch/(spitch - ueff) = spitch/(spitch - fac*u)
22  % fac is derived given at the case areas S1 + S1 = S2
23  % The equivalent slot opening (equivalent slot depression width) is defined
24  % when the real flux density is replaced with constant flux density under
25  % teeth and zero under slot.
26
27  spitch = 2*pi*Ri/Ns; % slot pitch
28  fac    = (2/pi)*(atan(u/2/g) - 2*g/u*log(sqrt(1+(u/2/g)^2)));
29  % approximation of fac: fac = u/g/(5 + u/g)
30  ueff  = fac*u; % effective slot opening width
31  cc = 1/(1- ueff/spitch);
32
33  end
```

- wf.m

```
1   function kw = wf(n,nss,m)
2   % This function calculates the winding factor
3
4   %--- Inputs
5   % n: space harmonic order
6   % nss: number of slots being short pitched
7   % m: number of slots per pole per phase
8   %--- Output
9   % kw: winding factor at the nth order harmonic
10
11
12  gama = pi/(3*m); % slot-slot angular displacement in elect. rad
13  alpha = pi - nss*gama;
14
15  % or
16  % nct = 3*m - nss; % coil throw after short pitching
17  % alpha = gama*nct; % or winding-pitch angle in elect. rad
```

```
18
19 % Pitch factor
20 kp = sin(n*alpha/2)*sin(n*pi/2); % the +-1 factor will not affect the
21 % inductances but will effect the Br(theta) if you're plotting it
22
23 % kp = cos(n*(nss*gama)/2); % here no need to worry about the +-1 factor
24 % since the cosine is always positive.
25
26 % Distribution/breadth factor
27 kb = sin(n*m*gama/2)/(m*sin(n*gama/2));
28
29 kw = kp*kb;
30
31 end
```

- **skewf.m**

```
1  function ks = skewf(n,sk)
2  % skewf calculates the skew factor for a given flux density space harmonic
3  % component and a skew angle.
4  % input:
5  % n : space harmonic order
6  % sk: skew angle in electrical radians
7  % Output:
8  % ks: skew factor
9
10 % Eqivalent ckt for skew leakage.
11
12 %_____________    1:ks   ______ Xm(1-ks^2) ______
13 %      |        |        (
14 %      |        )        (
15 %     Xm        )   ||    (
16 %      |        )        (
17 %      |        )        (
18 %______|________|        |_____________________
19     % Note: there are no unique method to incorporate skew leakage. Many EQV
20     % circuits are mathemetically equivalent in accounting for the skew leakage
21     % However we are going to adopt the intuitive equivalent circuit which
22     % considers the skew leakage on the rotor side with a transformer model of
23     % 1:ksk ratio since it fully conforms with the essential physical
24     % conditions in flux tube model/electromagnetic ckt of the induction motor.
25     % In other words, it is the safest method to avoid incorrect use of the
26     % the priniciple of superposition when magnetic saturation is present
27
28     % For more on this, refer to "Comparison of alternative skew-effect
29     % parameters of cage induction motors, O. I. Butler"
30
31 ks = sin(n*sk/2)/(n*sk/2);
32
33 end
```

- **dispmotordata.m**

```
1  fprintf('\n')
2  fprintf('          3ph Motor for ceiling fans designed data          \n')
3  fprintf('============================================================ \n')
4
5  fprintf('\n')
6  fprintf('Winding Configuration: \n');
7  fprintf('Distributed (m>1) double layer lap coil \n');
8  fprintf('Number of slots/pole/phase, m  = %g \n',m);
9  fprintf('\n')
10
11 fprintf('Number of pole pairs, p        = %g \n',p);
12 fprintf('Number of stator slots, Ns     = %g \n',Ns);
13 fprintf('Number of rotor bars, Nr       = %g \n',Nr);
14 fprintf('Number of turns per coil       = %g \n',Nc);
15 fprintf('Total number of turns/phase    = %g \n',Na);
16
```

```
fprintf('\n')
fprintf('Active length                    = %g cm \n',l*100);
fprintf('Rotor outer diameter (2*Rry)              = %g cm \n',2*Rry*100);
fprintf('Rotor inner diameter (2*Rrg)              = %g cm \n',2*Rrg*100);
fprintf('Rotor core radial depth          = %g cm \n',dcr*100);
fprintf('Physical airgap (g)                 = %g mm \n', g*1e3);
fprintf('Stator diameter (2*Rsg)                   = %g cm \n',2*Rsg*1e2);

fprintf('\n')
fprintf('Stator slot pitch                = %g mm \n',sslotp*1000);
fprintf('Tooth to slot-pitch ratio        = %g \n',stsp);
fprintf('Tooth width                      = %g mm \n',t0*1000);
fprintf('Stator slot top width            = %g mm \n',wst*1000);
fprintf('Stator slot bottom width         = %g mm \n',wsb*1000);
fprintf('Stator slot height               = %g mm \n',hs*1000);
fprintf('Stator depression depth          = %g mm \n',ds*1000);
fprintf('Stator depression width          = %g mm \n',us*1000);
fprintf('Stator slot area                 = %g mm^2 \n',sarea*1e6);

fprintf('\n')
fprintf('Rotor slot height                = %g mm \n',hr*1000);
fprintf('Rotor slot width                 = %g mm \n',wr*1000);
fprintf('Rotor depression depth           = %g mm \n',dr*1000);
fprintf('Rotor depression width           = %g mm \n',ur*1000);
fprintf('Rotor tooth to slot-pitch ratio= %g \n',rtsp);
fprintf('Rotor endring radial hieght = %g mm \n',her*1000);
fprintf('Rotor endring  axial length = %g mm \n',ler*1000);


fprintf('\n')
fprintf('Physical airgap = %g mm, Equivalent airgap = %g mm \n \n',...
    g*1e3,ge*1e3);


fprintf('                              Stator                                  \n')
fprintf('======================================================================= \n')

fprintf('\n')
fprintf('1) Airgap inductances: \n \n')

fprintf('Fundamental airgap magnetizing inductance and reactance: \n')
fprintf('Lm = %g mH          Xm = %g Ohm \n',Lm*1e3, Xm);

fprintf('\n')
fprintf('Airgap space harmonic leakage elements: \n')

fprintf('Lm,5 = %g mH        Xm,5 = %g Ohm \n',Lm5*1e3,Xm5)
fprintf('Lm,7 = %g mH        Xm,7 = %g Ohm \n',Lm7*1e3,Xm7)
if m>1
fprintf('Lm,p = %g mH        Xm,p = %g Ohm \n',Lmp*1e3,Xmp)
fprintf('Lm,m = %g mH        Xm,m = %g Ohm \n',Lmm*1e3,Xmm)
end

fprintf('\n')
fprintf('2) Stator leakage inductances: \n')
fprintf('  a) Slot leakage \n')
fprintf('      Ll,slot = %g mH        Xl,slot = %g Ohm\n',Lsslotleak*1e3,Xsslot);
fprintf('  b) Endwinding leakage \n')
fprintf('      Ll,ew = %g mH          Xl,ew = %g Ohm \n',Le*1e3,Xe)

fprintf('\n')
fprintf('Stator leakage Inductance Ll = Ll,slot + Ll,endwinding \n');
fprintf('Ll = %g mH \n',Ll*1e3);
fprintf('Stator leakage reactance Xl = Xl,slot + Xl,endwinding \n');
fprintf('Xl = %g Ohm \n',Xl)

fprintf('\n')
fprintf('3) Stator resistance: \n')
fprintf('Rl = %g Ohm \n', Rl)
fprintf('Slot Packing(fill) factor                                  = %g   \n',slotff)
fprintf('Stator effective length of wire per phase                  = %g meters \n',lwt)
fprintf('Stator slot area                                           = %g mm^2 \n',sarea*1e6);
fprintf('Effective slot area (packing_factor*slot_area)             = %g mm^2 \n ',slotff*sarea
    *1e6);
fprintf('Area of stator wire of 1 turn (per phase)                  = %g mm^2 \n',Aw*1e6);
```

```
91  fprintf('Wire diameter per phase                                    = %g mm \n',2*wire_radius
        *1e3);
92
93  fprintf('\n')
94  fprintf('4) Core branch: \n')
95  fprintf('Rc = %g kOhm\n', Rc*1e-3)
96  fprintf('Xc = %g kOhm \n', Xc*1e-3)
97
98
99  fprintf('\n')
100 fprintf('                                Rotor                                          \n')
101 fprintf('============================================================== \n')
102
103 fprintf('All rotor quantities are referred to stator')
104 fprintf('Rotor leakage inductances: \n')
105
106 fprintf('\n')
107 fprintf('1) Rotor leakage inductances: \n')
108 fprintf('   a) Rotor skew \n')
109 fprintf('      L21,skew = %g mH            X2,sk_1 = %g Ohm\n',Lsk1*1e3,Xsk1)
110 fprintf('      L25,skew = %g mH            X2,sk_5 = %g Ohm\n',Lsk5*1e3,Xsk5)
111 fprintf('      L27,skew = %g mH            X2,sk_7 = %g Ohm\n',Lsk7*1e3,Xsk7)
112 if m>1
113 fprintf('      L2p,skew = %g mH            X2,sk_p = %g Ohm\n',Lskp*1e3,Xskp)
114 fprintf('      L2m,skew = %g mH            X2,sk_m = %g Ohm\n',Lskm*1e3,Xskm)
115 end
116
117 fprintf('\n')
118 fprintf('   b) Rotor slot leakage inductances: \n')
119 fprintf('      L21,slot = %g nH            X21,slot = %g Ohm \n',Lrslotleak*1e9, X2slot)
120 fprintf('      L25,slot = %g nH            X25,slot = %g Ohm \n',Lrslotleak5*1e9, X25slot)
121 fprintf('      L27,slot = %g nH            X27,slot = %g Ohm \n',Lrslotleak7*1e9, X27slot)
122 if m>1
123 fprintf('      L2p,slot = %g nH            X2p,slot = %g Ohm \n',Lrslotleakp*1e9, X2pslot)
124 fprintf('      L2m,slot = %g nH            X2m,slot = %g Ohm \n',Lrslotleakm*1e9, X2mslot)
125 end
126
127
128 fprintf('\n')
129 fprintf('   c) Rotor end winding leakage inductances: \n')
130
131 fprintf('      L2er,b-b (ith endring inductance over a pitch of rotor slot) = %g nH \n',Ler
        *1e9)
132
133 fprintf('      L21,er = %g nH            X21,er = %g Ohm \n',L2e*1e9, X2e)
134 fprintf('      L25,er = %g nH            X25,er = %g Ohm \n',L25e*1e9, X25e)
135 fprintf('      L27,er = %g nH            X27,er = %g Ohm \n',L27e*1e9, X27e)
136 if m>1
137 fprintf('      L2p,er = %g nH            X2p,er = %g Ohm \n',L2pe*1e9, X2pe)
138 fprintf('      L2m,er = %g nH            X2m,er = %g Ohm \n',L2me*1e9, X2me)
139 end
140
141
142 fprintf('\n')
143 fprintf('   d) Rotor zigzag leakage inductances: \n')
144 fprintf('      L21,zigzag = %g mH          X21,zigzag = %g Ohm \n',X2z/2/pi/fd*1e3, X2z)
145 fprintf('      L25,zigzag = %g mH          X25,zigzag = %g Ohm \n',X25z/2/pi/fd*1e3, X25z)
146 fprintf('      L27,zigzag = %g mH          X27,zigzag = %g Ohm \n',X27z/2/pi/fd*1e3, X27z)
147 fprintf('      L2p,zigzag = %g mH          X2p,zigzag = %g Ohm \n',X2pz/2/pi/fd*1e3, X2pz) %
        Ns+1, Ns-1 in case of m=1
148 fprintf('      L2m,zigzag = %g mH          X2m,zigzag = %g Ohm \n',X2mz/2/pi/fd*1e3, X2mz)
149
150 fprintf('\n')
151 fprintf('Rotor leakage reactance X2 = X2,slot + X2,skew + X2,zigzag \n');
152
153 fprintf('X2   = %g Ohm \n',X2)
154 fprintf('X2,5 = %g Ohm \n',X25)
155 fprintf('X2,7 = %g Ohm \n',X27)
156 if m>1
157 fprintf('X2,p = %g Ohm \n',X2p)
158 fprintf('X2,m = %g Ohm \n',X2m)
159 end
160
161 fprintf('\n')
162 fprintf('2) Rotor resistance: \n')
163 fprintf('\n')
```

```
164 if (skin_depth > (5*hr))
165     fprintf('Skin Depth at locked rotor (unity slip) = %g mm >> rotor_slot depth = %g mm \
        n',skin_depth*1e3,hr*1e3);
166     fprintf('No need to consider deep rotor bar effect \n');
167 end
168 fprintf('\n');
169 fprintf('R2slot                                                    = %g uOhm \n',R2b*1e6)
170 fprintf('R2end (of one endring)                                    = %g uOhm \n',R2e*1e6)
171 fprintf('R2b-b (ith endring resistance over a pitch of rotor slot) = %g uOhm \n',Rer*1e6)
172 fprintf('2) Rotor resistance: \n')
173 fprintf('R2   = %g Ohm \n',R2)
174 fprintf('R2,5 = %g Ohm \n',R25)
175 fprintf('R2,7 = %g Ohm \n',R25)
176 if m>1
177 fprintf('R2,p = %g Ohm \n',R2p)
178 fprintf('R2,m = %g Ohm \n',R2m)
179 end
180
181 fprintf('\n')
182 fprintf('                    Weight and Inertia                    \n')
183 fprintf('========================================================== \n')
184 fprintf('Weight of induction motor   = %g kg \n',mtot);
185
186 fprintf('\n')
187 fprintf('a. Mass of the stator          = %g kg \n',mstator);
188 fprintf('(a) Back iron                  = %g kg \n',mcores);
189 fprintf('(b) Teeth                      = %g kg \n',mteeths);
190 fprintf('(a) Winding                    = %g kg \n',mconds);
191
192 fprintf('\n')
193 fprintf('b. Mass of the rotor           = %g kg \n',mrotor);
194 fprintf('(a) Back iron                  = %g kg \n',mcorer);
195 fprintf('(b) Teeth                      = %g kg \n',mteethr);
196 fprintf('(a) Bars                       = %g kg \n',mcondr);
197 fprintf('-------------------------------------------------------------------------------\n');
198
199 fprintf('\n')
200 fprintf('-------------------------------------------------------------------------------\n');
201 fprintf('Moment of inertia of the IM    = %g kg.m^2 \n',J);
202 fprintf('Stator moment of inertia       = %g kg.m^2 \n',Js);
203 fprintf('Rotor moment of inertia        = %g kg.m^2 \n',Jr);
```

- **performance_eval.m**

```
1  function [y sp] = performance_eval(s)
2  % this function does the motor analysis
3
4  global m p omega R1 X1 Xm Xm5 Xm7 Xmm Xmp X2 X25 X27 X2m X2p R2 R25 R27 R2m...
5  R2p Rc Xc nm np V P0 nuair peB pef Rrtnls l g Rsg Na kwm kwp mteethr B0 omega0 ...
6  rhoair Pbase
7
8  % harmonic slips
9  s5 = 6-5*s;
10 s7 = -6+7*s;
11 if m>1
12     sm = 1+nm*(1-s);
13     sp = 1-np*(1-s);
14 end
15
16 % Stator Section Impedance
17 Z1 = j*X1 + R1;
18
19 % fundamental
20 Z21   = j*X2 + R2./s; % rotor impedence
21 Zm1   = 1/(1/(j*Xm)+ 1/Rc + 1/(j*Xc) + 1/Rrtnls);
22 Zag1  = 1./(1./Z21 + 1/Zm1);
23
24 % 5th
25 Z25   = j*X25 + R25./s5;
26 Zm5   = j*Xm5;
27 Zag5 = Zm5*Z25 ./ (Zm5+Z25);
28
```

```
% 7th
Z27  = j*X27 + R27./s7;
Zm7  = j*Xm7;
Zag7 = Zm7*Z27 ./ (Zm7+Z27);

Zag  = Zag1 + Zag5 + Zag7;

if m>1
    % pth
    Z2p  = j*X2p + R2p./sp;
    Zmp  = j*Xmp;
    Zagp = Zmp*Z2p ./ (Zmp+Z2p);
    % mth
    Z2m  = j*X2m + R2m./sm;
    Zmm  = j*Xmm;
    Zagm = Zmm*Z2m ./ (Zmm+Z2m);
    Zag = Zag + Zagp + Zagm;
end

Zt = Z1 + Zag;
It = V./Zt;

Zrest   = 1./(1/Rrtnls + 1/(j*Xc) + 1/(j*Xm)+1./Z21);
Ic = It.*Zrest./(Zrest+Rc); % current in Rc branch

% Zrest_  = 1./(1/Rc + 1/(j*Xc) + 1/(j*Xm)+1./Z21); % added on april 29,
% 2019 if it is the same as Prtnls
% Irtnls = It.*Zrest_./(Zrest_+Rrtnls); % current in Rc branch;

I21 = It.*Zm1./(Zm1+Z21);
I25 = It.*Zm5./(Zm5+Z25);
I27 = It.*Zm7./(Zm7+Z27);

if m>1
    I2p = It.*Zmp./(Zmp+Z2p);
    I2m = It.*Zmm./(Zmm+Z2m);
end

% Input power
Pin = 3*real(V*conj(It));

% Airgap electromagnetic power
Pag1 = 3*abs(I21.^2).*R2./s;
Pag5 = 3*abs(I25.^2).*R25./s5;
Pag7 = 3*abs(I27.^2).*R27./s7;
Pag  = Pag1 + Pag5 + Pag7;


% Pmech = Pag - Pslip - Pnls - Prtsl - Pwf

% Compute each loss component after the airgap power:

% (1) Slip losses (Pslip)
Pslip1 = s.*Pag1;
Pslip5 = s5.*Pag5;
Pslip7 = s7.*Pag7;
Pslip  = Pslip1 + Pslip5 + Pslip7;

if m>1
    Pagp = 3*abs(I2p.^2).*R2p./sp;
    Pagm = 3*abs(I2m.^2).*R2m./sm;
    Pag = Pag + Pagp + Pagm;

    Pslipm = sm.*Pagm;
    Pslipp = sp.*Pagp;
    Pslip  = Pslip + Pslipm + Pslipp;
end

% (2) Armature loss
Pa = 3*abs(It).^2*R1;
Vr = abs(It).*R1; % voltage drop to estimate Vag

% (3) core loss
Pc = 3*abs(Ic).^2*Rc;
% Pc = 3*(V-R1*It).^2/Rc;

```

```
105 % (4) Rotor teeth no load stray losses
106 % due to modulation of the fundamental flux due to stator slot openings
107
108 Prtnls = 3*abs(V)^2/Rrtnls*ones(1,numel(s)); % in rotor teeth laminations
109 % Prtnls = 3*abs(Irtnls).^2*Rrtnls;
110
111 % (5) Rotor teeth stray load losse
112 % (due to the stator mmf higher space harmonics)
113
114 % If the rotor is laminated, we should estimate
115 % losses in the rotor teeth due to zigzag fluxes
116 % use only the highest frequency components
117 % this is a component of stray load loss
118 % harmonic conduction losses are the rest of stray load loss
119
120 if m>1
121   Bm = abs(nm*p*(It-I2m).*Zmp./(2*l*Rsg*Na*kwm*omega)); % changed it from Zagp to Zmp on
          April 29, 2019
122   % or It only since I2m and I2p are very small
123   Bp = abs(np*p*(It-I2p).*Zmm./(2*l*Rsg*Na*kwp*omega));
124   omsp = abs(sp).*omega;
125   omsm = abs(sm).*omega;
126
127   Prtls = mteethr * Pbase*abs(Bm/B0).^peB .*abs(omsm/omega0).^pef ...
128     + mteethr * Pbase*abs(Bp/B0).^peB .*abs(omsp/omega0).^pef;
129 else
130   Bm = abs(5*p*It.*Zm5./(2*l*Rsg*Na*kw5*omega));
131   Bp = abs(7*p*It.*Zm7./(2*l*Rsg*Na*kw7*omega));
132   oms5 = abs(s5).*omega;
133   oms7 = abs(s7).*omega;
134
135   Prtls = mteethr * Pbase*abs(Bm/B0).^peB .*abs(oms5/omega0).^pef ...
136     + mteethr * Pbase*abs(Bp/B0).^peB .*abs(oms7/omega0).^pef;
137 end
138
139 % (6) Windage and friction losses:
140 omegam = omega/p*(1-s);
141 ren = omegam*Rsg*g/nuair; % Reynold's Number in the gap (unitless)
142 ff = .0076./(ren.^(.25));      % friction factor (N.m.s/Rad)
143 Pwf = 2*pi*Rsg^4*omegam.^3*l*rhoair.*ff;
144
145 % total losses
146 Ploss = Pa + Pc + Pslip + Prtnls + Prtls + Pwf;
147 % Converted power
148 % Pmech = Pag - Pslip;
149 Pmech = Pag - Pslip - Prtnls - Prtls - Pwf;
150 % Pmech = Pin - Ploss;
151
152 S   = 3*V*abs(It); % apparent power
153 eff = Pmech./Pin*100;
154 pf  = Pin./S;
155
156 Te = p/omega*(Pag1 - 5*Pag5 + 7*Pag7);
157 if m>1
158     Te = Te + p/omega*(np*Pagp - nm*Pagm);
159 end
160 Tm = p*Pmech/omega;
161
162 % find s corresponding to 175kW output power
163 [Pconvpk idx]= max(Pmech);
164 Pout = P0;
165 for i = 1:idx
166     if Pconvpk >= Pout
167         if Pmech(i)<Pout && Pmech(i+1)>Pout
168         % linear interpolation:
169         sp = s(i) + (s(i+1)-s(i)) * (Pout-Pmech(i))/(Pmech(i+1)-Pmech(i));
170         break
171         end
172     else
173         fprintf('Peak converter power is %g < required output power of %g \n', Pconvpk,
              Pout);
174         sp = [];
175         break
176     end
177
```

```
178 end
179
180 y = [It; Pin; S; Pag1; Pag5; Pag7; Pagm; Pagp; Pag; Pslip1; Pslip5; Pslip7;...
181       Pslipm; Pslipp; Pslip; Pa; Pc; Prtnls; Prtls; Pwf;...
182       Ploss; Pmech; Te;Tm; eff; pf; I21; I25; I27; I2m; I2p; Ic; Vr; ff];
183
184 end
```

- **dispresults.m**

```
1  fprintf('\n')
2  fprintf('                              Analysis                                \n')
3  fprintf('======================================================================= \n')
4
5
6  fprintf('\n')
7  fprintf('-------------------------------------------------------------------------\n');
8  fprintf('Flux Densities (peak) \n');
9  fprintf('Airgap flux density              = %g T\n',Bg*sqrt(2));
10 fprintf('Stator teeth flux density        = %g T\n',Bst*sqrt(2));
11 fprintf('Stator back iron flux density    = %g T\n',Bcs*sqrt(2));
12 fprintf('Rotor tooth flux density         = %g T\n',Brt*sqrt(2));
13 fprintf('Rotor back iron flux density     = %g T\n',Bcr*sqrt(2));
14 fprintf('-------------------------------------------------------------------------\n');
15
16
17 fprintf('\n')
18 fprintf('-------------------------------------------------------------------------\n');
19 % fprintf('Operating data: \n')
20 fprintf('Operating slip (s0)                 = %g\n',sp);
21 fprintf('RPM (N0)                            = %g\n',N0);
22 fprintf('Phase voltage (Vt)                  = %g V \n',V);
23 fprintf('supply frequency (f)                = %g Hz \n',f0);
24 fprintf('inverter frequency (fd)            = %g Hz \n',fd);
25 fprintf('-------------------------------------------------------------------------\n');
26
27 fprintf('At %g slip (rated speed): \n Skin Depth = %g mm >> rotor_slot depth = %g mm \n',
       sp, skin_depth_rated_speed*1e3,hr*1e3);
28 fprintf('Delta_rated_speed/hr = %g \n',skin_depth_rated_speed_to_hr);
29
30 fprintf('\n');
31 fprintf('-------------------------------------------------------------------------\n');
32 fprintf('\n');
33 fprintf('Current Density Limit for Natural Cooling:\n');
34 fprintf('Jl,limit                        = %g Arms/mm^2, %g A/mm^2 \n',Jslimit,Jslimit*sqrt(2))
35 fprintf('Jb,limit (bars)                 = %g Arms/mm^2, %g A/mm^2 \n',Jblimit,Jblimit*sqrt(2))
36
37 fprintf('\n');
38 fprintf('Current Density at locked rotor condition(0 RPM)\n');
39 fprintf('Jl,limit (stator winding)  = %g Arms/mm^2, %g A/mm^2 \n',Jb0RPM, Jb0RPM*sqrt(2));
40 fprintf('Jb,limit (bars)            = %g Arms/mm^2, %g A/mm^2 \n',Js0RPM, Js0RPM*sqrt(2));
41 fprintf('Je,limit (endring segment) = %g Arms/mm^2, %g A/mm^2 \n',Je0RPM, Je0RPM*sqrt(2));
42
43 fprintf('\n');
44 fprintf('Current Density at rated speed(%g RPM):\n',N0);
45 fprintf('Jl,limit (stator winding)  = %g Arms/mm^2, %g A/mm^2 \n',JsRated,JsRated*sqrt(2))
       ;
46 fprintf('Jb,limit (bars)            = %g Arms/mm^2, %g A/mm^2 \n',JbRated,JbRated*sqrt(2))
       ;
47 fprintf('Jb,limit (endring segment) = %g Arms/mm^2, %g A/mm^2 \n',JeRated,JeRated*sqrt(2))
       ;
48 fprintf('-------------------------------------------------------------------------\n');
49
50 fprintf('\n')
51 fprintf('Terminal current(It)                                                = %g
       Arms \n',abs(It0));
52 fprintf('\n')
53
54 fprintf('Fundamental rotor current (Referred to Stator),I2                   = %g
       Arms \n',abs(I210));
55 fprintf('I2,5                                                                = %g
       Arms \n',abs(I250));
```

```
56  fprintf('I2,7                                                                    = %g
        Arms \n',abs(I270));
57  fprintf('I2,11                                                                   = %g
        Arms \n',abs(I2m0));
58  fprintf('I2,13                                                                   = %g
        Arms \n',abs(I2p0));
59  fprintf('\n')
60
61  fprintf('Fundamental Rotor Bar Current (Ib) at locked rotor condition(0 RPM)     = %g
        Arms \n',abs(Ib0RPM));
62  fprintf('Fundamental Rotor Bar Current (Ib) at raten speed (%g RPM)          = %g Arms \n'
        ,N0, abs(IbRated));
63  fprintf('Fundamental Rotor End Ring Current (Ie) at locked rotor condition(0 RPM) = %g
        Arms \n',abs(Ie0RPM));
64  fprintf('Fundamental Rotor End Ring Current (Ie) at rated speed (%g RPM)     = %g Arms \n'
        ,N0, abs(IeRated));
65  fprintf('\n')
66
67  fprintf('Starting torque                  = %g N.m \n',Tstarting)
68  fprintf('EM torque at nominal speed       = %g N.m \n',Te0);
69
70  fprintf('\n');
71
72  fprintf('Input Power                      = %g W \n', Pin0);
73  fprintf('Apparent Power                   = %g VA \n', S0);
74
75  % Or
76  % fprintf('(Terminal Current/wire_area_per_phase_per_layer_per_turn_all_slots)  \n');
77
78  fprintf('\n');
79  fprintf('Airgap power: \n')
80  fprintf('Fundamental                      = %.7g W \n', Pag10);
81  fprintf('5th                              = %.7g W \n', Pag50);
82  fprintf('7th                              = %.7g W \n', Pag70);
83  fprintf('11th                             = %.7g W \n', Pagm0);
84  fprintf('13th                             = %.7g W \n', Pagp0);
85  fprintf('Total airgap power               = %.7g W \n', Pag0);
86
87  fprintf('\n');
88  fprintf('Losses: \n')
89  fprintf('Slip losses                      = %.7g W \n', Pslip0);
90  fprintf('Fundamental                      = %.7g W \n', Pslip10);
91  fprintf('5th                              = %.7g W \n', Pslip50);
92  fprintf('7th                              = %.7g W \n', Pslip70);
93  fprintf('11th                             = %.7g W \n', Pslipm0);
94  fprintf('13th                             = %.7g W \n', Pslipp0);
95
96  fprintf('Armature losses                  = %g W \n',Pa0);
97  fprintf('Core losses                      = %g W \n',Pc0);
98  fprintf('Windage loss                     = %g W \n',Pwf0);
99  fprintf('Rotor tooth no load stray loss = %g W \n',Prtnls0);
100 fprintf('Rotor tooth load stray loss     = %g W \n',Prtls0);
101 fprintf('Total losses                     = %g W \n', Ploss0);
102
103 fprintf('\n')
104 fprintf('VARloss: score&teeth +rteeth     = %g VAR \n',Qc);
105
106 fprintf('\n')
107 fprintf('Converted mechanical power: \n')
108 fprintf('Pconv    = Pag - Pslip - Prtnls - Prtls - Pwf     = %g W \n', Pmech0);
109 fprintf('Pconv''  = Pin - Ploss                             = %g W \n', Pin0 - Ploss0);
110
111 fprintf('\n')
112 fprintf('Efficiency = Pconv/Pin           = %g \n',eff0);
113 fprintf('Power factor                     = %g \n',pf0);
114 fprintf('-------------------------------------------------------------------------\n');
```

- **RunOptim.m**

```
1  % This script run genetic algorihms to optimize the motor design
2
3  clear; clc; close all;
```

```
4
5  % Constraints:
6
7  % 1) Bounds on optimization vars
8  x0(1)  = 1;                    % Nc,min
9  x0(2)  = 100e-3/2;             % Rry,min
10 x0(3)  = 20e-3;                % dcr,min
11 x0(4)  = 0.5e-3;               % g,min
12 x0(5)  = 10e-3;                % l,min
13 x0(6)  = 0.5e-3;               % dr,min
14 x0(7)  = 0.5e-3;               % ur,min
15 x0(8)  = 1e-3;                 % hr,min
16 x0(9)  = 0.3;                  % rtsp,min %Previously it was wr_min
17 x0(10) = 1e-3;                 % her,min
18 x0(11) = 1e-3;                 % ler,min
19 x0(12) = 115;                  % Vd_min
20 x0(13) = 0.5e-3;               % ds_min
21 x0(14) = 1e-3;                 % us,min % so that the wire can fit
22 x0(15) = .3;                   % stsp,min
23 x0(16) = 1e-3;                 % hs,min (in case of normal method in wire)
24 x0(17) = 0;                    % nsp,min
25 % x0(18)  = 2;                   % p,min
26 % x0(18)  = 18;                  % Nr,min
27
28 xf(1) = 300;                    % Nc_manx % let's set this to a maximum such that the guage
       is reasonable
29 xf(2) = 200e-3/2;              % Rry,max
30 xf(3) = 25e-3;                 % dcr,max
31 xf(4) = 1e-3;                  % g,max
32 xf(5)  = 40e-3;                % l,max
33 xf(6)  = 3e-3;                 % dr,max
34 xf(7) = 3e-3;                  % ur,max
35 xf(8) = 6e-3;                  % hr,max
36 xf(9) = 0.7;                   % rtsp,max
37 xf(10) = 10e-3;                % her,max
38 xf(11) = 15e-3;                % ler,max
39 xf(12) = 115;                  % Vd,max
40 xf(13) = 3e-3;                 % ds,max
41 xf(14) = 3e-3;                 % us,,max
42 xf(15) = .7;                   % stsp,max
43 xf(16) = 35e-3;                % hs,max (in case of normal method in wire)
44 xf(17) = 1;                    % nsp,max
45 % xf(18) = 3;                   % pmax
46 % xf(18)  = 29;                  % Nr,min
47
48 D      = numel(x0);            % number of variables to be optimized against
49 IntCon = [];                   % Define integer variables by their indices:
50
51 gaoptions = optimoptions('ga',...
52                          'FunctionTolerance',1e-6,...
53                          'ConstraintTolerance',1e-6,...
54                          'MaxGenerations',6*D,...
55                          'MaxTime',inf,...
56                          'Display','iter',...
57                          'PlotFcn', {@gaplotbestf,@gaplotbestindiv,@gaplotexpectation}...
58                          );
59 startTime = tic;
60 [x,fval,exitflag,output] = ga(@costfunc4,D,[],[],[],[],x0,xf,[],IntCon,gaoptions);
61 time_ga_sequential = toc(startTime);
62 fprintf('Serial GA optimization takes %g seconds.\n',time_ga_sequential);
63 gaAvailable = true;
64
65 fprintf('The number of generations was : %d\n', output.generations);
66 fprintf('The number of function evaluations was : %d\n', output.funccount);
67 fprintf('The best function value found was : %g\n', fval);
```

- **costfunc.m**

```
1 % Cost function to run optimization model
2 % Created Dec 11, 2018
3 % Mohammad Qasim
```

```
4
5  function OF = costfunc(x)
6
7  %%
8  global m p omega R1 X1 Xm Xm5 Xm7 Xmm Xmp X2 X25 X27 X2m X2p R2 R25 R27 R2m...
9  R2p Rc Xc nm np V P0 nuair peB pef Rrtnls l g Rsg Na kwm kwp mteethr B0 omega0 ...
10 rhoair Pbase
11
12 % some constants
13 sigAlum    = 2.3e7; %3.8e7;              % rotor bars conductivity (S/m)
14 sigCopper  = 6e7;                       % stator conductor cond (S/m)
15 rhocopper = 8400;                       % copper density in (kg/m^3)
16 rhoalum    = 2800;                      % rotor bars mass density (kg/m^3)
17 rhofe      = 7650;                      % steel density (kg/m^3) M1926G
18 u0         = 4*pi*1e-7;                 % permeability of air (H/m)
19 rhoair     = 1.225;                     % air density kg/m^3
20 nuair      = 1.56e-5;                   % kinematic viscosity of air (m^2/s)
21 %%
22 %=========================================================================
23                                  % Design data
24 %=========================================================================
25
26 % Optimization variables:
27 p     = 2;                          % pole pairs
28 m     = 2;                          % number of slots/pole/phase
29 Ns    = 6*p*m;                      % number of stator slots
30
31 % (1) Winding data
32 Nc    = x(1); %x(2)                 % number of turns per coil
33 Na    = 2*p*m*Nc;                   % Armature # turns per phase
34 nsp   = x(17);                      % # slots short pitched
35 nct   = 3*m -nsp;                   % # slots coil throw
36
37 % (2) motor dimensions
38 Rry   = x(2);                       % outer radius of rotor
39 dcr   = x(3);                       % radial depth of rotor annulus
40 Rrg   = Rry - dcr;                  % inner radius of rotor
41 g     = x(4);                       % physical airgap
42 Rsg = Rry - dcr - g;                % stator radius
43 l     = x(5);                       % active/axial length
44
45
46 % (3) rotor slots
47 Nr = 18; %x(8);                     % number of rotor slots
48 Nr = ceil(Nr);
49
50 dr   = x(6);                        % depression depth
51 ur   = x(7);                        % depression width
52 hr   = x(8);                        % slot depth
53 rslotp = 2*pi*(Rrg+dr+hr/2)/Nr;     % rotor slot pitch
54 rtsp = x(9);
55 rt = rtsp*rslotp;
56 wr   = rslotp - rt; %rslotp*(1-rtsp);  % slot width
57 rssp = wr/rslotp;                    % rotorslotopening-slotpitch ratio
58 rtsp = 1 - rssp;                     % rotor-tooth to slot-pitch ratio
59
60 her = x(10);                        % end ring radial height
61 ler = x(11);                        % end ring axial height
62
63 gama = p*2*pi/Ns;                   % stator slot pitch in elect.
64 sk    = 1e-17; %x(15);              % rotor skew in elect. rad
65
66 % (4) Nominal and operating values
67 f0     = 50;
68 omega0 = 2*pi*f0;
69 V      = x(12);
70 fd      = 360/60*p;
71 omega  = 2*pi*fd;
72 P0     = 15;                        % Desired output power at rated speed
73 % (6) Data for hysteresis core losses calculation
74 Pbase  = 1.3;                       % Core iron base dissp (W/kg)
75 B0     = 1;                         % for loss calculation
76 peB    = 1.88;%2.5, %1.88;          % B power exponent of steel
77 pef    = 1.53; %1.53;               % f power exponent of steel
78 Q01    = 1.08;                      % core iron var base 1
```

```
Q02     = 0.0144;                       % core iron var base 2
epq1    = 1.7;                          % core iron var expon 1
epq2    = 16.1;                         % core iron var expon 2

% (7) Stator slots

slotff = 0.45;                           % stator slot fill factor by copper
stf    = 0.95;                          % steel laminations stacking factor
ds     = x(13);                         % depression depth
us     = x(14);                         % depression width
sslotp = 2*pi*(Rsg-ds)/Ns;              % stator slot pitch airgap (top) side
hsmax  = Rsg*0.8;                       % maximum allowed stator slot height

%% Correct airgap
ccs = carterf(us,Rsg,Ns,g);  % carter factor stator
ccr = carterf(ur,Rrg,Nr,g);  % carter factor rotor
ge  = ccs*ccr*g;
R   = Rsg + ge/2;            % mean airgap radius
%%
%===================================   ===================================
                                    % EQV CKT
%=============================================================================

% 1) Stator resitance

% normal method where a gauge is not specified and is chosen later
    % based on the calculated radius
hs     = x(16);                         % slot height
stsp   = x(15);                          % toothwidth-slotpitch ratio
t0     = stsp*sslotp;                   % tooth-width
wst    = sslotp - t0;                   % stator slot top width
wsb = 2*pi*(Rsg-ds-hs)/Ns-t0;
sarea               = 1/2*(wsb +wst)*hs;              % slot trapezodial area
% Correction March 18, 2019 (there was extra sqrt(Ns) in the denominator of
% wire_radius :(
Aw                  = slotff*sarea/(2*Nc);            % OR slotff*sarea*(Ns/(3*2*Na)) %
    wire area per phase
wire_radius         = sqrt(Aw/pi);                    % wire radius per phase
lw                  = 2*(1+pi*(Rsg-ds-hs/2)/p);       % length of wire
lwt                 = lw*Na;                          % effective length of winding per
    phase
Rl = lwt/sigCopper/Aw;

% print some warnings if dimensions voilate physics
if hs>hsmax
    fprintf('warning: stator slot height is too large: max hs is %f mm \n',hsmax*1e3)
end

if wst<0 || wsb<0
    fprintf('Warning: Stator slot width bottom or top is negative\n');
end

if wsb < 2*pi*(Rsg-ds-hs)/Ns-t0
    fprintf('Warning: Stator slot width bottom or top is negative\n');
end

% Calculate winding factors needed later to calculate inductances

kw1 = wf(1,nsp,m);
kw5 = wf(5,nsp,m); % belt 5th
kw7 = wf(7,nsp,m); % belt 7th 8

% Zigzag order harmonics winding factors
if m>1
    np = Ns/p + 1; % or 6m + 1
    nm = Ns/p - 1; % or 6m - 1
else % if m = 1 => Ns = 6p => the harmonic order are 5 and 7
    np = Ns + 1;
    nm = Ns - 1;
end
kwp = wf(np,nsp,m);
kwm = wf(nm,nsp,m);

% Stator
% =============================================================================

```

```
% 1) Airgap magnetizing inductance: fundamental magnetizing inductance

Lm = 3/2*4/pi*u0*R*l*(kw1*Na)^2/(p^2*ge);
Xm = omega*Lm;

% 2) Stator leakage inductance

% a) Airgap leakage inductance: Space harmonic leakage induct components

% Belt leakage
Lm5 = Lm*(kw5/kw1/5)^2;
Xm5 = omega*Lm5;
Lm7 = Lm*(kw7/kw1/7)^2;
Xm7 = omega*Lm5;

% Zigzag leakage
if m>1
Lmp = Lm*(kwp/kw1/np)^2;
Xmp = omega*Lmp;

Lmm = Lm*(kwm/kw1/nm)^2;
Xmm = omega*Lmm;
end

% b) Slot leakage
wave        = (wst+wsb)/2;
Psslot      = u0*l*(hs/3/wave + ds/us);
Lsslotleak = Na^2/p*Psslot*(2/m - 5/4*nsp/m^2);
Xsslot      = Lsslotleak*omega;

% c) End-winding leakage inductance

wp = nct/(3*m); % winding pitch as a ratio of coil throw to pole pitch
Xe = 7*fd*3*Na^2*(2*Rsg)/p^2*le-6*(wp - 0.3);
Le = Xe/omega;
% Xe = 14*3/2*(u0*10/4/pi^2)*omega*r*Na^2/p^2*(wp   0.3)

Ll = Lsslotleak + Le;
Xl = Xsslot + Xe;

% Rotor
% ========================================================================
% 1) Skew leakage (we are consider it on the rotor side)

ks1 = skewf(1,sk);
ks5 = skewf(5,sk);
ks7 = skewf(7,sk);
ksp = skewf(np,sk);
ksm = skewf(nm,sk);

% Rotor skew leakage inductances reffered to stator
Lsk1 = Lm *(1 - ks1^2)/ks1^2 ; Xsk1 = omega*Lsk1;
Lsk5 = Lm5*(1 - ks5^2)/ks5^2 ; Xsk5 = omega*Lsk5;
Lsk7 = Lm7*(1 - ks7^2)/ks7^2 ; Xsk7 = omega*Lsk7;
if m>1
    Lskp = Lmp*(1 - ksp^2)/ksp^2 ; Xskp = omega*Lskp;
    Lskm = Lmm*(1 - ksm^2)/ksm^2 ; Xskm = omega*Lskm;
end

% 2) Rotor slot harmonics:

skin_depth = 1/sqrt(pi*fd*u0*sigAlum); % skin depth = 33mm >> hr
% For now no diffusion. Update this later to incorporate diffusion

Lrslotleak  = u0*l*(hr/3/wr + dr/ur); % H
Lrslotleak5 = Lrslotleak*(kw5/kw1)^2;
Lrslotleak7 = Lrslotleak*(kw7/kw1)^2;
if m>1
    Lrslotleakp = Lrslotleak*(kwp/kw1)^2;
    Lrslotleakm = Lrslotleak*(kwm/kw1)^2;
end

% Fundamental:
X2slot      = (12*omega*Na^2*kw1^2/Nr*Lrslotleak)/ks1^2; % divide by ks1^2
% when referring to the stator side
% Belt:
```

```
X25slot     = (12*omega*Na^2*kw1^2/Nr*Lrslotleak5)/ks5^2;
X27slot     = (12*omega*Na^2*kw1^2/Nr*Lrslotleak7)/ks7^2;
% Zigzag:
if m>1
    X2pslot = (12*omega*Na^2*kw1^2/Nr*Lrslotleakp)/ksp^2;
    X2mslot = (12*omega*Na^2*kw1^2/Nr*Lrslotleakm)/ksm^2;
end

% 3) End ring leakage extended to slot/rotor-bar leakage

% Based on Grover's formula for the self inductance of a circular ring
% with mean radius (Ri+her/2) with a sqaure cross section (ignore depression):
er_mean_radius = Rrg+her/2;
Ler = u0*er_mean_radius*1/2/Nr*...
    ( 1/2*(1+wr*hr/er_mean_radius^2/6)*log(8*er_mean_radius^2/wr/hr)...
      -.8434 + .2041*wr*hr/er_mean_radius^2 );
L2e = Ler/2/(sin(p*pi/Nr))^2; % leakage inductance of one endring

L25e = L2e*(kw5/kw1)^2;
L27e = L2e*(kw7/kw1)^2;
if m>1
    L2pe = L2e*(kwp/kw1)^2;
    L2me = L2e*(kwm/kw1)^2;
end

% Fundamental:
X2e     = (12*omega*Na^2*kw1^2/Nr*L2e)/ks1^2; % divide by ks1^2
% when referring to the stator side
% Belt:
X25e    = (12*omega*Na^2*kw1^2/Nr*L25e)/ks5^2;
X27e    = (12*omega*Na^2*kw1^2/Nr*L27e)/ks7^2;
% Zigzag:
if m>1
    X2pe = (12*omega*Na^2*kw1^2/Nr*L2pe)/ksp^2;
    X2me = (12*omega*Na^2*kw1^2/Nr*L2me)/ksm^2;
end

% 4) Rotor zigzag harmonics

% Fundamental
X2z  = Xm*p^2*( 1/(Nr+p)^2 + 1/(Nr-p)^2 )/ks1^2;
% Belt
X25z = Xm*p^2*(kw5/kw1)^2*( 1/(Nr+5*p)^2 + 1/(Nr-5*p)^2 )/ks5^2;
X27z = Xm*p^2*(kw7/kw1)^2*( 1/(Nr+7*p)^2 + 1/(Nr-7*p)^2 )/ks7^2;
% Zigzag
X2pz = Xm*p^2*(kwp/kw1)^2*( 1/(Nr+np*p)^2 + 1/(Nr-np*p)^2 )/ksp^2;
X2mz = Xm*p^2*(kwm/kw1)^2*( 1/(Nr+nm*p)^2 + 1/(Nr-nm*p)^2 )/ksm^2;

% Compute Total leakage reactance
X2  = X2slot  + X2e + X2z + Xsk1;
X25 = X25slot + X25e + X25z + Xsk5;
X27 = X27slot + X27e + X27z + Xsk7;
if m>1
X2p = X2pslot + X2pe + X2pz + Xskp;
X2m = X2mslot + X2me + X2mz + Xskm;
end

% 5) Rotor resitance (reffered to stator)

R2b = 1/(sigAlum*(wr*hr + ur*dr));
Rer = 2*pi*Rrg/Nr/her/ler/sigAlum;
Re_method = 'detailed'; % choose between 'reduced_order' or 'detailed'

if(strcmp(Re_method,'reduced_order')) % (Alger's)
    R2e = R2b*Nr*Rrg*wr/(pi*l*ler*p^2);
else % detailed (Lippo's)
    R2e = Rer/2/(sin(p*pi/Nr))^2;
end


R2be = R2b + R2e;

R2  = 12*Na^2*kw1^2/Nr*R2be/ks1^2;
R25 = 12*Na^2*kw5^2/Nr*R2be/ks5^2;
R27 = 12*Na^2*kw7^2/Nr*R2be/ks7^2;
```

```
if m>1
R2p = 12*Na^2*kwp^2/Nr*R2be/ksp^2;
R2m = 12*Na^2*kwm^2/Nr*R2be/ksm^2;
end

%%

% Calculate Core elements
% =========================================================================

% (1) First calculate the stator hysteresis core loss density (W/)of
% (a) stator teeth, (b) stator back iron, (c) rotor teeth, (d) rotor bars
% and end rings

Bg = p*V/(2*Rsg*l*Na*kw1*omega); % air gap flux density

% (a) Stator teeth

Bst  = Bg/stsp*stf; % stator tooth flux density;
Keddy = 8.1564; % W.m/V^2
Kh = 0;
Kex = 0;
% Pst = Pcloss(Keddy,Kh,Kex,f,Bst); % W/Vol
Pst  = Pbase*abs(Bst/B0)^peB*abs(omega/omega0)^pef; % tooth loss density (W/kg)
Qst  = (Q01*abs(Bst/B0)^epq1 + Q02*abs(Bst/B0)^epq2)*abs(omega/omega0);

% (b) Stator back iron

Bcs = Bg*Rsg/(p*(Rsg-hs))*stf; % stator back iron flux density

% Pdc = Pcloss(Keddy,Kh,Kex,f,Bcs); % W/Vol
Pdc = Pbase*abs(Bcs/B0)^peB*abs(omega/omega0)^pef; % back iron loss density
Qdc = (Q01*abs(Bcs/B0)^epq1 + Q02*abs(Bcs/B0)^epq2)*abs(omega/omega0);
% back iron VAR density

% (c) Rotor teeth
Brt = Bg/rtsp; % rotor tooth flux density
Qrt = (Q01*abs(Brt/B0)^epq1 + Q02*abs(Brt/B0)^epq2)*abs(omega/omega0);
% rotor teeth var density

% (d) Rotor back iron  <==== added this March 20, 2017
% ask kirtley if I should add rotor back iron losses to core losses Pc

Bcr = Bg*Rrg/( p*(dcr-hr) )*stf; % rotor back iron flux density
Pdrc = Pbase*abs(Bcr/B0)^peB*abs(omega/omega0)^pef; % back iron loss density

% 2) calcualte the mass of (a) back iron , (b) teeth, and (c) conductor

% (a) Mass of back iron
mcores = pi*(Rsg-ds-hs)^2*l*rhofe;
mcorer = pi*(Rry^2-(Rrg+dr+hr)^2)*l*rhofe;

% (b) Mass of tooth
% mtooths = 2*pi*Rsg*(hs+ds)*l*rhofe*stsp; % What is this? Ask Jim
mteeths =( ds*(sslotp-us) + hs/2*(2*sslotp-wst-wsb) )*l*Ns*rhofe; % my expr
mteethr = pi*((Rrg+dr+hr)^2-(Rrg)^2)*l*rhofe*rtsp;

% (c) Conductor mass
rslot_area  = wr*hr+ur*dr;
mconds = 3*lwt*Aw* rhocopper; % stator conductor mass (multiply by three to get mass for
    the copper weight of the three phases). Modified on April 15,2019
mcondr = Nr*rslot_area*l*rhoalum + 2*(pi*((Rrg+dr+her)^2-(Rrg+dr)^2)*ler*rhoalum);
% rotor conductor mass inculding end ring

mstator = mcores + mteeths + mconds; % total mass of stator
mrotor  = mcorer + mteethr + mcondr; % total mass of rotor
mtot    = mstator + mrotor; % total active mass of the IM

% Motor moment of inertia: (only for result display)
% stator
Ds = 2*Rsg;
Jsx = 1/8*mstator*Ds^2;
Jsy = 1/4*mstator*(Ds^2/4 + 1^2/3);
Js = sqrt(Jsx^2+Jsy^2);
% rotor
D1 = 2*Rry;
```

```
D2 = 2*Rrg;
Jrx = 1/8*mrotor*(D1^2 + D2^2);
Jry = 1/4*mrotor*( (D1^2 + D2^2)/4 + 1^2/3);
Jr = sqrt(Jrx^2+Jry^2);

J = sqrt(Js^2+Jr^2);

% total stator core loss at nominal flux density
Pc = Pst*mteeths + Pdc * mcores;
% Pc = Pst*pi*Rsg^2*l + Pdc * pi*(Rsg-hs)^2*l/p;
%%
% total VAR loss (stator core + stator teeth + rotor teeth)at nominal B0
Qc = Qst*mteeths + Qdc*mcores + Qrt*mteethr;

% then core parallel resistance is %
Rc = 3*V^2/Pc;
% and parallel reactance is:
Xc = 3*V^2/Qc;
% Xc = inf;

% No load loss in rotor teeth because of stator slot opening modulation
% of fundamental flux density:

% parallel resistance element for zigzag flux loss
% first, generate nominal zigzag flux variation:
% thetad is the normalized angular slot opening
thetad = Ns*us/Rsg;

% BH is the nominal flux variation
BH = Bg * (2/pi) * sin (0.5*thetad);
% Prtnls = Ploss(Keddy,Kh,Kex,f,BH); % W/Vol
Prtnls = P0*abs(BH/B0)^peB*abs(Ns*omega/omega0)^pef; % back iron loss density
% so then the equivalent resistance is:
Rrtnls = 3 * V^2 / Prtnls;

dispmotordata_v2

%%
%=========================================================================
                                % Motor Analysis
%=========================================================================

% Motor analysis

s        = logspace(-6,0,1e3);
[y sp]   = motoranalysis_edited_need_revision(s);
It       = y(1,:);
Pin      = y(2,:);
S        = y(3,:);
Pag1     = y(4,:);
Pag5     = y(5,:);
Pag7     = y(6,:);
Pagm     = y(7,:);
Pagp     = y(8,:);
Pag      = y(9,:);
Pslip1   = y(10,:);
Pslip5   = y(11,:);
Pslip7   = y(12,:);
Pslipm   = y(13,:);
Pslipp   = y(14,:);
Pslip    = y(15,:);
Pa       = y(16,:);
Pc       = y(17,:);
Prtnls   = y(18,:);
Prtls    = y(19,:);
Pwf      = y(20,:);
Ploss    = y(21,:);
Pmech    = y(22,:);
Te       = y(23,:);
Tm       = y(24,:);
eff      = y(25,:);
pf       = y(26,:);
I21      = y(27,:);
I25      = y(28,:);
I27      = y(29,:);
```

```
455 I2m      = y(30,:);
456 I2p      = y(31,:);
457 Ic       = y(32,:);
458 Vr       = y(33,:);
459
460
461
462 %%
463 Tstarting = Te(end); % starting torque at slip = 1
464
465 if isempty(sp) % when the linear search cannot find Pout = 23 W
466     fprintf('Pconv,pk < Pout,rating \n');
467     OF = 1e8; % to force the optim. algorithm to try another x
468 else
469     yp = motoranalysis_edited_need_revision(sp);
470     It0      = yp(1);
471     Pin0     = yp(2);
472     S0       = yp(3);
473     Pag10    = yp(4);
474     Pag50    = yp(5);
475     Pag70    = yp(6);
476     Pagm0    = yp(7);
477     Pagp0    = yp(8);
478     Pag0     = yp(9);
479     Pslip10  = yp(10);
480     Pslip50  = yp(11);
481     Pslip70  = yp(12);
482     Pslipm0   = yp(13);
483     Pslipp0  = yp(14);
484     Pslip0   = yp(15);
485     Pa0      = yp(16);
486     Pc0      = yp(17);
487     Prtnls0  = yp(18);
488     Prtls0   = yp(19);
489     Pwf0     = yp(20);
490     Ploss0   = yp(21);
491     Pmech0   = yp(22);
492     Te0      = yp(23);
493     Tm0      = yp(24);
494     eff0     = yp(25);
495     pf0      = yp(26);
496     I210     = yp(27);
497     I250     = yp(28);
498     I270     = yp(29);
499     I2m0     = yp(30);
500     I2p0     = yp(31);
501     Ic0      = y(32,:);
502     Vr0      = y(33);
503
504
505     % calculate current densities:
506
507     % stator
508     Jslimit = 5; % Arms/mm^2 (based on Lippo's table6 6 for ODP motors chp 6 pg 285)
509
510     Js0RPM    = abs(It(end))/Aw*1e-6;
511     JsRated   = abs(It0)/Aw*1e-6;
512
513     % rotor
514
515     I20RPM   = sqrt(abs(I21(end))^2+abs(I25(end))^2+abs(I27(end))^2+abs(I2m(end))^2+abs(I2p
        (end))^2);
516     I2Rated = sqrt(abs(I210)^2+abs(I250)^2+abs(I270)^2+abs(I2m0)^2+abs(I2p0)^2);
517
518     % bar current desnity
519     Ib0RPM   = 6*Na*kw1/Nr*I20RPM;
520     IbRated = 6*Na*kw1/Nr*I2Rated;
521
522     Jblimit = 7.75; %Arms/mm^2 or 5000 Arms/in^2 as indicated by Lippo chp6 pg 285
523
524     Jb0RPM     = Ib0RPM/rslot_area*1e-6;
525     JbRated    = IbRated/rslot_area*1e-6;
526
527         % end ring
528     endring_current = 'exact'; %1stOrderTylor
529     if(strcmp(endring_current,'exact'))
```

```
530             IeORPM = abs(IbORPM/(1-exp(j*2*pi*p/Nr)));
531             IeRated = abs(IbRated/(1-exp(j*2*pi*p/Nr)));
532         elseif(strcmp(endring_current,'1stOrderTylor'))
533             IeORPM = IbORPM*Nr/2/pi/p;
534             IeRated = IbRated*Nr/2/pi/p;
535         end
536
537         JeORPM      = IeORPM/rslot_area*1e-6;
538         JeRated     = IeRated/rslot_area*1e-6;
539
540         % Calculate skin_depth at slip:
541         skin_depth_rated_speed = 1/sqrt(sp*pi*fd*u0*sigAlum);
542         skin_depth_rated_speed_to_hr = skin_depth_rated_speed/hr;
543
544         omegam = omega/p*(1-s);
545         N = omegam*60/(2*pi);
546         N0 = omega/p*(1-sp)*60/2/pi;
547
548         % display results in case of meeting the power requirement
549         dispresults
550
551         % objective function
552         b1 = 1;
553         b2 = 4;
554         b3 = 0;
555         b4 = 0;
556         Bmax = max(sqrt(2)*[Bg Bst Brt Bcs Bcr]);
557
558         ff = (eff0^b1)/(mtot^b2); % Cost Function
559         if Bmax > 1.7
560             OF  = 1/ff  + 1e3;
561         else
562             OF  = 1/ff;
563         end
564
565         if eff0<0
566             OF = 1e6;
567         end
568
569         figure (2);
570         hold on;
571
572         if (eff0>30 && mtot>2)
573         plot(eff0,mtot,'-o','color',[0 173 187]./255);
574
575         ylabel('Active weight (kg)');
576         xlabel('Efficiency %');
577         title('Pareto frontier')
578
579         hold off;
580         end
581
582     end
583     end
```

- **sensitivity_analysis_dr_ur.m**

```
1  % Sensitivity analysis on two variables
2
3  %'x is the motor variables
4  % var1 is the first variable to run sensitivity against
5  % var2 is the second variable to run sensitivity against
6  % Pout is the required output power
7
8  function [Eff Mactive Torque mechPower] = sensitivity_analysis_dr_ur(x,var1,var2,Pout)
9
10 % clear; clc; close all;
11 % choose the two variables and range you want to do it on
12 dr  = var1; %3e-3                          % depression depth
13 ur  = var2; %0.54e-3;
14 M = numel(dr);
15 Eff = zeros(M);
```

```
Mactive = zeros(M);
Torque = zeros(M);
mechPower = zeros(M);
for i = 1:M %dr
%%
for j = 1:M %ur
%%
global m p omega R1 X1 Xm Xm5 Xm7 Xmm Xmp X2 X25 X27 X2m X2p R2 R25 R27 R2m...
R2p Rc Xc nm np V P0 nuair peB pef Rrtnls l g Rsg Na kwm kwp mteethr B0 omega0 ...
rhoair Pbase

% some constants
sigAlum    = 2.3e7; %3.8e7;              % rotor bars conductivity (S/m)
sigCopper  = 6e7;                        % stator conductor cond (S/m)
rhocopper  = 8400;                       % copper density in (kg/m^3)
rhoalum    = 2800;                       % rotor bars mass density (kg/m^3)
rhofe      = 7650;                       % steel density (kg/m^3) M1926G
u0         = 4*pi*1e-7;                  % permeability of air (H/m)
rhoair     = 1.225;                      % air density kg/m^3
nuair      = 1.56e-5;                    % kinematic viscosity of air (m^2/s)
%%
%=========================================================================
                                % Design data
%=========================================================================

% Optimization variables:
p     = 2;                             % pole pairs
m     = 2;                             % number of slots/pole/phase
Ns    = 6*p*m;                         % number of stator slots

% (1) Winding data
Nc    = x(1); %x(2)                          % number of turns per coil
Na    = 2*p*m*Nc;                      % Armature # turns per phase
nsp   = x(17);                          % # slots short pitched
% remember fractional pitch makes it possible to use number of stator slots
% which is not an exact multiple of the number of poles, thus tending to
% supress pulsations of flux as the teeth move relative to the pole faces,
% and so largly eliminates tooth ripple in the voltage waveform
nct   = 3*m-nsp;                        % # slots coil throw

% (2) motor dimensions
Rry   = x(2);                           % outer radius of rotor
dcr   = x(3);                           % radial depth of rotor annulus
Rrg   = Rry - dcr;                      % inner radius of rotor
g     = x(4);                           % physical airgap
Rsg = Rry - dcr - g;                    % stator radius
l     = x(5);                           % active/axial length


% (3) rotor slots
Nr = 18; %x(8);                             % number of rotor slots
Nr = ceil(Nr);

% dr   = x(6);                            % depression depth
% ur   = x(7);                            % depression width
hr   = x(8);                            % slot depth
rslotp = 2*pi*(Rrg+dr(i)+hr/2)/Nr;          % rotor slot pitch
rtsp = x(9);
rt = rtsp*rslotp;
wr   = rslotp - rt; %rslotp*(1-rtsp);   % slot width
rssp = wr/rslotp;                       % rotorslotopening-slotpitch ratio
% rtsp = 1 - rssp;                        % rotor-tooth to slot-pitch ratio

her = x(10);                            % end ring radial height
ler = x(11);                            % end ring axial height

gama = p*2*pi/Ns;                       % stator slot pitch in elect.
sk    = 1e-17; %x(15);                          % rotor skew in elect. rad

% (4) Nominal and operating values
f0     = 50;
omega0 = 2*pi*f0;
V      = x(12);
fd      = 360/60*p;
omega  = 2*pi*fd;
```

```
P0      = Pout;                                 % Desired output power at rated speed
% (6) Data for hysteresis core losses calculation
Pbase   = 1.3;                                  % Core iron base dissp (W/kg)
B0      = 1;                                    % for loss calculation
peB     = 1.88;%2.5; %1.88;                     % B power exponent of steel
pef     = 1.53; %1.53;                          % f power exponent of steel
Q01     = 1.08;                                 % core iron var base 1
Q02     = 0.0144;                               % core iron var base 2
epq1    = 1.7;                                  % core iron var expon 1
epq2    = 16.1;                                 % core iron var expon 2

% (7) Stator slots

slotff = 0.45;                                  % stator slot fill factor by copper
stf    = 0.95;                                  % steel laminations stacking factor
ds     = x(13);                                 % depression depth
us     = x(14);                                 % depression width
sslotp = 2*pi*(Rsg-ds)/Ns;                      % stator slot pitch airgap (top) side
hsmax  = Rsg*0.8;                               % maximum allowed stator slot height

%% Correct airgap
ccs = carterf(us,Rsg,Ns,g);  % carter factor stator
ccr = carterf(ur(j),Rrg,Nr,g);  % carter factor rotor
ge  = ccs*ccr*g;
R   = Rsg + ge/2;              % mean airgap radius
%%
%=================================== ==================================
                                % EQV CKT
%=========================================================================

% 1) Stator resitance

% normal method where a gauge is not specified and is chosen later
    % based on the calculated radius
hs     = x(16);                                 % slot height
stsp   = x(15);                                  % toothwidth-slotpitch ratio
t0     = stsp*sslotp;                           % tooth-width
wst    = sslotp - t0;                           % stator slot top width
wsb = 2*pi*(Rsg-ds-hs)/Ns-t0;
sarea               = 1/2*(wsb +wst)*hs;                % slot trapezodial area
% Correction March 18, 2019 (there was extra sqrt(Ns) in the denominator of
% wire_radius :(
Aw                  = slotff*sarea/(2*Nc);              % OR slotff*sarea*(Ns/(3*2*Na)) %
    wire area per phase
wire_radius         = sqrt(Aw/pi);                      % wire radius per phase
lw                  = 2*(1+pi*(Rsg-ds-hs/2)/p);         % length of wire
lwt                 = lw*Na;                            % effective length of winding per
    phase
R1 = lwt/sigCopper/Aw;

% print some warnings if dimensions voilate physics
if hs>hsmax
    fprintf('warning: stator slot height is too large: max hs is %f mm \n',hsmax*1e3)
end

if wst<0 || wsb<0
    fprintf('Warning: Stator slot width bottom or top is negative\n');
end

if wsb < 2*pi*(Rsg-ds-hs)/Ns-t0
    fprintf('Warning: Stator slot width bottom or top is negative\n');
end

% Calculate winding factors needed later to calculate inductances

kw1 = wf(1,nsp,m);
kw5 = wf(5,nsp,m); % belt 5th
kw7 = wf(7,nsp,m); % belt 7th 8

% Zigzag order harmonics winding factors
if m>1
    np = Ns/p + 1; % or 6m + 1
    nm = Ns/p - 1; % or 6m - 1
else % if m = 1 => Ns = 6p => the harmonic order are 5 and 7.
    % Thus remove p to makes sure that you get the zigzag harmonic order
```

```
164         np = Ns + 1;
165         nm = Ns - 1;
166     end
167     kwp = wf(np,nsp,m);
168     kwm = wf(nm,nsp,m);
169
170     % Stator
171     % ================================================================================
172
173     % 1) Airgap magnetizing inductance: fundamental magnetizing inductance
174
175     Lm = 3/2*4/pi*u0*R*l*(kwl*Na)^2/(p^2*ge);
176     Xm = omega*Lm;
177
178     % 2) Stator leakage inductance
179
180     % a) Airgap leakage inductance: Space harmonic leakage induct components
181
182     % Belt leakage
183     Lm5 = Lm*(kw5/kwl/5)^2;
184     Xm5 = omega*Lm5;
185     Lm7 = Lm*(kw7/kwl/7)^2;
186     Xm7 = omega*Lm5;
187
188     % Zigzag leakage
189     if m>1
190     Lmp = Lm*(kwp/kwl/np)^2;
191     Xmp = omega*Lmp;
192
193     Lmm = Lm*(kwm/kwl/nm)^2;
194     Xmm = omega*Lmm;
195     end
196
197     % b) Slot leakage
198     wave        = (wst+wsb)/2;
199     Psslot      = u0*l*(hs/3/wave + ds/us);
200     Lsslotleak  = Na^2/p*Psslot*(2/m - 5/4*nsp/m^2);
201     Xsslot      = Lsslotleak*omega;
202
203     % c) End-winding leakage inductance
204
205     wp = nct/(3*m); % winding pitch as a ratio of coil throw to pole pitch
206     Xe = 7*fd*3*Na^2*(2*Rsg)/p^2*le-6*(wp - 0.3);
207     Le = Xe/omega;
208     % Xe = 14*3/2*(u0*10/4/pi^2)*omega*r*Na^2/p^2*(wp -0.3)
209
210     Ll = Lsslotleak + Le;
211     Xl = Xsslot + Xe;
212
213     % Rotor
214     % ================================================================================
215     % 1) Skew leakage (we are consider it on the rotor side)
216
217     ksl = skewf(1,sk);
218     ks5 = skewf(5,sk);
219     ks7 = skewf(7,sk);
220     ksp = skewf(np,sk);
221     ksm = skewf(nm,sk);
222
223     % Rotor skew leakage inductances reffered to stator
224     Lsk1 = Lm *(1 - ksl^2)/ksl^2 ; Xsk1 = omega*Lsk1;
225     Lsk5 = Lm5*(1 - ks5^2)/ks5^2 ; Xsk5 = omega*Lsk5;
226     Lsk7 = Lm7*(1 - ks7^2)/ks7^2 ; Xsk7 = omega*Lsk7;
227     if m>1
228         Lskp = Lmp*(1 - ksp^2)/ksp^2 ; Xskp = omega*Lskp;
229         Lskm = Lmm*(1 - ksm^2)/ksm^2 ; Xskm = omega*Lskm;
230     end
231
232     % 2) Rotor slot harmonics:
233
234     skin_depth = 1/sqrt(pi*fd*u0*sigAlum); % skin depth = 33mm >> hr
235     % For now no diffusion. Update this later to incorporate diffusion
236
237     Lrslotleak  = u0*l*(hr/3/wr + dr(i)/ur(j)); % H
238     Lrslotleak5 = Lrslotleak*(kw5/kwl)^2;
239     Lrslotleak7 = Lrslotleak*(kw7/kwl)^2;
240     if m>1
```

```
    Lrslotleakp = Lrslotleak*(kwp/kw1)^2;
    Lrslotleakm = Lrslotleak*(kwm/kw1)^2;
end

% Fundamental:
X2slot     = (12*omega*Na^2*kw1^2/Nr*Lrslotleak)/ks1^2; % divide by ks1^2
% when referring to the stator side
% Belt:
X25slot    = (12*omega*Na^2*kw1^2/Nr*Lrslotleak5)/ks5^2;
X27slot    = (12*omega*Na^2*kw1^2/Nr*Lrslotleak7)/ks7^2;
% Zigzag:
if m>1
    X2pslot = (12*omega*Na^2*kw1^2/Nr*Lrslotleakp)/ksp^2;
    X2mslot = (12*omega*Na^2*kw1^2/Nr*Lrslotleakm)/ksm^2;
end

% 3) End ring leakage extended to slot/rotor bar leakage

% Based on Grover's formula for the self inductance of a circular ring
% with mean radius (Ri+her/2) with a sqaure cross section (ignore depression).
er_mean_radius = Rrg+her/2;
Ler = u0*er_mean_radius*1/2/Nr*...
    ( 1/2*(1+wr*hr/er_mean_radius^2/6)*log(8*er_mean_radius^2/wr/hr)...
      -.8434 + .2041*wr*hr/er_mean_radius^2 );
L2e = Ler/2/(sin(p*pi/Nr))^2; % leakage inductance of one endring

L25e = L2e*(kw5/kw1)^2;
L27e = L2e*(kw7/kw1)^2;
if m>1
    L2pe = L2e*(kwp/kw1)^2;
    L2me = L2e*(kwm/kw1)^2;
end

% Fundamental:
X2e      = (12*omega*Na^2*kw1^2/Nr*L2e)/ks1^2; % divide by ks1^2
% when referring to the stator side
% Belt:
X25e     = (12*omega*Na^2*kw1^2/Nr*L25e)/ks5^2;
X27e     = (12*omega*Na^2*kw1^2/Nr*L27e)/ks7^2;
% Zigzag:
if m>1
    X2pe = (12*omega*Na^2*kw1^2/Nr*L2pe)/ksp^2;
    X2me = (12*omega*Na^2*kw1^2/Nr*L2me)/ksm^2;
end

% 4) Rotor zigzag harmonics

% Fundamental
X2z  = Xm*p^2*( 1/(Nr+p)^2 + 1/(Nr-p)^2 )/ks1^2;
% Belt
X25z = Xm*p^2*(kw5/kw1)^2*( 1/(Nr+5*p)^2 + 1/(Nr-5*p)^2 )/ks5^2;
X27z = Xm*p^2*(kw7/kw1)^2*( 1/(Nr+7*p)^2 + 1/(Nr-7*p)^2 )/ks7^2;
% Zigzag
X2pz = Xm*p^2*(kwp/kw1)^2*( 1/(Nr+np*p)^2 + 1/(Nr-np*p)^2 )/ksp^2;
X2mz = Xm*p^2*(kwm/kw1)^2*( 1/(Nr+nm*p)^2 + 1/(Nr-nm*p)^2 )/ksm^2;

% Compute Total leakage reactance
X2  = X2slot  + X2e + X2z + Xsk1;
X25 = X25slot + X25e + X25z + Xsk5;
X27 = X27slot + X27e + X27z + Xsk7;
if m>1
X2p = X2pslot + X2pe + X2pz + Xskp;
X2m = X2mslot + X2me + X2mz + Xskm;
end

% 5) Rotor resitance (reffered to stator)
R2b = 1/(sigAlum*(wr*hr + ur(j)*dr(i)));
Rer = 2*pi*Rrg/Nr/her/ler/sigAlum;
Re_method = 'detailed'; % choose between 'reduced_order' or 'detailed'

if(strcmp(Re_method,'reduced_order')) % (Alger's)
    R2e = R2b*Nr*Rrg*wr/(pi*1*ler*p^2);
else % detailed (Lippo's)
    R2e = Rer/2/(sin(p*pi/Nr))^2;
end
```

```
316
317
318 R2be = R2b + R2e;
319
320
321 R2  = 12*Na^2*kw1^2/Nr*R2be/ks1^2;
322 R25 = 12*Na^2*kw5^2/Nr*R2be/ks5^2;
323 R27 = 12*Na^2*kw7^2/Nr*R2be/ks7^2;
324 if m>1
325 R2p = 12*Na^2*kwp^2/Nr*R2be/ksp^2;
326 R2m = 12*Na^2*kwm^2/Nr*R2be/ksm^2;
327 end
328
329 %%
330
331 % Calculate Core elements
332 % ========================================================================
333
334 Bg = p*V/(2*Rsg*l*Na*kw1*omega); % air gap flux density
335
336 % (a) Stator teeth
337
338 Bst  = Bg/stsp*stf; % stator tooth flux density;
339 Keddy = 8.1564; % W m/V^2
340 Kh = 0;
341 Kex = 0;
342 % Pst = Ploss(Keddy,Kh,Kex,f,Bst); % W/Vol
343 Pst  = Pbase*abs(Bst/B0)^peB*abs(omega/omega0)^pef; % tooth loss density (W/kg)
344 Qst  = (Q01*abs(Bst/B0)^epq1 + Q02*abs(Bst/B0)^epq2)*abs(omega/omega0);
345
346 % (b) Stator back iron
347
348 Bcs = Bg*Rsg/(p*(Rsg-hs))*stf; % stator back iron flux density
349
350 % Pdc = Ploss(Keddy,Kh,Kex,f,Bcs); % W/Vol
351 Pdc = Pbase*abs(Bcs/B0)^peB*abs(omega/omega0)^pef; % back iron loss density
352 Qdc = (Q01*abs(Bcs/B0)^epq1 + Q02*abs(Bcs/B0)^epq2)*abs(omega/omega0);
353 % back iron VAR density
354
355 % (c) Rotor teeth
356 Brt = Bg/rtsp; % rotor tooth flux density
357 Qrt = (Q01*abs(Brt/B0)^epq1 + Q02*abs(Brt/B0)^epq2)*abs(omega/omega0);
358 % rotor teeth var density
359
360 % (d) Rotor back iron  <==== added this March 20, 2017
361 % ask kirtley if I should add rotor back iron losses to core losses Pc
362
363 Bcr = Bg*Rrg/( p*(dcr-hr) )*stf; % rotor back iron flux density
364 Pdrc = Pbase*abs(Bcr/B0)^peB*abs(omega/omega0)^pef; % back iron loss density
365
366 % 2) calcualte the mass of (a) back iron , (b) teeth, and (c) conductor
367
368 % (a) Mass of back iron
369 mcores = pi*(Rsg-ds-hs)^2*l*rhofe;
370 mcorer = pi*(Rry^2-(Rrg+dr(i)+hr)^2)*l*rhofe;
371
372 % (b) Mass of tooth
373 % mtooths = 2*pi*Rsg*(hs+ds)*l*rhofe*stsp; % What is this? Ask Jim
374 mteeths =( ds*(sslotp-us) + hs/2*(2*sslotp-wst-wsb) )*l*Ns*rhofe; % my expr
375 mteethr = pi*((Rrg+dr(i)+hr)^2-(Rrg)^2)*l*rhofe*rtsp;
376
377 % (c) Conductor mass
378 rslot_area  = wr*hr+ur(j)*dr(i);
379 mconds = 3*lwt*Aw* rhocopper; % stator conductor mass (multiply by three to get mass for
      the copper weight of the three phases). Modified on April 15,2019
380 mcondr = Nr*rslot_area*l*rhoalum + 2*(pi*((Rrg+dr(i)+her)^2-(Rrg+dr(i))^2)*ler*rhoalum);
381 % rotor conductor mass inculding end ring
382
383 mstator = mcores + mteeths + mconds; % total mass of stator
384 mrotor  = mcorer + mteethr + mcondr; % total mass of rotor
385 mtot    = mstator + mrotor; % total active mass of the IM
386
387 % Motor moment of inertia: (only for result display)
388 % stator
389 Ds = 2*Rsg;
390 Jsx = 1/8*mstator*Ds^2;
```

```
391 Jsy = 1/4*mstator*(Ds^2/4 + l^2/3);
392 Js = sqrt(Jsx^2+Jsy^2);
393 % rotor
394 Dl = 2*Rry;
395 D2 = 2*Rrg;
396 Jrx = 1/8*mrotor*(Dl^2 + D2^2);
397 Jry = 1/4*mrotor*( (Dl^2 + D2^2)/4 + l^2/3);
398 Jr = sqrt(Jrx^2+Jry^2);
399
400 J = sqrt(Js^2+Jr^2);
401
402 % total stator core loss at nominal flux density
403 Pc = Pst*mteeths + Pdc * mcores;
404 % Pc = Pst*pi*Rsg^2*l + Pdc * pi*(Rsg hs)^2*l/p;
405 %%
406 % total VAR loss (stator core + stator teeth + rotor teeth)at nominal B0
407 Qc = Qst*mteeths + Qdc*mcores + Qrt*mteethr;
408
409 % then core parallel resistance is %
410 Rc = 3*V^2/Pc;
411 % and parallel reactance is:
412 Xc = 3*V^2/Qc;
413 % Xc = inf;
414
415 % No load loss in rotor teeth because of stator slot opening modulation
416 % of fundamental flux density:
417 thetad = Ns*us/Rsg;
418
419 % BH is the nominal flux variation
420 BH = Bg * (2/pi) * sin (0.5*thetad);
421 % Prtnls = Pcloss(Keddy,Kh,Kex,f,BH); % W/Vol
422 Prtnls = P0*abs(BH/B0)^peB*abs(Ns*omega/omega0)^pef; % back iron loss density
423 % so then the equivalent resistance is:
424 Rrtnls = 3 * V^2 / Prtnls;
425
426 dispmotordata_v2
427
428 %%
429 %=========================================================================
430                                   % Motor Analysis
431 %=========================================================================
432
433 % Motor analysis
434
435 s       = logspace(-6,0,1e3);
436 [y sp]  = motoranalysis_edited_need_revision(s);
437 It      = y(1,:);
438 Pin     = y(2,:);
439 S       = y(3,:);
440 Pag1    = y(4,:);
441 Pag5    = y(5,:);
442 Pag7    = y(6,:);
443 Pagm    = y(7,:);
444 Pagp    = y(8,:);
445 Pag     = y(9,:);
446 Pslip1  = y(10,:);
447 Pslip5  = y(11,:);
448 Pslip7  = y(12,:);
449 Pslipm  = y(13,:);
450 Pslipp  = y(14,:);
451 Pslip   = y(15,:);
452 Pa      = y(16,:);
453 Pc      = y(17,:);
454 Prtnls  = y(18,:);
455 Prtls   = y(19,:);
456 Pwf     = y(20,:);
457 Ploss   = y(21,:);
458 Pmech   = y(22,:);
459 Te      = y(23,:);
460 Tm      = y(24,:);
461 eff     = y(25,:);
462 pf      = y(26,:);
463 I21     = y(27,:);
464 I25     = y(28,:);
465 I27     = y(29,:);
```

```
I2m      = y(30,:);
I2p      = y(31,:);
Ic       = y(32,:);
Vr       = y(33,:);


%%
Tstarting = Te(end); % starting torque at slip = 1

if isempty(sp) % when the linear search cannot find Pout = 23 W
    fprintf('Pconv,pk < Pout,rating \n');
    OF = 1e8; % to force the optim. algorithm to try another x
else
    yp = motoranalysis_edited_need_revision(sp);
    It0      = yp(1);
    Pin0     = yp(2);
    S0       = yp(3);
    Pag10    = yp(4);
    Pag50    = yp(5);
    Pag70    = yp(6);
    Pagm0    = yp(7);
    Pagp0    = yp(8);
    Pag0     = yp(9);
    Pslip10  = yp(10);
    Pslip50  = yp(11);
    Pslip70  = yp(12);
    Pslipm0   = yp(13);
    Pslipp0  = yp(14);
    Pslip0   = yp(15);
    Pa0      = yp(16);
    Pc0      = yp(17);
    Prtnls0  = yp(18);
    Prtls0   = yp(19);
    Pwf0     = yp(20);
    Ploss0   = yp(21);
    Pmech0   = yp(22);
    Te0      = yp(23);
    Tm0      = yp(24);
    eff0     = yp(25);
    pf0      = yp(26);
    I210     = yp(27);
    I250     = yp(28);
    I270     = yp(29);
    I2m0     = yp(30);
    I2p0     = yp(31);
    Ic0      = y(32,:);
    Vr0      = y(33);

    % Store efficiency and active weight here

    Eff(i,j) = eff0;
    Mactive(i,j) = mtot;
    Torque(i,j) = Te0;
    mechPower(i,j) = Pmech0;

    % calculate current densities:

    % stator
    Jslimit = 5; % Arms/mm^2 (based on Lippo's table6 6 for ODP motors chp 6 pg. 285)

    Js0RPM    = abs(It(end))/Aw*1e-6;
    JsRated   = abs(It0)/Aw*1e-6;

    % rotor

    I20RPM  = sqrt(abs(I21(end))^2+abs(I25(end))^2+abs(I27(end))^2+abs(I2m(end))^2+abs(I2p
        (end))^2);
    I2Rated = sqrt(abs(I210)^2+abs(I250)^2+abs(I270)^2+abs(I2m0)^2+abs(I2p0)^2);

    % bar current desnity
    Ib0RPM  = 6*Na*kw1/Nr*I20RPM;
    IbRated = 6*Na*kw1/Nr*I2Rated;

    Jblimit = 7.75; %Arms/mm^2 or 5000 Arms/in^2 as indicated by Lippo chp6 pg 285
```

```
541         Jb0RPM      = Ib0RPM/rslot_area*1e-6;
542         JbRated     = IbRated/rslot_area*1e-6;
543
544             % end ring
545         endring_current = 'exact'; %1stOrderTylor
546         if(strcmp(endring_current,'exact'))
547             Ie0RPM = abs(Ib0RPM/(1-exp(j*2*pi*p/Nr)));
548             IeRated = abs(IbRated/(1-exp(j*2*pi*p/Nr)));
549         elseif(strcmp(endring_current,'1stOrderTylor'))
550             Ie0RPM = Ib0RPM*Nr/2/pi/p;
551             IeRated = IbRated*Nr/2/pi/p;
552         end
553
554         Je0RPM      = Ie0RPM/rslot_area*1e-6;
555         JeRated     = IeRated/rslot_area*1e-6;
556
557         % Calculate skin_depth at slip:
558         skin_depth_rated_speed = 1/sqrt(sp*pi*fd*u0*sigAlum);
559         skin_depth_rated_speed_to_hr = skin_depth_rated_speed/hr;
560
561         omegam = omega/p*(1-s);
562         N = omegam*60/(2*pi);
563         N0 = omega/p*(1-sp)*60/2/pi;
564
565         % display results in case of meeting the power requirement
566         dispresults
567
568         % objective function
569         b1 = 1;
570         b2 = 1;
571         b3 = 0;
572         b4 = 0;
573         Bmax = max(sqrt(2)*[Bg Bst Brt Bcs Bcr]);
574 %         penalty = 100*(Bmax -1.6);
575
576         ff = (eff0^b1)/(mtot^b2); % Cost Function
577         if Bmax > 1.7
578             OF  = 1/ff  + 1e3;
579         else
580             OF  = 1/ff;
581         end
582
583         if eff0<0
584             OF = 1e6;
585         end
586     end
587
588     end % j
589     end % i
590     end
```

Bibliography

[1] ABB. ABB High Voltage Induction Motors. Technical report, 2007.

[2] ABB. Low voltage: Process Performance Motors according to EU MEPS. Technical report, 2014.

[3] P. L. Alger. *Induction Machines Their Behavior and Uses*. New York: Gordon and Breach Science Publishers, 1970.

[4] M. Andriollo, M. De Bortoli, G. Martinelli, A. Morini, and A. Tortella. Design improvement of a single-phase brushless permanent magnet motor for small fan appliances. *IEEE Transactions on Industrial Electronics*, 57(1):88–95, Jan 2010.

[5] ANSYS. Ansys Maxwell. Available at `https://www.ansys.com/products/electronics/ansys-maxwell` (5/18/2019).

[6] ANSYS. Maxwell Help. Available at `https://ansyshelp.ansys.com/Views/Secured/Electronics/v192/PDFs/Maxwell.pdf` (5/18/2019).

[7] T. H. Barton and B. C. Doxey. Three-phase motors with unsymmetrical secondary circuits. *Journal of the Institution of Electrical Engineers*, 1(2):87–88, February 1955.

[8] T. H. Barton and J. C. Dunfield. Polyphase to two-axis transformation for real windings. *IEEE Transactions on Power Apparatus and Systems*, PAS-87(5):1342–1346, May 1968.

[9] R. Bojoi, M. Lazzari, F. Profumo, and A. Tenconi. Digital field-oriented control for dual three-phase induction motor drives. *IEEE Transactions on Industry Applications*, 39(3):752–760, May 2003.

[10] W. J. Branson. Polyphase induction motors a labor saving method of calculating performance from previously determined constants. *Transactions of the American Institute of Electrical Engineers*, 49(1):319–328, Jan 1930.

[11] N. J. Braun. Some aspects of the application of induction motors to aircraft. *Electrical Engineering*, 63(10):769–772, Oct 1944.

[12] O. I. Butler and T. S. Birch. Comparison of alternative skew-effect parameters of cage induction motors. *Proceedings of the Institution of Electrical Engineers*, 118(7):879–883, July 1971.

[13] O. I. Butler and A. K. Wallace. Generalised theory of induction motors with asymmetrical primary windings, and its application to the analysis and performance prediction of shaded-pole motors. *Proceedings of the Institution of Electrical Engineers*, 115(5):685–694, May 1968.

[14] S. S. L. Chang. A high-power-factor one-running-capacitor 2-motor system. *Transactions of the American Institute of Electrical Engineers. Part III: Power Apparatus and Systems*, 76(3):720–724, April 1957.

[15] S. Chen, G. Liu, and L. Zhu. Sensorless control strategy of a 315 kw high-speed bldc motor based on a speed-independent flux linkage function. *IEEE Transactions on Industrial Electronics*, 64(11):8607–8617, Nov 2017.

[16] A. Chunekar and D. Singh. A guidebook on super-efficient equipment program (seep). *Prayas, Energy Group*, Dec 2013.

[17] I. E. Davidson and J. F. Gieras. Performance analysis of a shaded-pole linear induction motor using symmetrical components, field analysis, and finite element method. *IEEE Transactions on Energy Conversion*, 15(1):24–29, March 2000.

[18] Dawei Zhou, C. B. Rajanathan, A. T. Sapeluk, and C. S. Ozveren. Finite-element-aided design optimization of a shaded-pole induction motor for maximum starting torque. *IEEE Transactions on Magnetics*, 36(5):3551–3554, Sep. 2000.

[19] Stephane de la Rue du Can, Virginie E. Letschert, Michael A. McNeil, Nan Zhou, and Jayant A. Sathaye. Residential and transport energy use in india: Past trend and future outlook. 2/26/2009 2009.

[20] M. Depenbrock. Direct self-control (dsc) of inverter-fed induction machine. *IEEE Transactions on Power Electronics*, 3(4):420–429, Oct 1988.

[21] S. Dunkl, A. Muetze, and G. Schoener. Design constraints of small single-phase permanent magnet brushless dc drives for fan applications. *IEEE Transactions on Industry Applications*, 51(4):3178–3186, July 2015.

[22] J. F. Eastham and E. R. Laithwaite. Pole-change motors using phase-mixing techniques. *Proceedings of the IEE - Part A: Power Engineering*, 109(47):397–409, October 1962.

[23] M. Fazil and K. R. Rajagopal. Nonlinear dynamic modeling of a single-phase permanent-magnet brushless dc motor using 2-d static finite-element results. *IEEE Transactions on Magnetics*, 47(4):781–786, April 2011.

[24] F. P. Flynn, R. D. Slater, and W. S. Wood. Transient negative torques in induction motors due to rapid reconnection of the supply. *Proceedings of the Institution of Electrical Engineers*, 116(12):2009–2014, December 1969.

[25] F. Grover. *Inductance Calculations*. Dover Publications, 1st edition, 2009.

[26] M. Hagiwara, I. Hasegawa, and H. Akagi. Start-up and low-speed operation of an electric motor driven by a modular multilevel cascade inverter. *IEEE Transactions on Industry Applications*, 49(4):1556–1565, July 2013.

[27] A. Hota, M. Qasim, J. L. Kirtley, and V. Agarwal. A novel three-phase induction motor drive for domestic fan application with improved reliability. *IEEE Power Electron. Drives Energy Syst. Conf. (PEDES)*, 2019. (in press).

[28] Huangsheng Xu, H. A. Toliyat, and L. J. Petersen. Five-phase induction motor drives with dsp-based control system. *IEEE Transactions on Power Electronics*, 17(4):524–533, July 2002.

[29] W. Jiang, H. Huang, J. Wang, Y. Gao, and L. Wang. Commutation analysis of brushless dc motor and reducing commutation torque ripple in the two-phase stationary frame. *IEEE Transactions on Power Electronics*, 32(6):4675–4682, June 2017.

[30] J. L. Kirtley Jr. *6.685 Electric Machines, Class Notes 10: Induction Machine Control and Simulation*. Massachusetts Institute of Technology: MIT OpenCourseWare, 2011.

[31] J. L. Kirtley Jr. *6.685 Electric Machines, Class Notes 8: Analytic Design Evaluation of Induction Motors*. Massachusetts Institute of Technology: MIT OpenCourseWare, Fall 2013.

[32] P. C. Krause, O. Wasynczuk, and S. D. Sudhoff. *Analysis of Electric Machinery and Drive Systems*. IEEE Press series on power engineering. IEEE Press, 2002.

[33] A. S. Langsdorf. Air-gap flux in induction motors. *Proceedings of the American Institute of Electrical Engineers*, 24(9):973–984, Sep. 1905.

[34] D. Lee and Y. Kim. Control of single-phase-to-three-phase ac/dc/ac pwm converters for induction motor drives. *IEEE Transactions on Industrial Electronics*, 54(2):797–804, April 2007.

[35] E. C. Lee. Brushless dc-a modern approach to variable speed drives. In *Forty-Second Annual Conference of Electrical Engineering Problems in the Rubber and Plastics Industries*, pages 16–20, Apr 1990.

[36] H. Li, S. Zheng, and H. Ren. Self-correction of commutation point for high-speed sensorless bldc motor with low inductance and nonideal back emf. *IEEE Transactions on Power Electronics*, 32(1):642–651, Jan 2017.

[37] J. Li, T. Abdallah, and C. R. Sullivan. Improved calculation of core loss with nonsinusoidal waveforms. In *Conference Record of the 2001 IEEE Industry Applications Conference. 36th IAS Annual Meeting (Cat. No.01CH37248)*, volume 4, pages 2203–2210 vol.4, Sep. 2001.

[38] T. A. Lipo. *Introduction to AC Machine Design*. Wiley-IEEE Press, 2018.

[39] Y. Liu, J. Zhao, M. Xia, and H. Luo. Model reference adaptive control-based speed control of brushless dc motors with low-resolution hall-effect sensors. *IEEE Transactions on Power Electronics*, 29(3):1514–1522, March 2014.

[40] C. Ma, Q. Li, H. Lu, Y. Liu, and H. Gao. Analytical model for armature reaction of outer rotor brushless permanent magnet dc motor. *IET Electric Power Applications*, 12(5):651–657, 2018.

[41] B. McCormick. Comparison of two- and three-phase motors. *Transactions of the American Institute of Electrical Engineers*, XXV:295–306, Jan 1906.

[42] T.J.E. Miller. *Brushless Permanent-Magnet and Reluctance Motor Drives*. Oxford: Clarendon Press, 1989.

[43] Melanie Mitchell. *An Introduction to Genetic Algorithms*. MIT Press, Cambridge, MA, USA, 1998.

[44] M. Ojaghi and S. Daliri. Analytic model for performance study and computer-aided design of single-phase shaded-pole induction motors. *IEEE Transactions on Energy Conversion*, 32(2):649–657, June 2017.

[45] A. M. Osheiba, K. A. Ahmed, and M. A. Rahman. Performance prediction of shaded pole induction motors. *IEEE Transactions on Industry Applications*, 27(5):876–882, Sep. 1991.

[46] Y. Park, J. Cho, and D. Kim. Cogging torque reduction of single-phase brushless dc motor with a tapered air-gap using optimizing notch size and position. *IEEE Transactions on Industry Applications*, 51(6):4455–4463, Nov 2015.

[47] M. Rosu, P. Zhou, D. Lin, D. M. Ionel, M. Popescu, F. Blaabjerg, V. Rallabandi, and D. Staton. *Multiphysics Simulation by Design for Electrical Machines, Power Electronics and Drives*. Wiley-IEEE Press, 2018.

[48] M. B. Sawyer. Design considerations of 400-cycle aircraft motors. *Electrical Engineering*, 63(12):877–879, Dec 1944.

[49] H. Seol, J. Lim, D. Kang, J. S. Park, and J. Lee. Optimal design strategy for improved operation of ipm bldc motors with low-resolution hall sensors. *IEEE Transactions on Industrial Electronics*, 64(12):9758–9766, Dec 2017.

[50] Nihar Shah, Nakul Sathaye, Amol Phadke, and Virginie Letschert. Efficiency improvement opportunities for ceiling fans. *Energy Efficiency*, 8(1):37–50, Feb 2015.

[51] R. Shanmugasundram, K. M. Zakariah, and N. Yadaiah. Implementation and performance analysis of digital controllers for brushless dc motor drives. *IEEE/ASME Transactions on Mechatronics*, 19(1):213–224, Feb 2014.

[52] A. Straughen, P. P. Biringer, and G. R. Slemon. Three-phase induction-motor control using static-frequency doublers. *Transactions of the American Institute of Electrical Engineers, Part II: Applications and Industry*, 77(2):58–66, May 1958.

[53] F. J. Teago. The nature of the magnetic field produced by the stator of a three-phase induction motor, with special reference to pole-changing motors. *Journal of the Institution of Electrical Engineers*, 61(323):1087–1096, October 1923.

[54] Atomberg Technologies. Gorilla Efficio Energy Energy Energy Fan with BLDC Motor. Available at `https://atomberg.com/fans/ceiling-fan/gorilla-efficio/` (5/18/2019).

[55] H. A. Toliyat, T. A. Lipo, and J. C. White. Analysis of a concentrated winding induction machine for adjustable speed drive applications. i. motor analysis. *IEEE Transactions on Energy Conversion*, 6(4):679–683, Dec 1991.

[56] P. H. Trickey. An analysis of the shaded pole motor. *Transactions of the American Institute of Electrical Engineers*, 55(9):1007–1014, Sept 1936.

[57] S. D. Umans. *Fitzgerald & Kingsley's Electric Machinery, 7^{th} ed.* Boston, MA: McGraw-Hill Education, 2013.

[58] Usha. Usha Sewing Machines, Air Coolers, Fans, Kitchen Home Appliances. Available at `https://www.usha.com/fans/ceiling-fans/energy-saving-fans/technix-decorative-gold-1200` (5/18/2019).

[59] J. Varga and D. Basic. Analysis of the characteristics of single phase shaded pole induction motor with two short-circuited auxiliary phases. *IEEE Transactions on Energy Conversion*, 12(4):269–274, Dec 1997.

[60] C. G. Veinott. Performance calculations on induction motors. *Electrical Engineering*, 51(4):264–264, April 1932.

[61] C. G. Veinott. Performance calculations on induction motors practical straightforward means for calculating performance of single-phase or polyphase induction motors. *Transactions of the American Institute of Electrical Engineers*, 51(3):743–754, Sep. 1932.

[62] C. G. Veinott. *Theory and Design of Small Induction Motors*. McGraw-Hill Book Company, Inc., 1959.

[63] C. F. Wagner. Self-excitation of induction motors. *Transactions of the American Institute of Electrical Engineers*, 58(2):47–51, Feb 1939.

[64] Paul Waide and Conrad U. Brunner. Energy-efficiency policy opportunities for electric motor-driven systems. IEA Energy Papers 2011/7, OECD Publishing, 2011.

[65] S. Williamson and M. A. Mueller. Calculation of the impedance of rotor cage end rings. *IEE Proceedings B - Electric Power Applications*, 140(1):51–60, Jan 1993.

[66] T. G. Wilson and P. H. Trickey. D-c machine with solid-state commutation. *Electrical Engineering*, 81(11):879–884, Nov 1962.

[67] T. Yazdan, W. Zhao, T. A. Lipo, and B. Kwon. A novel technique for two-phase bldc motor to avoid demagnetization. *IEEE Transactions on Magnetics*, 52(7):1–4, July 2016.

[68] Yifan Zhao and T. A. Lipo. Space vector pwm control of dual three-phase induction machine using vector space decomposition. *IEEE Transactions on Industry Applications*, 31(5):1100–1109, Sep. 1995.

[69] M. Z. Youssef. Design and performance of a cost-effective bldc drive for water pump application. *IEEE Transactions on Industrial Electronics*, 62(5):3277–3284, May 2015.